BLIDA 1 university

Faculty of Technology
Electronics Department

DOCTORAL THESIS
In Electrical Engineering

IMPLEMENTATION OF MAXIMUM POWER POINT TRACKING ALGORITHMS FOR PARTIALLY SHADED PHOTOVOLTAIC GENERATORS

Defended by:

BOUKENOUI Rachid

Before a jury composed of:

A. GUESSOUM	Professor, Blida 1 University	chairman
K. KARA	Professor, Blida 1 University	Examiner
H. BENTARZI	Professor, Boumerdes MB University	Examiner
H. SALHI	Professor, Blida 1 University	Thesis supervisor
A. MELLIT	Professor, Jijel University	Thesis Co-supervisor

Blida, 2017

ABSTRACT

In this thesis, the latest progress in Maximum Power Point Tracking (MPPT) techniques for Photovoltaic (PV) systems under uniform and non-uniform irradiance conditions is covered. Moreover, a survey of some recent progress in PV device technologies is provided. A PV model based on manufacturer's datasheet has been developed to predict the Current-Voltage and Power-Voltage characteristics of some PV technologies. Test facility has been employed to assess the developed PV model and experimental results have been provided. A standalone PV system is designed to increase the energy extraction by using new MPPT methods. The first proposed MPPT is based on the use of Golden Section Optimization (GSO) technique. GSO-MPPT has many advantages under uniform irradiance conditions. However, it cannot track the Global MPP (GMPP) under complicated shading patterns. In order to address this issue, another MPPT is proposed, it combines a scanning-storing procedure as well as a tracking loop which is based on Fuzzy Logic Controller (FLC). Based on simulation and comparison results, it can be concluded that this MPPT is able to track the GMPP and improve the dynamic and steady state performance simultaneously under complicated shading patterns. However, using FLC as MPPT tracker leads to an increase in the complexity level of the control system as well as to high memory requirement during implementation. The third MPPT has been proposed in order to solve the drawback associated with the second MPPT, meanwhile, keeping its advantages. It is based on cascading two loops to handle the problem of Partial Shading Conditions (PSCs) and improve the PV system performance. Finally, experimental evaluation is carried out to evaluate the performance of some MPPTs. The hardware implementation platform has been designed at Quartz laboratory EA 7393 located in ‘‘l’École Nationale Supérieure de l'Èlectronique et de ses Applications’’ (ENSEA), France.

Keywords: Photovoltaic system, maximum power point tracking, performance assessment, dSPACE, comparison, experimental validation, photovoltaic technology, Simscape, golden section optimization, fuzzy logic controller, variable step size hill climbing.

RÈSUMÈ

Dans cette thèse, une étude bibliographique sur les différents types de commandes MPPT destinées à contrôler les systèmes Photovoltaïques (PV) soumis à des conditions d'irradiation uniforme et non uniforme (présence d'ombrage) a été présenté. Les récents progrès de certaines technologies des panneaux PV sont aussi présentés. Un modèle PV basé sur les données du datasheet a été développé pour prévoir les caractéristiques électriques Tension-Puissance et Tension-Courant des différentes technologies photovoltaïques. Le modèle photovoltaïque développé a été évalué et les résultats expérimentaux ont été fournis. Aussi, trois contrôleurs MPPT dédiées à la commande des systèmes photovoltaïques ont été proposés pour extraire le point de puissance maximale disponible. Le premier contrôleur MPPT basé sur une technique connue sous le nom Golden Section Optimisation, présente plusieurs avantages lorsque l'irradiation du générateur photovoltaïque est uniforme. Cependant, il montre des limitations dans le cas des conditions où le motif d'ombrage est compliqué. A cet effet, un autre contrôleur MPPT basé sur la combinaison de la procédure balayage-stockage avec une boucle de suivi floue a été proposé. Cette solution, présente une grande précision et une robustesse dans différents conditions de fonctionnement. Cependant, l'utilisation du contrôleur flou conduit à une grande complexité lors d'une implémentation. Le troisième contrôleur MPPT élaboré utilise deux boucles en cascade. La première est la boucle d'identification, tandis que, la deuxième est la boucle de suivi. Ce contrôleur offre une grande précision et robustesse. L'implémentation hardware a été effectuée pour évaluer et comparer les performances du contrôleur MPPT. La plate-forme d'implémentation a été conçue dans le laboratoire Quartz EA 7693 situé à l'École Nationale Supérieure de l'Èlectronique et de ses Applications (ENSEA), France.

Mots clés : Système photovoltaïque, contrôleur de point de puissance maximale, évaluation de performance, dSPACE, comparaison, Validation expérimentale. Technologie photovoltaïque, Simscape, golden section optimiseur, contrôleur flou, hill climbing basé sur un pas variable.

ملخص

في هذه الأطروحة، تم تقديم أحدث التطورات في تقنيات محسن القوة المعروفة باسم متتبع نقطة الإستطاعة العظمى *(MPPT)* الذي يجب أن يستعمل مع النظم الكهروضوئية تحت ظروف إشعاعية متجانسة وغير متجانسة. علاوة على ذلك، تم تقديم آخر التطورات في تكنولوجيات أجهزة الكهروضوئية. وقد تم تطوير نموذج للأجهزة الكهروضوئية حيث أن هذا الأخير يستند فقط إلى ورقة البيانات التي يقدمها المصنع, هذا النموذج تم إخضاعه إلى إختبارات تجريبية .

تم تصميم نظام كهروضوئي مستقل يعمل مع أساليب جديدة من محسنات القوة *(MPPTs)* لزيادة الطاقة المستخرجة. يستند أول محسن قوة مقترح إلى تقنية *(GSO)* . هذه التقنية لديها العديد من المزايا في ظل ظروف إشعاعية متجانسة. غير أن لا يمكنها تتبع الإستطاعة العظمى بدقة تحت ظروف إشعاعية غير متجانسة, خاصة في أنماط تظليل معقدة.

من أجل معالجة هذه المسألة، تم إقتراح محسن قوة جديد يجمع بين عملية المسح والتخزين وكذلك حلقة التتبع التي تقوم على تقنية منطق التحكم الغامض *(FLC)*. بالإعتماد على النتائج المحصل عليها تبين أن محسن القوة الأخير قادرة على تتبع الإستطاعة العظمى وتحسين الأداء المستقر والديناميكي في آن واحد ,تحت أنماط تظليل معقدة. غير أن إستخدام تقنية منطق التحكم الغامض *(FLC)* يؤدي إلى زيادة في مستوى تعقيد وحدة التحكم وكذلك متطلبات الذاكرة العالية أثناء التنفيذ.

محسن القوة الثالث تم إقترحه لتخفيض مستوى التعقيد المرتبط بمحسن القوة الثاني مع الحفاظ على مزاياه. هو يقوم على حلقتين متتاليتين لتحسين أداء النظم الكهروضوئية . تم إجراء تحقيق تجريبي لتقييم أداء محسن القوة الأخير حيث تم تصميم منصة تنفيذ التجارب في مختبر كوارتز إي *7393* (فرنسا). ولأجل إبراز مزايا محسن القوة الأخير تم مقارنته مع عدة محسنات القوة .

الكلمات الرئيسية: نظام كهروضوئي ، متتبع نقطة الإستطاعة العظمى *(MPPT)* ، تقييم الأداء، dSPACE ، المقارنة، التحقق من صحة التجريبية, تكنولوجيا الكهروضوئيات ، Simscape ، GSO، منطق التحكم الغامض *(FLC)* ، تسلق التل خطوة متغيرة .

DEDICATION

My deepest gratitude goes out to my parents, for their prayers, love, continuous encouragement and unlimited support, and also to my brothers, who provided much support. It is to them that I dedicate this thesis.

ACKNOWLEDGEMENTS

"Over all those endowed with knowledge is the All-Knowing (ALLAH)".

In the name of Allah, the Most Gracious and the Most Merciful. Thanks to ALLAH who is the source of all the knowledge in this world, for the strengths and guidance in completing this thesis.

The printed pages of this thesis hold far more than the culmination of years of study. These pages also reflect the relationships with many generous and inspiring people I have met since the beginning of my PhD study. I would like to take this opportunity to thank those who have helped me in some way or another. Without their help, it would not have been possible for me to complete this thesis.

First of all, I would like to express my special thanks of gratitude to my supervisors: Prof. *Hassen SALHI*, Prof. *Adel MELLIT*, and Dr. *Rafik BRADAI*, who gave me the golden opportunity to do this project. Throughout the supervision process, I have not only learned the technical knowledge, but also acquired the attitude and spirit of research. Their support did not stop at the scientific supervision but extended to facilitate many administrative issues. I highly appreciate all what they have done for me.

My sincere gratitude also goes to Prof. *Aissa KHELDOUN*, Prof. *Malek GHANES*, Prof. *J-P BARBOT* for their excellent advice and help during my PhD studies.

My heartfelt appreciation also goes to my examiners Prof. *Abderrezak GUESSOUM*, Prof. *Kamel KARA*, Prof. *Hamid BENTARZI*, for their insightful comments and suggestions.

Many thanks and appreciation to my best friends at Blida 1 university, *Sid Ali BLAIFI*, *Elyes GAROUDJA* and *Rabeh BOUHEDIR*, for their friendship and support. I will treasure our friendship forever.

Words cannot express enough my very grateful to my parents for all the sacrifices they had to make and for their support and encouragement. Their prayers and blessings were no doubt the true reason behind any success I have realized in my life.

Rachid Boukenoui

2017

TABLE OF CONTENTS

LIST OF ILLUSTRATIONS, GRAPHICS AND TABLES

ILLUSTRATIONS and GRAPHICS

CHAPTER 1

CHAPTER 2

CHAPTER 3

CHAPTER 4

CHAPTER 5

TABLES

CHAPTER 1

CHAPTER 2

CHAPTER 3

CHAPTER 4

CHAPTER 5

GENERAL INTRODUCTION

Context

With the rapid growth in industrial field worldwide as well as ever increasing sophistication of modern lifestyles; the world energy supply tends to be subject of tremendous strain. Furthermore, most of power plants are based on conventional energy sources (i.e., coal, petroleum and natural gas, etc) that experience a fast depletion and cause serious environmental issues (global warming and climate change). These phenomena have driven nations and power producers/suppliers around the world, seeking alternative energy sources that are sustainable, green and more efficient [1]. Electrical energy supplied by renewable sources has been targeted as an effective optimal pathway to cope with the aforementioned critical challenges [2]. It is worth mentioning that sunlight is considered as an interesting renewable source to produce electricity. In developing countries, for population who are living in remote areas and having no access to grid utility while solar radiation is abundantly available (i.e., South Asia, Southeast Asia, and Sub-Saharan Africa) [3], solar energy becomes critically important. It is envisaged to be one of the key sources of the future in Algeria. Moreover, it has become a necessity for people living in the southern to cope with the long hot season [4].

The primary energy of Photovoltaic (PV) based conversion systems is the sunlight and its conversion to electric energy involves no rotating machines. This process of conversion needs only the use of semiconductors and no fuel burning is required. This fact results in several advantages when using such PV systems in producing electricity such as: noiseless, safe, green, environmentally friendliness and almost no maintenance is required [5]. Moreover, PV systems can be effectively utilized in unused spaces, such as: rooftops of homes, universities, shopping malls and factories in order to harvest solar energy [6-8]. In addition to the PV systems ability in supplying the rural areas. Hence, the use of PV source in distributed generation or solar power plant as well as standalone systems, has recently known a big growth and attention [3].

Problem statement

PV systems have many drawbacks and one of the most important of them is the very low conversion efficiency. A great part of the power loss may be noticed which is due to the process of harvesting solar energy that is related to the conversion of limited wavelengths of photons being absorbed by the semiconductor. In other words, photons having less energy and those having energy greater than the band-gap energy of the semiconductor contribute in overheating rather than generating electricity [9].

Besides other factors, such as: structure defects of the PV cell and the area of contacts on the top of PV cell, the power conditioning (chopper or inverter) to which is connected the PV affects a lot its conversion efficiency. Many models to predict this efficiency as well as the electrical behavior of PV module/string/array under different working conditions are now available [10-13]. These models have been employed in the performance evaluation of Maximum Power Point Tracking (MPPT) algorithms [14, 15] as well as in analyzing the PV system performance (e.g., energy yield prediction, efficiency calculation etc) [16-18]. There are many models proposed in the literature to model PV generators (cells, modules, string or array). However, these models are sometimes unable to predict the electrical characteristics when the PV Generator (PVG) has complicated configurations of modules or undergoes PSCs, and often require additional information besides the standard data provided by the manufacturer's datasheet. Since the latter is the only source of data available to designers, hence developing an accurate model of PVG based on the datasheet is very beneficial.

Considering the uniformity of irradiance, there is only one point on the Power-Voltage (P-V) characteristic of the PVG where maximum electric power can be extracted and hence maximum operation efficiency is obtained [19]. To ensure that PV systems work at their Maximum Power Point (MPP), a chopper or inverter with voltage or current control are inserted between the PV and the load and a MPPT algorithm is run every time to seek this point. However, considering real life situations, the sunlight striking the PV system being constituted of many PV modules connected in series or/and in parallel can be non-uniform. It is worth mentioning that non-uniformity of irradiance is one of the major sources of reduction in energy yield of PV systems as confirmed by many studies [13, 17]. As a matter of fact, the energy

productivity of shaded PV systems can drop down to 20% of that of the unshaded PV systems [20]. Shaded cells inhibit power generation from other fully illuminated series-connected cells and become hot spots. Therefore, to protect the shaded cells from thermal destruction, bypass diodes should be integrated within the PV module [21]. However, adding bypass diodes in parallel to some set of cells or modules within PV string will result in multimodal P-V characteristic [22, 23].

Looking for places without frequent shadowing to install PV systems can be an effective solution to alleviate the impact of Partial Shading (PS) but cannot totally get rid of it. Many factors lead to PS problem, for instance, in building integrated PV installations, PV cells/modules can be subjected to shadows cast by both predictable surrounding objects, which may be nearby trees/antenna, utility towers, power lines, or unpredictable sources, e.g., fallen leaves or bird dung covering parts of the PV module surface. In large PV plants occupying a wide area of land, where PV modules are usually placed far from any surrounding obstacles, different orientations of PV modules belonging to the same PV string, moving clouds and shadows of adjacent rows of PV modules also lead to PS problem. Furthermore, PS effects can take place if there is a mismatch between modules composing the same PV system. This mismatch is the result of connecting together PV modules with different technologies or electrical characteristics [24]. This phenomenon is called as mismatching losses [25]. However, manufacturers set the tolerances in PV module characteristics to reduce the power losses as this problem continuously exists due to the uneven aging of PV modules that belong to the same PV string. Regarding PS problem, many solutions have been proposed to improve the efficiency of PV system. These solutions can fall within two main groups, hardware and software solutions. Hardware solutions include array connections [13, 17, 26, 27], PV system architectures [28-30] and circuit topologies [31, 32], aim to mitigate the PS effects. Array connections define how PV modules of an array are connected. Choosing, instead of series-parallel connections, total-cross-tied or bridge-linked PV modules allow decreasing the current that flows through shaded PV cells and hence keep the bypass diodes reverse biased. This would improve the MPP of the PV system. PV system architecture pertains to the way the chopper/inverter is connected. Unlike centralized architecture where all PV modules are connected to the main converter (chopper & inverter), in series and parallel-

connected micro-converter architectures, each PV module is connected to its own converter. The latter connections allow tracking the MPP of individual PV modules and hence improving the overall efficiency. The third solution that is circuit topologies consists in using different topologies of converters together with their connections to PV modules and are well investigated in the work of Bidram *et al.* [31]. Important improvement of efficiency has been obtained by using circuit topology methods.

Software solutions are pertaining to the upgraded MPPT methods that properly identify and track the desired MPP of the PV system [22, 33]. Conventional MPPTs are all based on pursuing the point on the P-V characteristics at which the derivative of power with respect to either voltage or duty cycle is null. Therefore, when used to track the MPP of partial shaded PV modules, they would fail to track the appropriate MPP and subsequently extra power losses result [34]. In this context, some conventional MPPT techniques have been modified or combined with other methods to escape Local Maximum Power Points (LMPPs) and hence properly identified the GMPP on the P-V characteristic curve.

In the light of the above discussion, proposed hardware solutions until now are limited and suffer from power dissipation and are not cost effective [17]. Furthermore, the majority of the proposed GMPPTs in the literature incur complex computational process as they use intelligent or soft computing algorithms. Complex computational process may provide drawbacks in terms of time response and hence inaccuracy in tracking the GMPP when the irradiation changes rapidly.

Objectives

The aim of the research presented in this thesis is to contribute to increasing PV systems efficiency. This goal can be achieved by developing suitable MPPT methods that have a low complexity as well as they can cope with PS problems and subsequently ensuring better tracking efficiency. To achieve this, the following key objectives are set:

- Investigate various types of MPPT techniques which have been proposed over the years as well as highlighting their advantages and disadvantages.

- Survey the recent progress in PV device technologies (such as: Crystalline Silicon and thin film based technologies), focusing on the fabrication cost, the conversion efficiency and the ability to the large scale deployment.
- Find an easier approach which considers only the manufacturer's datasheet to model PVGs under UICs and PSCs, the developed model should be efficient, accurate, easily to be applied by designers and must be able to model any configuration of PV sources (cells, modules) in one hand, and it should incorporate the bypass diodes behavior.
- Perform simulations and statistical errors calculation to measure the accuracy of the proposed PV model in predicting the I-V and P-V characteristics of different PV technologies.
- Clarify the effect of UICs and PSCs on the PV characteristics of series and parallel connected PV sources (cells or modules).
- Introduce new MPPT methods to track the true MPP and overcome PS problems. Simulation or experimental verification is to support the finding and comparison with recent MPPT is to figure out the advantages and disadvantages of the proposed MPPT.
- Design and construct of the hardware platform to be employed for the experimental assessment and validation of MPPT methods.

Organization of this thesis

The thesis is divided into five chapters, four of them present an original work. It is hoped that the work presented in this thesis will be a source of valuable information for PV professionals to keep abreast with the latest progress in the PV power source, as well as for new researchers to get started on MPPT methods and PV systems.

The first chapter covers the latest progress in the PV power plant control wherein the more recent MPPT methods, including LMPPTs as well as GMPPTs have been presented and discussed, their advantages and disadvantages are also clarified.

The second chapter deals with the recent progress in PV device technologies. Moreover, a PV model based on manufacturer's datasheet to predict the I-V and P-V characteristics of some PV technologies is introduced. The proposed model uses

Matlab-Simscape software to characterize any configuration of solar cells within the PV module. The ideality factor of solar cells is chosen according to their technologies. Moreover, the series resistance, is identified using a simple procedure which takes only the datasheet parameters into account. The test facility that has been employed to assess the developed PV model as well as experimental results are also given within the chapter.

The third chapter presents a new MPPT algorithm based on the use of Golden Section Optimization (GSO) technique in addition to its simulation and comparison results. GSO-MPPT has many advantages under UICs. However, it cannot track the GMPP under complicated shading patterns.

The fourth Chapter introduces a new intelligent MPPT method to track the GMPP of complicated partially shaded PVGs. It combines a scanning-storing procedure as well as a tracking loop based on FLC. According to simulation and comparison results it can be concluded that the proposed MPPT has many advantages under UICs and PSCs. However, the high complexity level is its main limitation.

The fifth chapter presents a new MPPT method besides its experimental results. This MPPT is based on cascading two loops with low complexity to handle the problem of PSCs. Meanwhile, to improve the PV system performance under both UICs and PSCs. The hardware implementation platform to be employed for the experimental evaluation of the proposed MPPT is provided with the chapter. The last section of the chapter provides comparative results that have been used to assess the proposed MPPT in controlling the PV system. To this end, in the first comparison, three LMPPTs (Perturb & Observe, Variable Step Size Incremental Conductance [35] and adaptive P&O-FLC [36]) have been experimentally implemented, tested and compared with the proposed MPPT. In the second comparison, the proposed MPPT has been compared with six recently published GMPPT methods [32, 37-41].

CHAPTER 1
LITERATURE REVIEW

1.1. Overview

The most economical way to improve the performance of PVGs is to keep them operating at their MPP irrespective of the environment conditions. This can be achieved by associating a MPPT controller to the power electronic converter (usually a DC-DC converter) in order to adjust the duty cycle to much the load. A great work has been done to improve the performance of PV systems through the development of new or upgrading already existed MPPTs. In this chapter, an attempt is made to review the more recent MPPT methods for PV systems under uniform and non-uniform irradiance conditions.

1.2. Maximum Power Point Tracking (MPPT)

The first MPPT technique was used in the 1970s for aerospace applications [42], by the company ‘’*Honeywell”* and the research centre ‘’*NASA”*. Sine that, many MPPT techniques have been developed and used as shown in figure (1.1). These techniques can be classified in two main groups, Local and Global MPPTs. LMPPTs can be employed only to track the MPP of PV systems under UICs. They include conventional, improved and artificial intelligent methods. While, GMPPTs include soft computing and hybrid MPPT methods. This group of MPPTs can extract the GMPP under PSCs.

1.3. Local MPPTs (LMPPTs)

1.3.1. Conventional MPPTs

1.3.1.1. Fractional Short-Circuit Current (FSCI) method

By sweeping the P-V characteristic curve of any PVG under UICs, there exists a single operating point $P_{pv}(V_{MPP}, I_{MPP})$ called MPP at which the produced power is maximum (P_{MPP}). Figure (1.2) shows the P-V and I-V characteristic curves of a PVG under UICs, with its main parameters such as: the short circuit current (I_{sc}), the current at P_{max} (I_{MPP}), the open circuit voltage (V_{oc}), the voltage at P_{max}(V_{MPP}) and the maximum power (P_{MPP}).

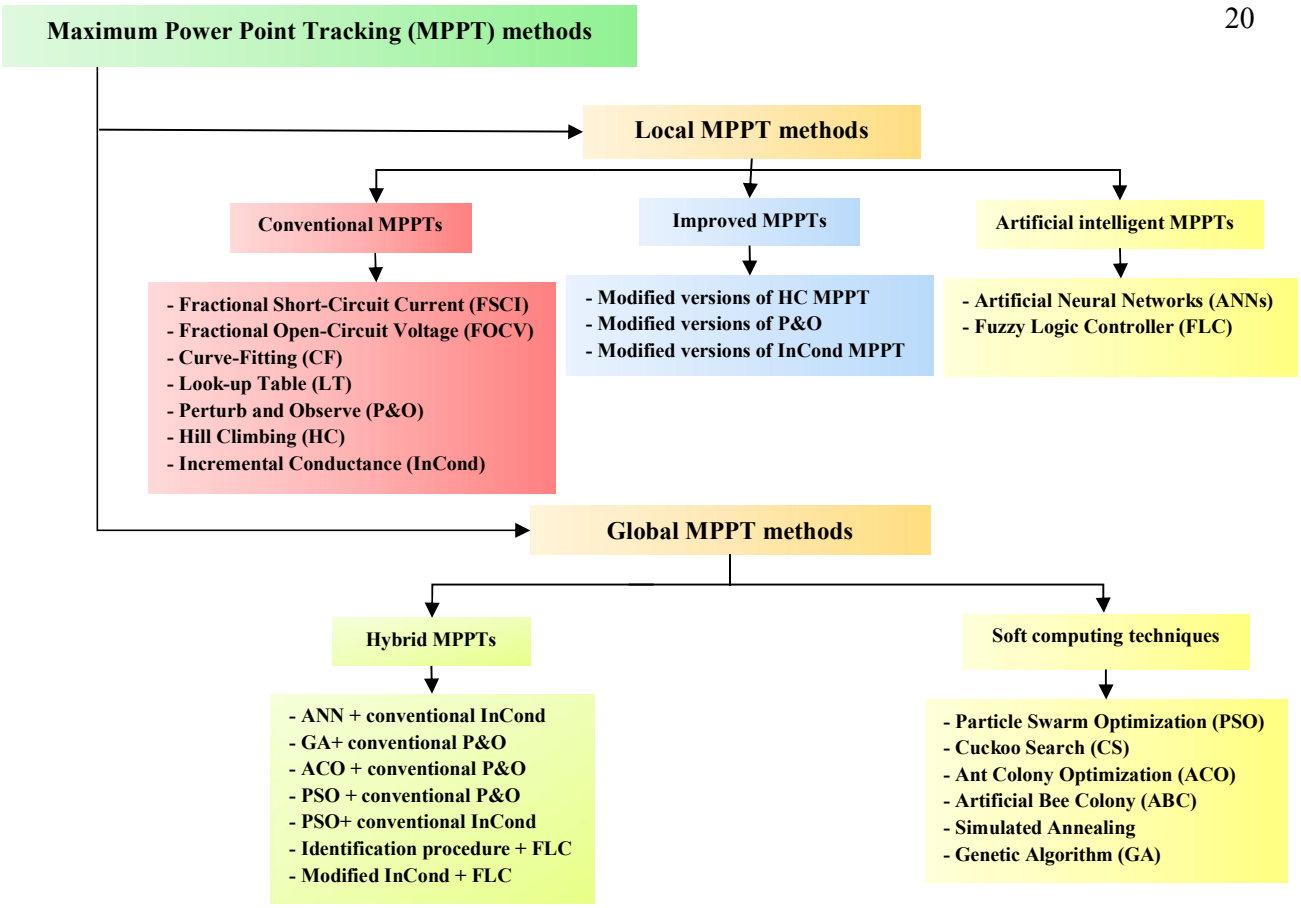

Figure 1. 1: Classification of MPPT techniques

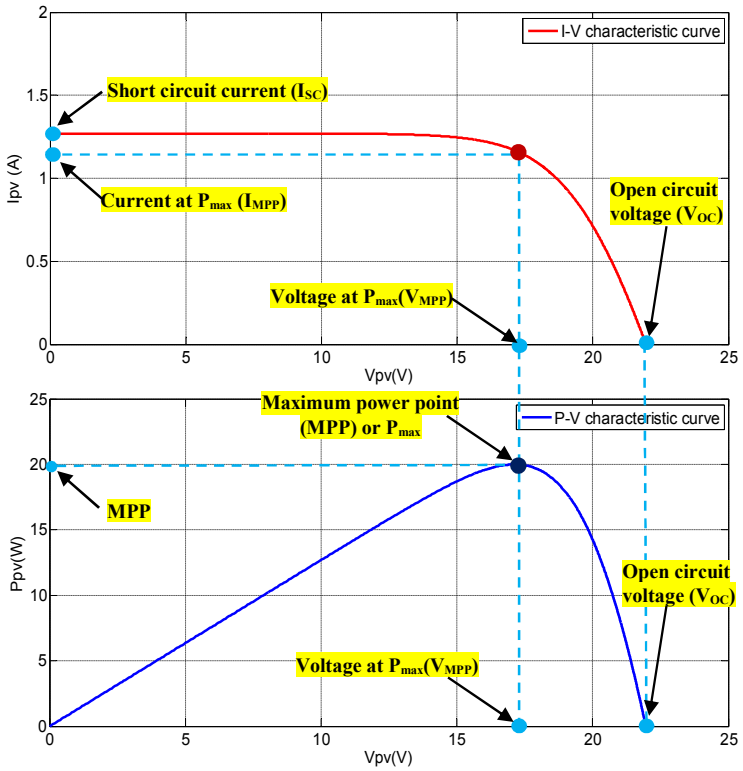

Figure 1. 2: I-V and P-V characteristics of a PVG under UICs

If any one of V_{MPP} or I_{MPP} are tracked by using MPPT method, the corresponding MPP can be tracked. In the FSCI method, the nonlinear I-V characteristic curve of a PVG under UICs is modeled using one of the exiting PV modelling approach (mathematical equations or numerical approximations) taking account of a wide range of irradiance and temperature levels. Then, a linear relationship between I_{MPP} and I_{sc} can be obtained, which is given by:

$$I_{MPP} \simeq K_{sc} I_{sc} \tag{1.1}$$

Where, the value of the current factor K_{sc} can be identified by analyzing the locus of I_{MPP} with respect to I_{sc} of many I-V characteristic curves at a wide range of irradiances and temperatures, which generally varies between 0.64 and 0.85 [43].

During the search process of FSCI MPPT, the PV system is short-circuited for a fraction of second and I_{sc} is measured, then I_{MPP} is calculated using the algorithm shown in Figure (1.3).

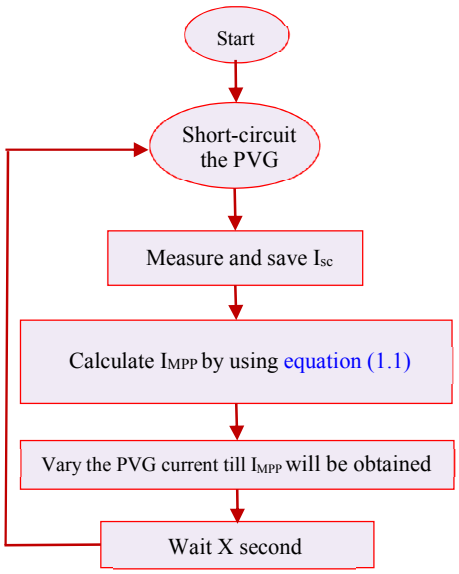

Figure 1. 3: Flowchart of FSCI MPPT

1.3.1.2. Fractional Open-Circuit Voltage (FOCV) method

In FOCV method, V_{MPP} can be calculated from the linear relationship given as follows:

$$V_{MPP} \simeq K_{oc} V_{oc} \tag{1.2}$$

The voltage factor K_{oc} can be identified by analyzing many I-V or P-V characteristic curves at a wide range of irradiances and temperatures. It is found that the value of K_{oc} varies between 0.7 and 0.85 [20, 43].

By employing FOCV MPPT to control the PV system, the PVG should be open-circuited for a fraction of second in order to measure V_{oc}, then V_{MPP} is calculated using equation (1.2). Repeating this process, V_{oc} is sampled repeatedly in every few seconds and the value of V_{MPP} is updated as illustrated in the flowchart of Figure 1.4.

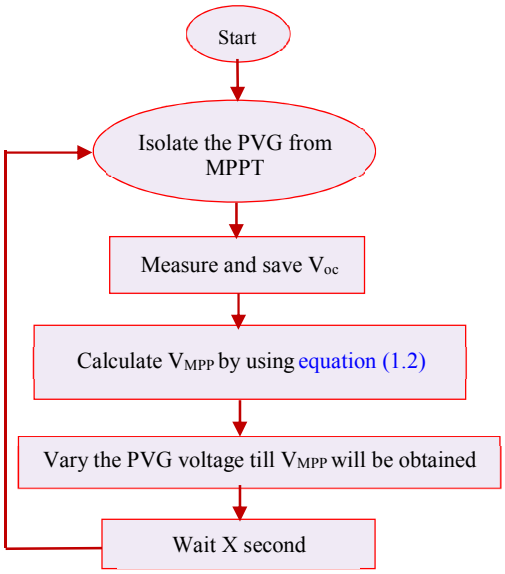

Figure 1. 4: Flowchart of FOCV MPPT

1.3.1.3. Curve-Fitting (CF) method

The MPP is the extreme value of the P-V characteristic curve at specific irradiance and temperature levels as shown in figure (1.2). Hence at first, the aforementioned curve should be predicted in this technique. Many existing methods in the literature can be employed for modelling and predicting the P-V characteristic curve [44, 45]. However, the CF based MPPT uses a third-order polynomial function to achieve an accurate fitting of this curve, which is given by,

$$P_{pv} = aV_{pv}^3 + bV_{pv}^2 + cV_{pv} + d \tag{1.3}$$

Where, the coefficients of the fitting function a, b, c and d are determined by sampling of PV voltage and power in some intervals. Differentiation of equation (1.3) gives,

$$\frac{dP_{pv}}{dV_{pv}} = 3aV_{pv}^2 + 2bV_{pv} + c \tag{1.4}$$

Equation (1.4) can be used to determine an optimum voltage at which the operating power (P_{pv}) is equal to the MPP by considering the following condition:

At MPP $$\frac{dP_{pv}}{dV_{pv}} = 0 \tag{1.5}$$

Thus, the voltage at MPP can be calculated as

$$V_{MPP} = \frac{-b \pm \sqrt{b^2 - 4ac}}{2a} \tag{1.6}$$

In this technique, the coefficients of the fitting function (a, b, c and d) are repeatedly sampled in a span of few milliseconds (using mathematical equations defined in [44]), then V_{MPP} is calculated.

1.3.1.4. Look-up Table (LT) Technique

In this technique, from theoretical calculations of MPP locus, V_{oc} and its corresponding V_{MPP} are calculated beforehand for each probable combination of irradiance and temperature then stored in the memory device (microprocessor) of MPPT's control system.

During the operation, V_{MPP} is obtained by measuring V_{oc} and searching in the Look-up table stored in MPPT's control system for V_{MPP} versus the measured V_{oc}. Then, the corresponding duty cycle for a particular condition is selected from that memory and used as input to the DC-DC converter.

It is worth mentioning that by using LT, CF, FOCV or FSCI based MPPTs, power oscillations around the MPP are avoided. However, these techniques suffer from a dependence on the PV system parameters (such as: the value of V_{oc} or I_{sc}) that may change over time. Moreover, significant power losses occurred by short-circuiting or open-circuiting the PVG in order to measure I_{sc} or V_{oc}, respectively.

1.3.1.5. Perturb and Observe (P&O) method

In practice, there is a widespread use of P&O MPPT [46, 47] to control PV systems, thanks to its low complexity and ease of implementation. P&O MPPT is considered as a sampling method, in which the process for arriving at the MPP is a result of repeating cycles of analysis (or iterations). At each step, the past and the present values of voltage and power are employed in the tracking process. For this,

measurements of the PV panel current and voltage are required at each sampling time (n), in order to compute the corresponding power. Considering the values of the current and voltage measured after the first terminal voltage perturbation ($V_{ref}(n)= V_{ref}(n-1)+ \Delta V_{ref}$ or $V_{ref}(n)= V_{ref}(n-1)- \Delta V_{ref}$), the new corresponding power will be calculated. If the power change ($\Delta P_{pv}(n) = P_{pv}(n) - P_{pv}(n-1)$) is positive, the voltage perturbation should be kept in the same direction. Otherwise, it should be reversed. The flowchart of the P&O MPPT is given in figure (1.5).

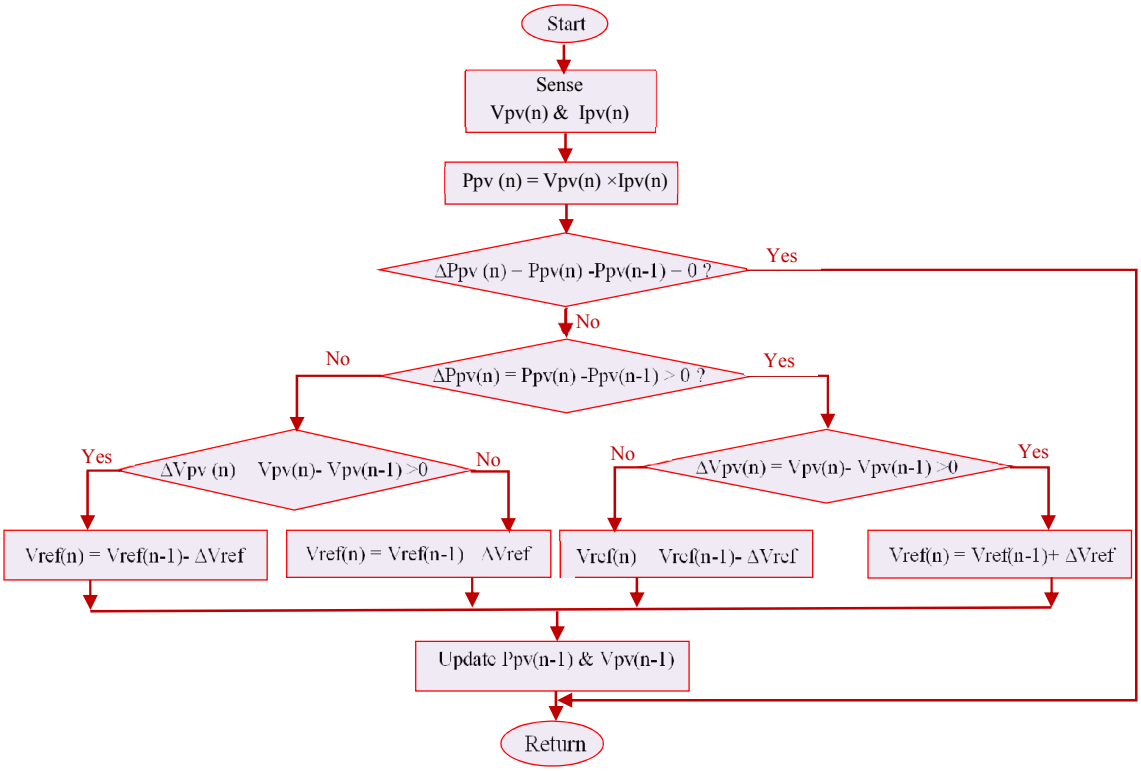

Figure 1. 5: Flowchart of P&O method

1.3.1.6. Hill Climbing (HC) method

As discussed in [48], HC and P&O are two different MPPT techniques having the same fundamental principle. The difference between them lies in the strategy used for controlling the power converter. Hence, P&O should be associated with a Proportional-Integral (PI) controller to generate an appropriate duty cycle for the DC–DC converter. Whereas, HC involves a direct perturbation on the duty cycle [49-51]. This in turn leads to perturbing the PV output current. Then, by achieving the condition at which the slope of power versus duty cycle is null, the MPP is reached

for a given irradiance and temperature [52]. In [53], a comparison between HC and P&O proves that P&O is more efficient, especially under varying weather conditions.

1.3.1.7. Incremental Conductance (InCond) method

InCond MPPT takes advantage of the fact that the slope of the P-V characteristic curve is zero at the MPP. It was proposed to improve the tracking efficiency and the dynamic performance in rapidly changing irradiance conditions [35, 54, 55]. In InCond, the measured PV output current and voltage are employed in calculating the values of both the conductance and incremental conductance. Then, by comparing their values, the MPPT is expected to make the right decision for changing the voltage reference. For more clarification, the PV output power can be expressed as:

$$P_{pv}(n)=V_{pv}(n)\times I_{pv}(n) \tag{1.7}$$

Where $P_{pv}(n)$, $V_{pv}(n)$ and $I_{pv}(n)$ are the PV output power, voltage and current, respectively.

InCond MPPT is obtained by differentiating the PV output power with respect to the PV output voltage, and setting the resulting equation to zero as follows:

$$\frac{\Delta P_{pv}(n)}{\Delta V_{pv}(n)}=\frac{\Delta(V_{pv}(n)\times I_{pv}(n))}{\Delta V_{pv}(n)}=I_{pv}(n)+V_{pv}(n)\frac{\Delta I_{pv}(n)}{\Delta V_{pv}(n)} \tag{1.8}$$

By dividing Equation (1.8) by $V_{pv}(n)$, as follows:

$$\frac{1}{V_{pv}(n)}\times\frac{\Delta P_{pv}(n)}{\Delta V_{pv}(n)}=\frac{I_{pv}(n)}{V_{pv}(n)}+\frac{\Delta I_{pv}(n)}{\Delta V_{pv}(n)} \tag{1.9}$$

By considering equation (1.9) and the fact that the slope of the P-V characteristic curve is zero at the MPP, decreasing on the right of the MPP and increasing on its left [56], three zones can be identified, each one associated with its related equations, as given in table (1.1).

The main objective of InCond MPPT is to find the optimal PV operating voltage at which the instantaneous conductance ($I_{pv}(n)$ / $V_{pv}(n)$) is equal to the incremental conductance ($\Delta I_{pv}(n)$ / $\Delta V_{pv}(n)$). By achieving this operating condition, it should be maintained till the value of the measured current changes, which indicates a change

in both the irradiance and the MPP position. Therefore, InCond increments or decrements its output ($V_{ref}(n)$) by a fixed step size (ΔV_{ref}) in order to track the new MPP position [57]. The flowchart of InCond MPPT is shown in figure. (1.6).

Table 1. 1: Procedure of InCond method

Left of the MPP	At the MPP	Right of the MPP
$\frac{\Delta P_{pv}(n)}{\Delta V_{pv}(n)} > 0$ **or** $\frac{\Delta I_{pv}(n)}{\Delta V_{pv}(n)} > -\frac{I_{pv}(n)}{V_{pv}(n)}$	$\frac{\Delta P_{pv}(n)}{\Delta V_{pv}(n)} = 0$ **or** $\frac{\Delta I_{pv}(n)}{\Delta V_{pv}(n)} = -\frac{I_{pv}(n)}{V_{pv}(n)}$	$\frac{\Delta P_{pv}(n)}{\Delta V_{pv}(n)} < 0$ **or** $\frac{\Delta I_{pv}(n)}{\Delta V_{pv}(n)} < -\frac{I_{pv}(n)}{V_{pv}(n)}$

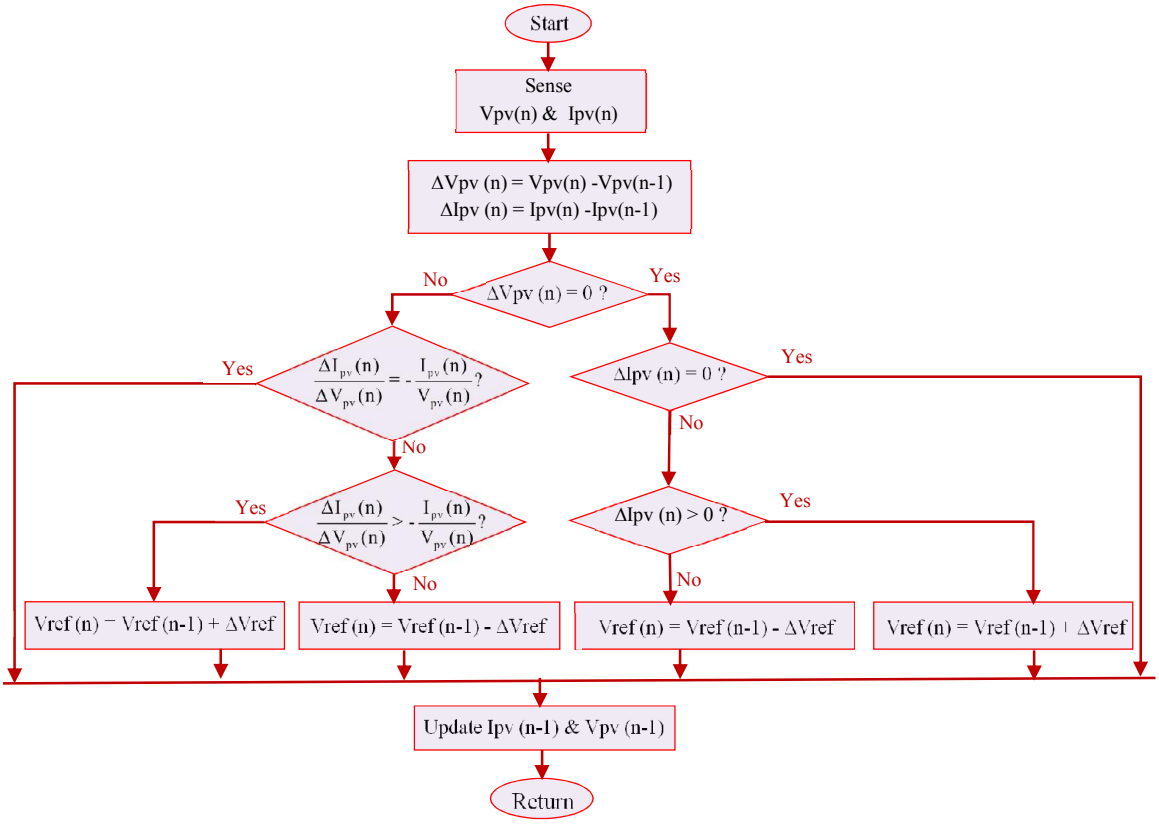

Figure 1. 6: Flowchart of InCond method

In P&O, HC and InCond MPPTs, choosing inappropriate perturbation step size leads to many drawbacks. Thereby, the small perturbation step size affects the convergence time under fast transient variations of irradiance. While the large perturbation leads to high ripples in the output power under steady-state conditions, reducing the power generation efficiency and affecting the stability of the whole PV system.

1.3.2. Improved MPPTs

To deal with the aforementioned problems that may arise from using a fixed perturbation step size, several improved MPPT techniques have been presented in the literature. For instance, various modified versions of HC MPPT have been proposed [50, 58] in order to improve the performance of conventional HC. Many modified versions of P&O have also been developed in [59-65], to adjust the step size of P&O technique, in order to find a tradeoff between fast response and low fluctuations in steady-state conditions. However, few research works have dealt with the drawbacks of conventional InCond MPPT.

1.3.2.1. Improved-InCond MPPT

Improved-InCond MPPT has been proposed in [54], in which the perturbation step size is automatically tuned according to the PV panel characteristics. In this technique, the perturbation step size is chosen to be large in order to accelerate the convergence to the MPP if the PV operating power is far from the MPP position. When it gets closer, the perturbation is smaller, leading to low oscillations around the MPP and hence minimal power losses in the steady-state conditions. The flowchart of improved-InCond MPPT is shown in figure (1.7).

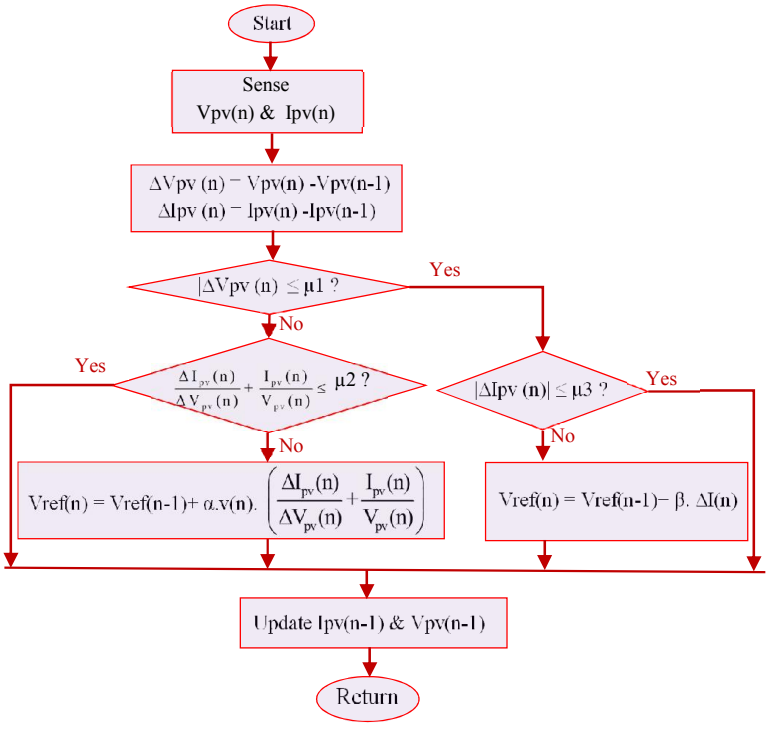

Figure 1. 7: Flowchart of improved-InCond method [54]

As shown in figure (1.7), $\mu 1$, $\mu 2$ and $\mu 3$ are small positive threshold values near zero, α and β represent the acceleration factors. It is worth mentioning that β is a small positive number near zero (e.g., 0.01), whereas the value of α is determined satisfying the following relation

$$\alpha \leq \frac{V_{step\text{-}max}}{\left| \frac{m.Ipv|_{Vref=m.Voc}}{m-1} \right|} \tag{1.10}$$

Where V_{step_max} is the allowable maximum step-size under the fixed step operating condition (e.g., 0.3V), m is a positive number near 1 (e.g., 0.97), V_{oc} is the open circuit voltage of the PV panel at Standard Test Condition (STC: 1000 W/m^2 and 25 °C), and $Ipv|_{verf=mVoc}$ is the value of PV output current when V_{ref} equals $mVoc$.

1.3.2.2. Variable Step Size InCond (VSS-InCond)

VSS-InCond [35] is dedicated to find an effective way to improve the accuracy in tracking the MPP in both dynamic and steady state conditions. The flowchart of VSS-InCond MPPT is shown in figure (1.8).

By employing equation (1.11), the iteration step size duty cycle of the DC-DC converter is automatically tuned.

$$D(n)=D(n-1) \pm dstep \tag{1.11}$$

Note that $D(n)$ and $dstep$ are the duty cycle and its step size, respectively. $dstep$ is defined as follow:

$$dstep = N\left|\frac{\Delta P(n)}{\Delta V(n)}\right| \tag{1.12}$$

Where, N is the scaling factor which is tuned at the design time to adjust the step size. To determine the scaling factor N, firstly, large step size ΔD_{max} should be chosen. Then, by evaluating the performance of the PV system when using ΔD_{max}, the dynamic performance is good enough, while the steady-state performance may not be satisfactory. Hence, it should be improved. To do that, the absolute value of the derivative of PVG output power to voltage ($|dP|/|dV|$) must be evaluated at the fixed step size $\Delta Dmax$, which will be chosen as the upper limiter as the VSS-InCond

MPPT (equation (1.13)). Based on the analysis done in [35], it is known that |dP|/|dV| is almost at its lowest value around the MPP. To ensure an accurate convergence to the MPP, the variable step rule must obey the following:

$$N.\left|\frac{\Delta P(n)}{\Delta V(n)}\right|_{\text{fixed step}=\Delta D_{max}} < \Delta D_{max} \tag{1.13}$$

Where, $\left|\frac{\Delta P(n)}{\Delta V(n)}\right|_{\text{fixed step}=\Delta D_{max}}$ is the derivative of PVG output power to voltage at the fixed step size ΔD_{max}.

The scaling factor N can therefore be chosen as

$$N < \frac{\Delta D_{max}}{\left|\frac{\Delta P(n)}{\Delta V(n)}\right|_{\text{fixed step}=\Delta D_{max}}} \tag{1.14}$$

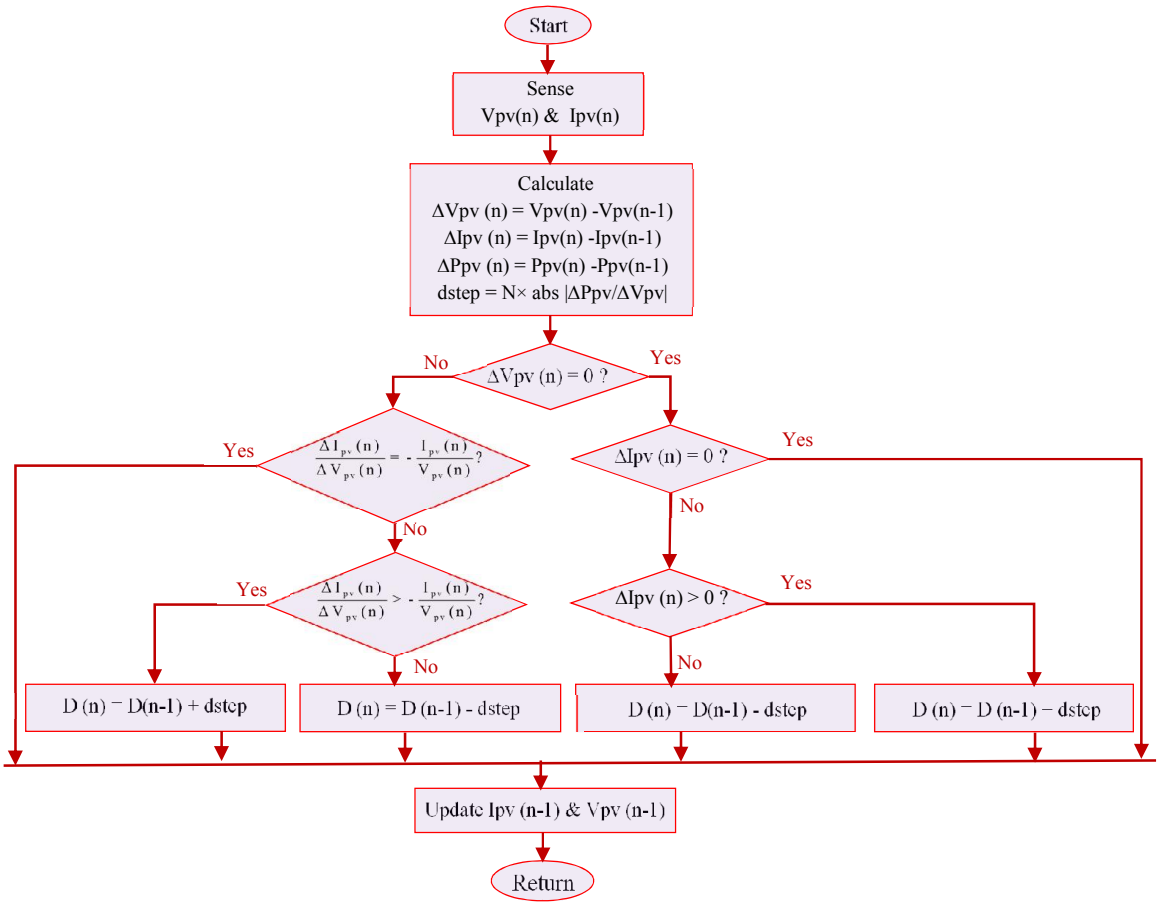

Figure 1. 8: Flowchart of VSS-InCond method [35]

1.3.3. Artificial intelligent MPPTs

The new trend of research works in renewable energy applications is the integration of artificial intelligence techniques to control, harvest energy and improve efficiency of different power generation systems, specially, in the field of PV systems [66].

1.3.3.1. Artificial Neural Networks (ANNs)

ANN is an inter connection of artificial neurons (nodes) that mimic a biological brain [22]. A possible structure of ANN, tailored for MPPT is shown in figure (1.9). It comprises of an input layer, a hidden layer and an output layer. In each layer the number of nodes varies and it is user defined. The link between the ith and jth nodes is the weight wij. Many measured parameters that relate to the employed PVG, like the output voltage and current, environmental data like irradiance and temperature, or any combination, can be used as inputs to ANN MPPT.

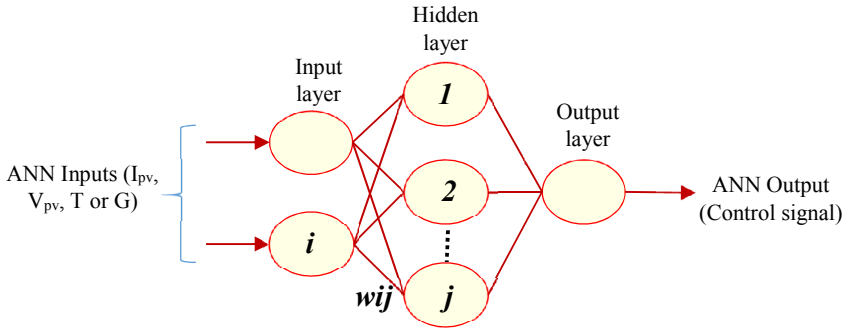

Figure 1. 9: A typical ANN structure for MPPT

Trained neural networks used to find the solution for the nonlinear PVG model, the output control signal (the solution of ANN) can be considered as either the voltage reference, the current reference or the duty cycle [20]. It is worth mentioning that the high performance of an ANN in tracking the MPP depends strongly on the hidden layer and how careful and extensively its networks are trained [22]. Typically, the ANN needs to be trained and tested for months (or even years) to ensure an accurate convergence to the MPP under various environmental conditions (irradiance and temperature).

Among the disadvantages of ANN-based MPPT is that finding reliable data as training set is a challenge, once a particular ANN is designed and trained for a specific PVG and climate conditions, it may not respond accurately by employing it

in different conditions. Moreover, an ANN-based MPPT designed with more hidden nodes can render accurate results, but at the expense of complex modeling, higher memory requirement and more computation time and efforts. Hence, an ANN with high number of nodes may not be able to respond quickly enough to cope with rapidly changing irradiance conditions. In the light of the previous discussion, it can be concluded that ANN is unsuitable for low cost microprocessors.

In certain applications, ANN is adopted to identify the optimized parameters of another MPPT controller rather than used as the MPP tracker itself. For instance, ANN is used as optimizer for conventional MPPTs such as: P&O or InCond [67, 68]. In other ones, ANN has been combined with other soft computing techniques like GA, FLC or DE. In general, these combinations result in an improved performance [69-71].

1.3.3.2. Fuzzy Logic Controller (FLC)

FLC is considered as one of the most popular artificial intelligence techniques applied as a MPPT controller to harvest maximum energy from PVGs. Due to its advantages as it can provide a good performance with imprecise inputs, does not need an accurate mathematical model and is very effective in handling non-linear problems [15]. FLC based MPPT integrates the human experience and knowledge into the control design process by employing fuzzy set theory to convert linguistic values directly into an automatic control strategy. Fuzzification, inference and defuzzification are the main stages of FLC to generate the required control.

The FLC adopted in this chapter to be presented is recently published by Zainuri *et al.* [36], where it is based on the combination of features experienced with P&O and classical FLC and hence the complexity is reduced simultaneously, with the aim of increasing the PV system efficiency. This FLC uses as inputs, the differential power and differential voltage at the n^{th} sampling time, equation (1.15) and (1.16), respectively;

$$\Delta P_{pv}(n) = P_{pv}(n) - P_{pv}(n-1) \tag{1.15}$$

$$\Delta V_{pv}(n) = V_{pv}(n) - V_{pv}(n-1) \tag{1.16}$$

The FLC output equation is

$$\Delta D(n) = D(n) - D(n-1) \tag{1.17}$$

Where $\Delta D(n)$ is the DC–DC converter duty cycle change.

The variable inputs (ΔP and ΔV) and output (ΔD) are divided into five fuzzy subsets (N: Negative, ZE: Zero, Ps: Positive Small, P: Positive, PB: Positive Big). Therefore, 25 fuzzy control rules are used by this FLC. Shapes and fuzzy subset partitions of membership functions used by this FLC are shown in figure (1.10). To operate fuzzy combinations and determine the FLC output, Mamdani fuzzy inference system (with max–min) is used. Fuzzy rules are shown in table (1.2).

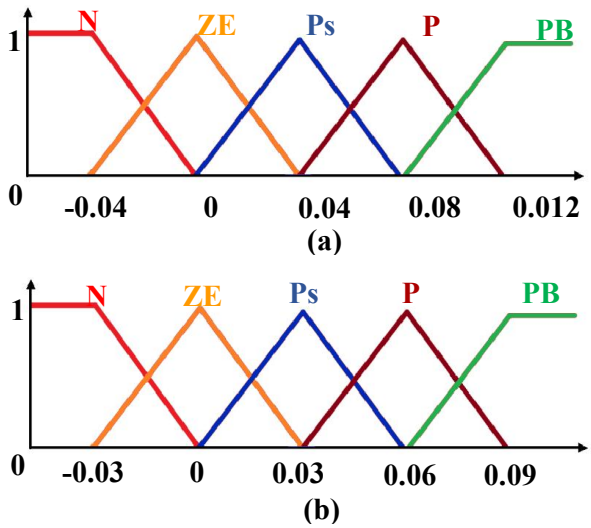

Figure 1. 10: Membership functions: (a) Input of ΔP and ΔV (b) Output of ΔD

Table 1. 2: Fuzzy rules

ΔP \ ΔV	N	ZE	Ps	P	PB
N	ZE	Ps	P	PB	PB
ZE	ZE	ZE	Ps	P	PB
Ps	N	ZE	ZE	Ps	P
P	N	N	ZE	ZE	Ps
PB	N	N	N	ZE	ZE

Many other FLCs have been proposed in the literature. Summary of the FLC related research works for MPPT are shown in table (1.3).

Table 1. 3: Summary of FLC related work for MPPT

Reference	Inputs	Control variable	Number of rules	Power conditioning type	Remarks
Simoes *et al.*[72]	$\Delta P_{pv}(n) = P_{pv}(n) - P_{pv}(n-1)$, $\Delta D(n-1)$	$\Delta D(n)$ (the duty cycle change)	15 fuzzy rules	Boost converter	Test results reveal that the dynamic response of the PV system has been improved. However, poor performance is achieved in steady-state conditions.
Won *et al.*[73]	$E(n) = \frac{P_{pv}(n) - P_{pv}(n-1)}{I_{pv}(n) - I_{pv}(n-1)}$, $\Delta E(n) = E(n) - E(n-1)$	$\Delta D(n)$ (the duty cycle change)	25 fuzzy rules	Boost converter	By testing this FLC, it can be concluded that steady-state oscillations around the MPP and wrong tracking direction under rapidly changing irradiance conditions are its main limitations.
Masoum *et al.*[74]	$E(n) = \frac{P_{pv}(n) - P_{pv}(n-1)}{I_{pv}(n) - I_{pv}(n-1)}$, $\Delta E(n) = E(n) - E(n-1)$ (used to improve the accuracy), D(n-1) (used to improve the dynamic performance)	$\Delta D(n)$ (the duty cycle change)	75 fuzzy rules	Buck converter	This FLC is based on the combination of FLCs presented in [72] and [73]. The shortcoming of this FLC lies in the difficulty of accurately computing its three inputs at the same time, especially under noisy environment conditions. Meanwhile, using 75 fuzzy rules burden the computation and the memory.
Kottas *et al.*[75]	$E(n) = \frac{P_{pv}(n) - P_{pv}(n-1)}{I_{pv}(n) - I_{pv}(n-1)}$, $\Delta E(n) = E(n) - E(n-1)$	$\Delta D(n)$ (the duty cycle change)	25 fuzzy rules	Boost converter	This FLC has been proposed to improve the energy conversion efficiency of PV systems as well as to deal with the dynamic performance of the FLC proposed in [73]. Therefore, *fuzzy cognitive network* (FCN) is proposed and combined with the FLC presented in [73]. FCN should be trained by using data about the PV system voltage, current, irradiance and temperature under a wide range of climatic conditions. According to numerical simulations, it can be concluded that the convergence time is improved as compared to [73]. However, the need for a short circuit current sensor and an additional switch in parallel with the PV system, leading to an increase in the implementation cost.
Wu *et al.*[76]	In **the grid connection mode**, the FLC inputs are the filter inductor current error and its change. Whereas, in **the standalone mode**, the FLC inputs are replaced by the variation of voltage ΔV_{pv} and its variation.	$\Delta D(n)$ (the duty cycle change)	25 fuzzy rules	Inverter	This FLC is designed to control the PV inverter systems in grid-connection and standalone modes. The scaling factors of both input and output are automatically tuned by employing a self-tuning algorithm. Simulation and experimental results demonstrate lower harmonic distortion under various load conditions. Moreover, the control scheme can be employed with various loads and different operation modes.
Larbes *et al.*[77]	$E(k) = \frac{P_{pv}(n) - P_{pv}(n-1)}{I_{pv}(n) - I_{pv}(n-1)}$, $\Delta E(n) = E(n) - E(n-1)$	D(n) (the instantaneous duty cycle)	25 fuzzy rules optimized by GA	Boost converter	Simulation results under different temperature and irradiance conditions show that the optimized FLC outperforms both P&O and classical FLC in terms of response time and accuracy.
Alajmi *et al.*[78]	$\Delta P_{pv}(n) = P_{pv}(n) - P_{pv}(n-1)$, $\Delta I_{pv}(n) = I_{pv}(n) - I_{pv}(n-1)$	$\Delta D(n)$ (the duty cycle change)	16 fuzzy rules	Boost converter	This FLC is designed by translating the search principle of conventional HC into 16 fuzzy rules. It aims to address limitations of conventional HC such as: slow convergence, steady-state oscillations and divergence from the MPP when the irradiance varies quickly. The obtained results show that this FLC offers fast and accurate tracking of the MPP during steady-state and varying weather conditions compared to conventional HC. Another comparison

					is carried out between FLC-based HC and two previous discussed FLCs [72] -[73], The results show limited tracking accuracy of [72] and poor performance of [73] during varying weather conditions. Whereas, FLC-based HC gives fast convergence to the MPP, small oscillations and high accuracy.
Messai *et al.*[79]	$E(n)=\frac{P_{pv}(n)-P_{pv}(n-1)}{I_{pv}(n)-I_{pv}(n-1)}$, $\Delta E(n)=E(n)-E(n-1)$	D(n) (the instantaneous duty cycle)	25 fuzzy rules	Boost converter	This FLC has been designed to well track the MPP under varying climate conditions. Simulation results show that this FLC has the ability to perform well under different conditions of irradiance and temperature. However, both the membership functions and the fuzzy control rules need to be optimized in order to more enhance the performance of PV systems.
Messai *et al.*[80]	$E(n)=\frac{P_{pv}(n)-P_{pv}(n-1)}{I_{pv}(n)-I_{pv}(n-1)}$, $\Delta E(n)=E(n)-E(n-1)$	D(n) (the instantaneous duty cycle)	25 fuzzy rules optimized by GA	Boost converter	An optimization technique based on GA has been applied to tune parameters of the FLC presented in [79], by simultaneously optimizing its membership functions and fuzzy rules. The test results show that the optimized FLC outperforms conventional P&O. Also, the response time in the transitional state is shortened and the fluctuations in the steady state are considerably reduced compared to the original FLC [79].
Al Nabulsi *et al.*[81]	$\left\lvert\frac{\Delta P_{pv}}{\Delta V_{pv}}\right\rvert=\left\lvert\frac{P_{pv}(n)-P_{pv}(n-1)}{V_{pv}(n)-V_{pv}(n-1)}\right\rvert$, The second input is the old perturbation step-size of P&O Vref (n-1).	The output of this FLC is the perturbation step size of P&O (ΔVref)	9 fuzzy rules	Buck converter	In [81], FLC with 9 fuzzy rules has been incorporated with conventional P&O in order to eliminate power oscillations at steady-state conditions. The output of this FLC is the perturbation step size of P&O (ΔVref) which is used to adaptively change the voltage perturbation (Vref) and subsequently controlling a buck converter. According to simulation results, the oscillating behavior is not completely eliminated by this MPPT technique. Moreover, a PI controller is required to generate the instantaneous duty cycle for the power converter, which leads to more complexity as well as an additional difficulty arising from the tuning of PI gains (Kp and Ki).
Rajesh *et al.*[82]	$\Delta P_{pv}(n)=P_{pv}(n)-P_{pv}(n-1)$, $\Delta V_{pv}(n)=V_{pv}(n)-V_{pv}(n-1)$, $\Delta D(n-1)$.	The reference current (I_{ref})	Unknown	Boost converter	This FLC intended to harvest maximum power from PV systems. According to experimental results, it can be noticed that low oscillations and fast convergence as compared with P&O MPPT, are the main advantages of this FLC.
Chao *et al.*[83]	$\Delta P_{pv}(n)=P_{pv}(n)-P_{pv}(n-1)$, $\Delta V_{pv}(n)=V_{pv}(n)-V_{pv}(n-1)$	ΔD(n) (the duty cycle change)	25 fuzzy rules	Two-stage DC–DC converter	Experimental tests show that this FLC can reach the MPP with slower convergence. The efficiency achieved by this FLC (ranged from 90% to 96%) is much lower compared to that achieved in [82] (around 99%).
El Khateb *et al.*[84]	$\Delta V_{pv}(n)=V_{pv}(n)-V_{pv}(n-1)$, $\Delta(\Delta V_{pv}(n))$.	D(n) (the instantaneous duty cycle)	50 fuzzy rules	SEPIC converter	This MPPT is based on two FLCs operating simultaneously with a Single-Ended-Primary-Inductor-Converter (SEPIC). Each FLC has two inputs and one output. Five fuzzy sets are proposed for each input in addition to nine for the output, which result in 50 fuzzy rules. The FLC based SEPIC converter exhibits a good performance. However, it has a high complexity level as well as sophisticated

					hardware equipment required for MPPT's real-time processing.
Guenounou *et al.*[85]	$E(n)=\frac{P_{pv}(n)-P_{pv}(n-1)}{I_{pv}(n)-I_{pv}(n-1)}$, $\Delta E(n)=E(n)-E(n-1)$	$\Delta D(n)$ (the duty cycle change)	25 fuzzy rules	Boost converter	This FLC has been used for online adjusting the controller's gain and subsequently the duty cycle of a boost DC–DC converter. Results indicate that this FLC outperforms conventional FLC.
Zainuri *et al.*[36]	$\Delta P_{pv}(n)=P_{pv}(n)-P_{pv}(n-1)$, $\Delta V_{pv}(n)=V_{pv}(n)-V_{pv}(n-1)$	D(n) (the instantaneous duty cycle)	25 fuzzy rules	Boost converter	Experimental results demonstrates that this FLC has low oscillations and fast convergence as compared to conventional P&O. The tracking efficiency obtained is around 99 .8%.
Chen et al.[86]	The judgement equation and auto-scaling step functions are employed as inputs of the proposed FLC	$\Delta D(n)$ (the duty cycle change)	77 fuzzy rules	Boost converter	In this work, the authors combined FLC with Auto-Scaling Variable Step-Size (ASVSS) MPPT method in order to improve the PV system performance and get a tradeoff between better steady-state performance and fast transient response. According to numerical simulations, high performance is achieved during variable irradiance conditions. However, the high number of fuzzy rules (77 fuzzy rules) would significantly contribute to increasing the controller complexity.

1.4. Global MPPTs (GMPPTs)

A PVG, which can be a module, a string or an array, when receiving a uniform irradiance, the resulting P-V characteristic curve exhibits a single MPP. However, the case in which different parts of a PVG receive different amounts of irradiance (PSCs), the P-V curve will be characterized by multiple peaks, i.e., one of them is the GMPP and the remaining peaks are LMMPs. It is very likely that conventional MPPTs will be trapped on LMPP, resulting in reduced output power and thus greatly deteriorates the efficiency of PV systems.

Unlike LMPPT techniques which may fail to converge to the GMPP when the PV module undergoes PS. GMPPT techniques are able to track the global peak as they have a mechanism to distinguish between local and global maxima. In the literature, many GMPPT techniques are proposed and implemented. These techniques can fall within two mean groups, Soft Computing (SC) and hybrid MPPT methods.

1.4.1. Soft Computing method

Soft computing (SC) techniques have gained attention from researchers to be employed in the study of MPPT for PV systems, especially under PSCs because they are equipped with exploration capability. Under UICs, the PV characteristic curve is considered by SC techniques as a unimodal optimization problem with a single optimum, whereas for PSCs, it is considered as a multimodal optimization

problem with multiple local optima. Therefore, finding the global maximum on the PV characteristic curve of PVGs is the main objective of SC techniques as MPPT. Due to their flexibility and ability to handle non-linear problems, robust SC-based MPPT schemes can be developed to improve the PV system performance. To date, there are several works on MPPT using SC, Some of the important research works on SC based MPPT are summarized in table (1.4).

Table 1. 4: Summary of SC related work for MPPT

Reference	Year	The employed method	Remarks
Ishaque *et al.*[87]	2012	Particle Swarm Optimization (PSO)	PSO takes inspiration from flocking behavior of birds and fishes. In this work, it has been used as a direct duty cycle control MPPT in order to eliminate the PI control loop. Its performance has been tested by employing 10 h (daytime) irradiance and temperature profile of a tropical country (Malaysia). Simulation results reveal that PSO based MPPT can achieve an average efficiency up to 99.5%. However, its main drawback is the difficulty of setting the four initial parameters including the initial number of particles, the inertia, population size and learning factors. To this, trial-error approach is the only way to tune these random parameters
Ishaque *et al.*[88]	2012	PSO	In this work, an efficient method is proposed to reinitialize the particles to search for the new MPP in order to improve the dynamic response of PSO. The developed algorithm was evaluated by implementing it along with a buck-boost converter while being compared to conventional PSO and HC methods. It is worth mentioning that the method has a simple structure of MPPT in comparison to conventional PSO since it needs only one parameter (the inertia weight) to be tuned. According to simulation and experimental results, this MPPT demonstrates superiority over conventional HC in terms of tracking speed and steady state oscillations.
Chao *et al.*[89]	2015	PSO	The authors proposed an improved PSO version to predict the GMPP of PVGs under PSCs. The improved PSO has better tracking speed, accuracy and response as compared to the conventional PSO.
Babu *et al.* [90]	2015	PSO	Conventional PSO has been modified wherein random initialisation is replaced by deterministic initialisation. Under UICs and for ten different PS patterns, the modified PSO outperforms conventional PSO, IC and HC in terms of tracking efficiency.
Jubaer *et al.* [91]	2014	Cuckoo Search (CS)	CS optimization takes inspiration from brood parasitic behavior of some cuckoo species that lay their eggs in nests of other birds. CS optimization is similar with PSO. However, its selection procedure is different. Lévy flight makes the randomization much more efficient, which provide faster convergence to the optimal solution. CS has been applied to control PV systems and improve their transient performance. Unlike conventional PSO that needs four parameters to be tuned, CS based MPPT needs only two parameters. According to comparison results presented in [91], CS based MPPT overcomes PSO and P&O in terms of convergence time. However, this MPPT has not been experimentally tested.
Lian *et al.*[92]	2013	Ant Colony Optimization (ACO)	ACO is a metaheuristic inspired from the behavior of ants seeking a path between their colony and a source of food. ACO also has been applied as MPPT for PV systems under PSCs. The feasibility of this optimization technique as MPPT was verified under different shading scenarios. Simulation results show that the algorithm can track the GMPP efficiently and its robustness to various shading patterns was observed.

Sundareswaran *et al.*[38]	2015	Artificial Bee Colony (ABC)	ABC algorithm is inspired from food foraging behavior of bees wherein the bees are categorized into three groups. The first group contains the employed bees, where it represents the half of the colony. The bees of this group are used to sweep the Power–Duty cycle (P–D) characteristic curve. The second group contains the other half of the colony. It gathers the onlooker bees that employed to move subsequently for improved positions. Finally, when the search process stagnates, the employed bees will become a scout bees (i.e., represents the third group), that will be used in seeking a new position. The PV output energy has been enhanced under PSCs through employing ABC based MPPT.
AbouSoufyane *et al*. [93]	2015	ABC	AbouSoufyane *et al*.[93] used ABC to track the GMPP of PVGs under PSCs. Then, the ABC based MPPT has been compared to PSO. Comparison results reveal that ABC outperforms PSO in terms of the number of successful convergence and the accuracy in tracking the GMPP. However, the ABC convergence time is longer than PSO.
Lyden *et al.* [39]	2016	Simulated Annealing (SA)	SA is inspired from the physical process of annealing in metals to find an optimal solution. Based on the seven experimental tests performed, only in five out of the seven tests, the SA MPPT could converge to the appropriate GMPP. However, in the two remaining tests, it converged to LMPP. Therefore, this MPPT may not always guarantee convergence to the GMPP, which leads to significant power losses. The last disadvantage is explained by the fact that this MPPT oscillates a lot before settling down to the GMPP.
Shaiek *et al.*[94]	2013	Genetic Algorithm (GA)	GA is inspired from natural evolution, mutation, crossover and selection. Shaiek *et al.*[94], carried out an assessment of GA and two conventional MPPTs. They concluded that InCond and P&O fail to achieve MPP of the PVG if it is Partially shaded. To solve this problem, GA algorithm was employed and it successfully enabled the system to reach the GMPP.
Daraban *et al.*[95]	2014	GA	In [95], GA has been modified to behave like conventional P&O by selecting individuals of three chromosomes: voltage, search direction and step size. New individuals are obtained by performing crossover and mutation which integrate the principle of P&O. This results in fast convergence to the GMPP.

1.4.2. Hybrid MPPT methods

Hybrid MPPTs can be defined as a combination of conventional MPPTs with SC based MPPTs or other mechanisms to escape LMPPs and hence properly identified the GMPP. The major aim of hybrid MPPTs is to accurately track the appropriate MPP for PV systems, regardless of irradiance variations, characteristics of the PVG and PSCs. Some of the important research works on hybrid MPPTs are summarized in table (1.5).

Table 1. 5: Summary of hybrid MPPTs.

Reference	Year	The employed methods	Remarks
Rizzo *et al.*[96]	2015	ANN + conventional InCond	In this MPPT, an ANN has been hybridized with InCond to track the GMPP of the PV system. The ANN is used to automatically predict the GMPP of the PVG. According to numerical simulations, it can be observed that ANN-based-MPPT provides a good robustness to parameter variations of PV system. However, high robustness requires a huge database which burdens the computation and the memory.

Sundareswaran *et al.*[97]	2015	GA+ conventional P&O	This MPPT aims to accelerate convergence and decrease the inherent oscillations due to the evaluation of chromosomes. The GA uses a population of 6 chromosomes (duty cycles) and applies the genetic operations on 4 of them only while the remaining two chromosomes are selected by elitism during each iteration. Three iterations are conducted and the best offspring (duty cycle) will be used as a starting point by the P&O which uses a variable step to accelerate convergence. Two patterns of shading have been tested and good results have been obtained. However, the number of iteration that is three (3) cannot guarantee the convergence to the near GMPP.
Sundareswaran *et al.*[41]	2016	ACO + conventional P&O	The authors proposed a hybrid MPPT that combines the features of ACO technique and convention P&O method in order to accurately converge to the GMPP. In the initial stage of tracking process, the foraging ants in the ACO method look for the GMPP by performing a finite number of ant movements. After that, the best solution achieved by ACO method is adopted as the starting point of the P&O.
Lian *et al.*[40]	2014	PSO + conventional P&O	Authors combine conventional P&O and PSO technique. At first, conventional P&O is employed to move the operating point into the first power peak, which reduces the search space of PSO. After that, and starting from that power peak, PSO technique is employed to search for the GMPP. The main contribution of this hybrid MPPT is that the PSO search space has been reduced. As a result, the time required for convergence to the GMPP is reduced.
Shi *et al.*[98]	2015	PSO+ conventional InCond	In this hybrid MPPT, PSO has been combined with InCond. First, PSO is used to look for the best power peak (exploration phase), then InCond is used to track it (exploitation phase). The simulation results show satisfactory performance in dynamic as well as steady state operation.
Manickam *et al.*[99]	2016	PSO + conventional P&O	PSO and P&O have been hybridized, where P&O is used to track the MPP under UICs as well as to detect the occurrence of PS. PSO is employed only on the onset of PSCs. Notably that the search space of PSO has been reduced by using a window-based search.
Alajmi *et al.*[37]	2013	scanning, storing, perturbing and observing procedures + FLC	The proposed fuzzy MPPT is based on scanning, storing, perturbing and observing procedures to locate the GMPP during PSCs. Then, a modified FLC to track the GMPP is applied. The proposed FLC uses 32 fuzzy rules based on the reference power and HC principle to track the identified GMPP. The method tracks the GMPP with low oscillations, but processing 32 fuzzy rules requires a long running time.
Punitha *et al.*[100]	2013	Modified inCond + FLC	This MPPT is based on an integrated model of a modified InCond with an adaptive FLC. The modified InCond is used for GMPP tracking under varying atmospheric and PSCs. In conjunction with this, an adaptive FLC is used to provide duty cycle calculation for the DC-DC converter and replace conventional PWM generator. Less fluctuations in steady state operation are achieved by this MPPT. However, it presents a high complexity level because of the consideration of two FLC systems and the input adaptation function.
Farhat *et al.*[14]	2016	Sliding Mode Controller (SMC)	This MPPT aims to maximize power extraction from standalone PV systems. In this MPPT technique, the voltage reference estimator has been used to estimate V_{ref} (i.e., $V_{ref} = V_{MPP}$, where V_{MPP} is the voltage at the MPP). Whereas, the SMC regulator has been employed to perform the system tracking by generating the appropriate PWM signal to control a boost DC-DC converter. Simulation results revealed that SMC-based-MPPT outperforms conventional P&O in terms of accuracy. However, the technique has not been tested experimentally under PSCs.
Ji *et al.* [101]	2011	Linear function + variable step size InCond	This MPPT uses a linear function based on the values of V_{oc} and I_{sc} of the PVG to detect the apparition of PSCs and change the voltage reference near the GMPP. Then, a variable step size InCond is applied to reach the GMPP. One can easily show that this technique is unable to track the GMPP in all shading patterns. Moreover, V_{oc} and I_{sc} should to be reset when changing other types of PV module.

1.5. Conclusion

The existing MPPT methods, can be grouped into LMPPTs and GMPPTs. It can be concluded that the extraction of MPP is not possible without using a MPPT controller. The PV system efficiency depends on how effectively the MPP is tracked, especially under PSCs. LMPPTs such as: conventional MPPTs, improved MPPTs and artificial intelligent MPPTs can fail to extract the GMPP under PSCs. Many researchers have addressed the problem of PS by developing GMPPT techniques such as: soft computing based MPPTs and hybrid MPPTs. However, the major drawbacks of the aforementioned GMPPTs are the high complexity of the control scheme and the excessive amount of calculation in order to identify and track the GMPP. Sometimes they fail to achieve the GMPP, especially under complicated shading patterns and fast moving clouds. Therefore, the aforementioned limitations remain to be addressed, which will be considered in next chapters (chapter 3, 4 and 5). The following chapter present essential studies related to PV generators.

CHAPTER 2
PV GENERATOR STUDIES - MODELING, SIMULATION, AND EXPERIMENTAL VALIDATION

2.1. Overview

Different valuable studies concerning PV device technologies and modeling under UICs and PSCs are presented. Starting by introducing the PVG structure, then the most commonly used PVG analytical model. Simscape approach for modelling PVGs is given along with simulation and experimental evaluation. To keep up with the latest developments in PV technologies, some recent progress in PV device technologies (such as: Crystalline Silicon and thin film based technologies), focusing on the fabrication cost, the conversion efficiency and the ability to the large scale deployment is also presented. Subsequently, Poly-Crystalline Silicon (Poly C-Si), Copper Indium Gallium Selenide (CIGS) and Cadmium Telluride (CdTe) based PV modules are investigated under different real working conditions of solar irradiance and temperature. Fill factor and efficiency are used as assessment parameters and comparison performed in order to eventually determine which technology fits well the given weather conditions. The last section of the chapter presents a contribution in improving the effectiveness of Simscape based model for predicting the I-V and P-V characteristics. The originality of this PV model consists in the usage of a simple procedure that is based on the module's datasheet in order to identify the series resistance of solar cells. Moreover, the ideality factor values are adapted to fit the above mentioned technologies. A test facility is employed to carry out the required tests for assessing the improved Simscape based model. Obtained experimental results under different climate conditions are compared with simulated ones. The comparison is carried out by evaluating four statistical errors with a view to measuring the accuracy of the improved Simscape based model in predicting the I-V and P-V characteristics.

2.2. PV Generator (PVG)

2.2.1. PVG structure

2.2.1.1. PV cell, module, string and array

A PVG is used to produce and generate an electric energy from the sunlight (solar irradiance, insolation). Typically, a PVG consists of PV cells (solar cells). Commercially PV devices are available as sets of series and/or parallel-connected PV cells combined into one item, which is commonly known as a PV module. The series connection of several PV modules constitutes a PV string. It's worth mentioning that the number of series-connected-PV-modules in a single PV string is related to the voltage required at the output. Finally, a PV array is formed by two or more parallel connected PV strings, with the purpose of generating a required power [102]. Figure (2.1) illustrates the PVG structure.

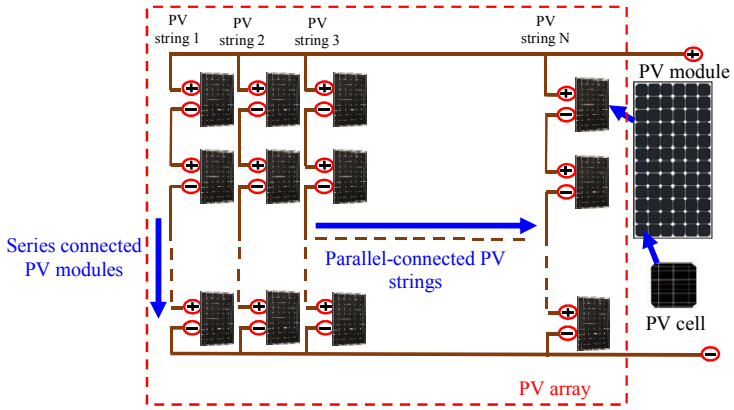

Figure 2. 1: PVG structure.

2.2.1.2. Bypass diodes

In a PVG, if some series-connected PV cells are shaded, they produce less power than the other fully illuminated series-connected cells (the differences in the produced power causes differences in the produced current). Once the high current that has been generated by the unshaded PV cells passes through the shaded ones (cells having low current generation), the voltage of these latter cells becomes negative, which makes them reverse biased and behave as a load. In this case, the shaded PV cells consume power instead of producing. Therefore, the consumed power causes an enormous heat up known as the hotspot phenomenon [103]. It is worth mentioning that the latter phenomenon can damage the shaded PV cells, or even distort the glass plate of the PV module (figure (2.2-a)). To protect the shaded cells from thermal distraction, each PV module should be equipped with one or

multiple antiparallel-diodes that known as bypass diodes [104] (figure (2.2-b)). As a result, the current generated by the unshaded PV cells is conducted across bypass diodes, which counteracts the shading effect and avoid deteriorations of the PV installation.

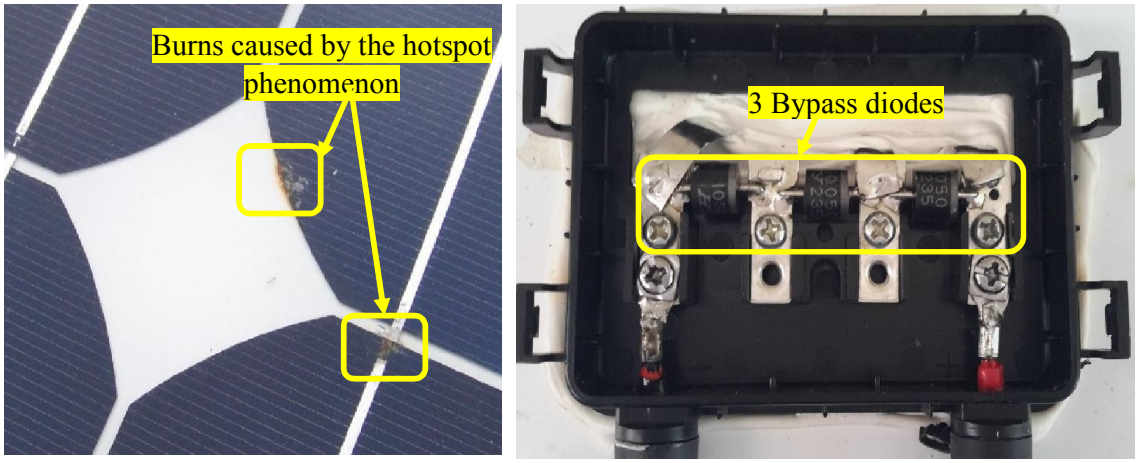

(a) (b)

Figure 2. 2: (a) Burns in a PV module due to hotspots (b) Bypass diodes insertion.

2.2.2. PVG model

This sub-section is devoted to PVG modelling which is a matrix of elementary cells that are the heart of PV systems. The modelling of PVG starts from the model of the elementary PV cell that is derived from that of the P-N junction. It is worth mentioning that the PV cell rated power has a great dependence on the cell-surface area and the technology of PV cells [37]. Figure (2.3) shows the model of the ideal PV cell that can be represented by a current source in parallel with a single diode, resulting in a non-linear I-V characteristic [105], and a real PV cell includes series and parallel resistances.

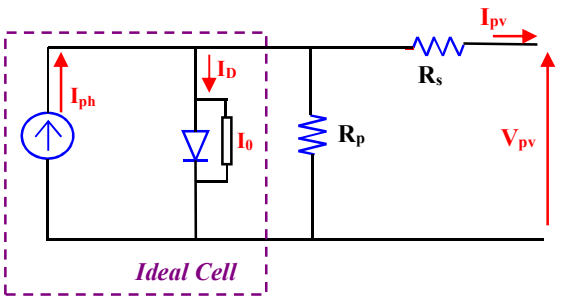

Figure 2. 3: Equivalent circuit of an ideal and real PV cell.

The analytical model describing the output current of a PVG that consists of series-and-parallel-connected PV cells is giving by [106]:

$$I_{pv} = n_p \left(I_{ph} - I_0 \left(\exp\left(\frac{q(V_{pv} + R_s I_{pv})}{A k T n_s} \right) - 1 \right) - \frac{(V_{pv} + R_s I_{pv})}{n_s R_p} \right) \quad (2.1)$$

Where V_{pv} and I_{pv} represent the PVG output voltage and current, respectively. R_s is the series resistance of a single PV cell, which has usually a small value representing the contact resistance. However, the parallel resistance R_p possesses a very large resistance that models the leakage current of the P-N junction. n_s and n_p are respectively the number of PV cells connected in series and in parallel. q is the charge of an electron (1.602×10^{-19} C) . I_{ph} is the light current that is proportional to the irradiance intensity. I_0 is the saturation current, A is the diode ideality factor, k is the Boltzmann's constant (1.38×10^{-23} J/K) and T is the cell temperature (in Kelvins).

The model presented in equation (2.1) is commonly used to simulate the PVG output characteristics (i.e., I-V and P-V curves). However, it suffers from the following limitations;

1- It can be used only when the irradiance over the PVG is uniform. However, the model cannot be reliable by considering the non-uniformity of irradiance.
2- It is utterly useless when the PVG has a complicated interconnection between PV cells or modules.
3- Finally, the model does not take into account the bypass diodes behaviour.

This leads to the need of a new model to simulate the PVG behavior as well as to cope with the above stated limitations. The next section introduces our novel PV modeling approach [15, 107] to model and simulate the PVG characteristics under UICs as well as PSCs. This approach takes into consideration the bypass diodes incorporation, besides, it can be used to model and simulate any configuration of PV cells, modules, strings and bypass diodes; for any shading pattern.

2.3. PVG Modeling under UICs and PSCs

2.3.1. Matlab-Simulink/Simscape presentation

Matlab® (MATrix LABoratory) is a high-level language and interactive programming environment created in 1984 by Mathworks, for mathematical computation, algorithm development, analysis and visualization [108]. Matlab can be used either by Matlab-Code or Matlab-Simulink.

Simulink is a block diagram environment integrated with Matlab, where it provides a graphical modeling blocks [109]. Simulink contains several tool blocks such as: Simscape, Stateflow, Aerospace blockset, etc.

Simscape is conceived to model and simulate a multi-domain physical systems, this is by using its components which cover more than 10 physical domains, comprising electric, mechanic and hydraulic, etc. For instance, semiconductors, sensors and sources are among the components included in the electrical domain, which are intended to be used for modelling of electric, electronic and mechatronic systems. Simscape employs a physical connections that aim to transmit power between different components and blocks [110].

Simscape offers the following advantages [110]:

- It enables user to rapidly establish and design models of physical or control systems by assembling the required fundamental components.
- It offers the possibility of modifying the initial design of the modeled system with ease and without deriving and implementing the system-level equations. This can be done either by modifying physical connections between components within the global block diagram, or by changing the initial setting parameters of components.
- It provides more analysis-capabilities and test-performance for complicated control systems.

2.3.2. Modeling of PVG using Simscape approach

A PVG model based on Matlab-Simscape toolbox for obtaining I-V and P-V characteristics is developed. The modeling tools consist of physical-component-blocks (such as: solar cell block, bypass diode block, etc) and physical-networks.

In Simscape environment, Solar cells and bypass diodes can be seamlessly used to model PVGs with any electrical characteristics. Moreover, Simscape physical networks are employed to connect together any configuration of PV parts (e.g., Solar cells and bypass diodes, etc) as well as to transmit power between them.

The output current of solar cell block is given by

$$I_{pv} = I_{ph} - I_0\left(\exp\left(\frac{q(V_{pv} + R_s I_{pv})}{AKT}\right) - 1\right) - \frac{(V_{pv} + R_s I_{pv})}{R_p} \tag{2.2}$$

So, to characterize a solar cell block, the open circuit voltage (V_{oc}), the short circuit current (I_{sc}) (i.e., both V_{oc} and I_{sc} are obtained from the datasheet), the ideality factor (i.e., the ideality factor is ranged from $1< A< 2$ [111]) and the series resistance (R_s) are the main electrical parameters required. While irradiance and temperature levels are the solar-cell-block input parameters pertaining to climatic conditions. The value of R_s can be tuned by trial-error method.

Figure (2.4) shows Simscape implementation of PV module "LORENTZ 75W" connected to a system for sweeping-acquiring I-V and P-V characteristics. According to ''PV module-Subsystem'' illustrated in figure (2.4), it can be seen that the PV module "LORENTZ 75W" with 32 PV cells and 4 bypass diodes is modelled by Simscape components. Its electrical features are reported in table (A.1-Appendix A). The outputs of the PV module "LORENTZ 75W'' are the positive and the negative terminals. So as to sweep the I-V and P-V characteristics, a variable resistor and ramp block are used. The current and voltage sensors are employed to measure I_{pv} and V_{pv}, respectively. The measured I_{pv} and V_{pv} are acquired and saved by the Measure-subsystem.

It is worth mentioning that any system modeled by Simscape requires exactly one Solver-Configuration-block to be connected to it. The latter block aims to determine the unknown variables for the entire modeled system; it can be connected anywhere on the physical network circuit by creating a branching point. It is imperative to fine-tune the solver parameters before running the simulation in order to avoid warning or error message. The developed Simscape-based model shown in figure (2.4) has been run by selecting the following solver parameters: the step-type is fixed step, the solver-type is Runge-Kutta and fixed step size is 0.001.

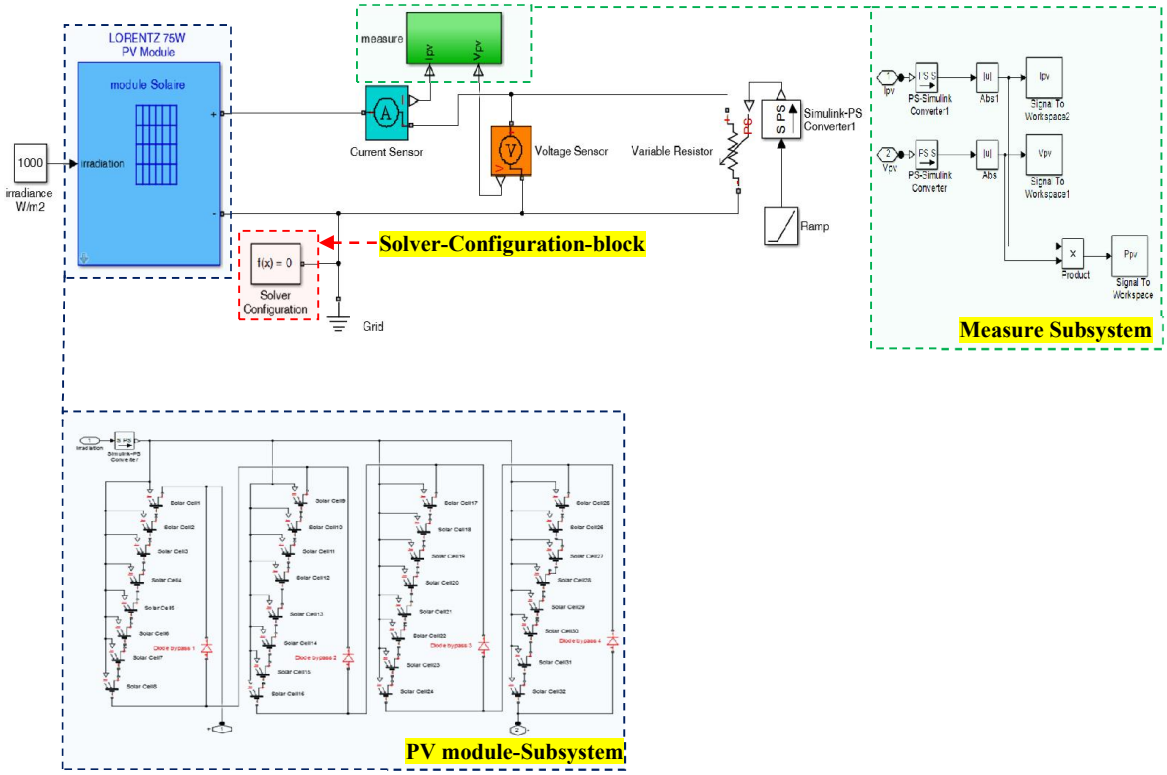

Figure 2. 4: Simscape implementation of PV module "LORENTZ 75W" (contains 4 bypass diodes) connected to system for sweeping-acquiring I-V and P-V characteristics

2.3.3. Influence of solar irradiance and temperature on the PV module

The Simscape-based model of "LORENTZ 75W" PV module is used to simulate the influence of temperature and irradiance on the I-V and P-V characteristics.

First, a constant temperature of 25 °C and different irradiance levels (i.e., ranged from 200W/m^2 to 1000W/m^2 with step of 100W/m^2) are applied on the PV module. In figure (2.5), it can be observed that the increase in the irradiance level gives rise to an increase in the PV output current and power.

Second, the influence of temperature is presented in figure (2.6-a) and (2.6-b). Where the irradiance is fixed at (1000 W/m^2) and different temperature levels (i.e., ranged from -25°C to 75°C with step of 25°C) are applied on the PV module. Therefore, it can be noted that a lower temperature level gives a larger open circuit voltage and a higher output power (i.e., high MPP) and vice versa.

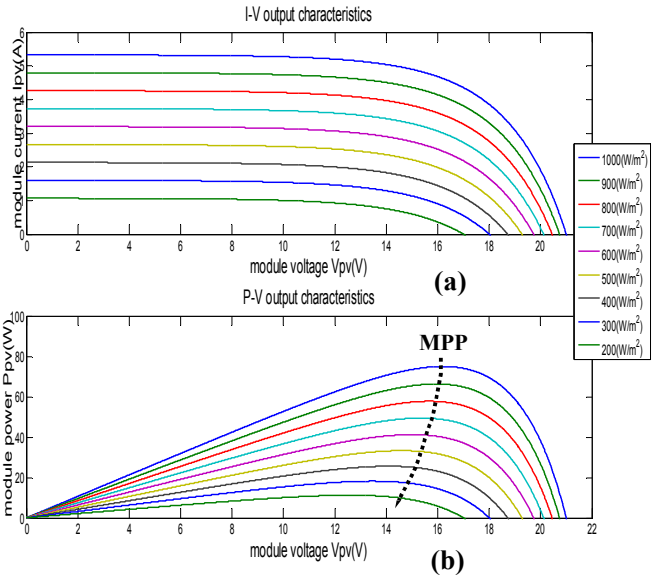

Figure 2. 5: Influence of irradiance on I-V and P-V characteristics.

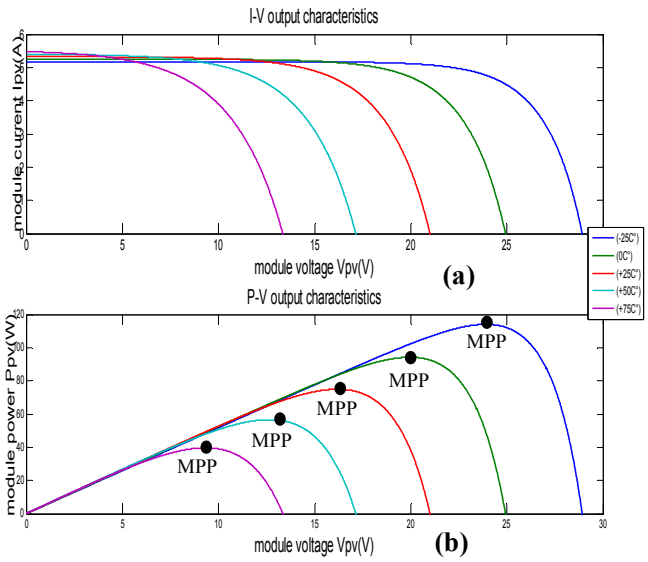

Figure 2. 6: Influence of temperature on I-V and P-V characteristics

2.3.4. Experimental validation of Simscape-based-model under PSCs

For the purpose of testing the effectiveness of the developed Simscape-based model in predicting the I-V and P-V characteristics. Three PV modules have different electrical-characteristics, configurations of PV cells and number of bypass diodes (i.e., the electrical characteristics are reported in table (A.1-Appendix A)) are modelled and experimentally tested. Moreover, to show the flexibility of the Simscape approach in modelling any case of shading pattern, firstly, the shading is applied to three series connected PV modules, secondly, it is applied to three parallel connected PV modules. Finally, the shading is applied at the cells level.

As reported in table (2.1), the first two cases of shading pattern (A and B) are applied to three series connected PV modules type "BP Solar MSX 120W" (as shown in figure (2.7-a)). Where the measured data that has been used for the purpose of assessing the Simscape based model are obtained from Renewable Energy Laboratory located at Jijel University. The third and the fourth cases (C and D) are carried out on three parallel connected PV modules type "LORENTZ 75W" (as shown in figure (2.7-b)), while the last two cases (E and F) are applied to a single PV module type "Sanyo HIT 200W". The experimental data of the PV modules LORENTZ 75W and Sanyo HIT 200W are obtained from refs [112, 113], respectively.

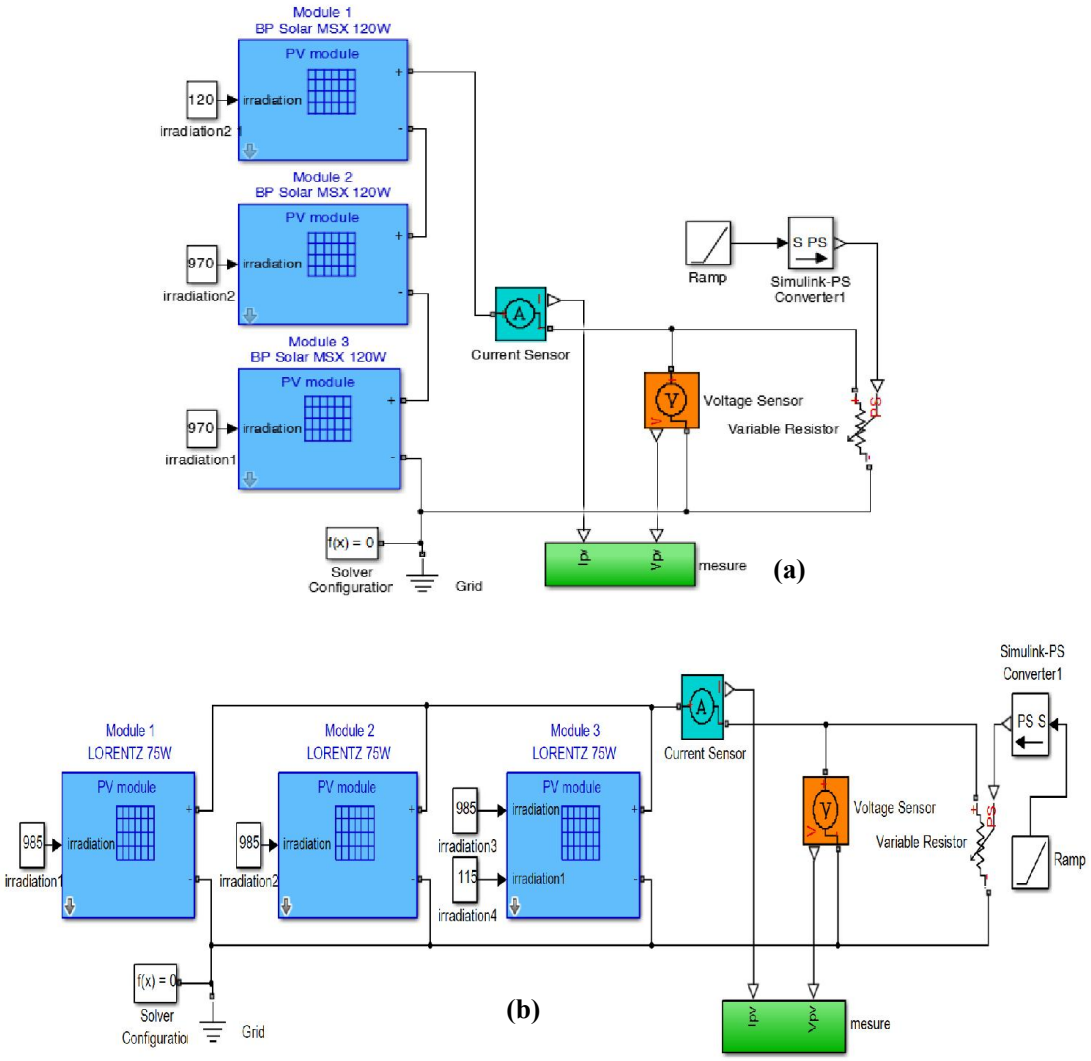

Figure 2. 7: Simscape implementation of (a) three series connected PV modules type “BP Solar MSX 120W” (b) three parallel connected PV modules type “LORENTZ 75W”

As shown in figures (2.5) and (2.6), when the PVG operates under UICs, its P-V characteristic curve exhibits a single MPP. However, if some parts of the PVG are shaded, two or more power peaks result in the P-V characteristic curve (as shown in figure (2.8)).

Figure (2.8) shows the simulated versus the experimental results of case (A), (B), (C), (D), (E) and (F). A good agreement is observed between the simulated and the measured P-V characteristics for the six shading-pattern cases. It is worth underlining that multiple power peaks resulting in P-V characteristic curves of figure (2.8) are caused by both the non-uniform irradiance and bypass-diodes integration.

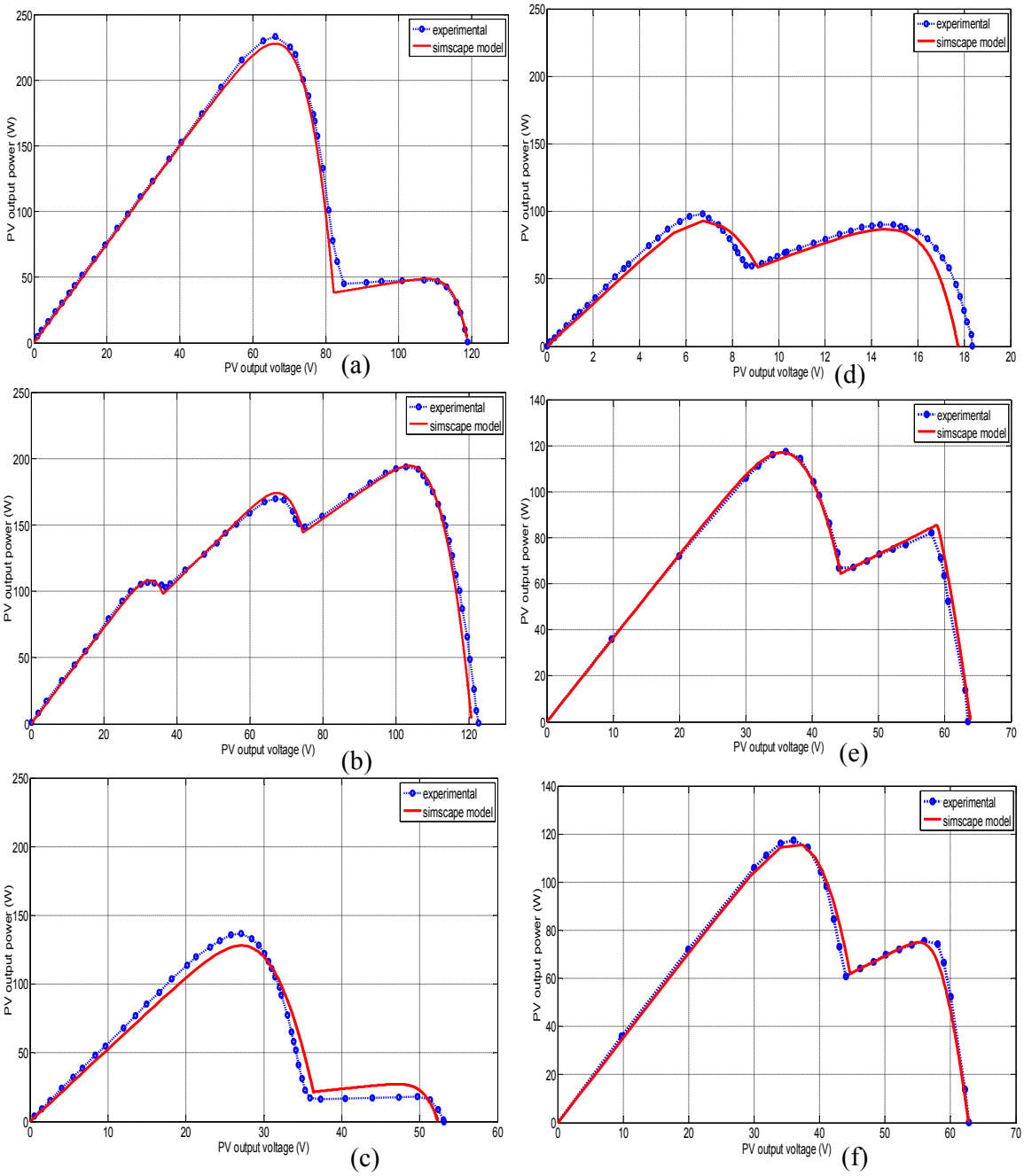

Figure 2. 8: (a) and (b) P-V characteristic of the cases A and B, (c) and (d) P-V characteristic of the cases C and D, (e) and (f) P-V characteristic of the cases E and F.

To assess the performance of the Simscape-based PV model in predicting the I-V and P-V characteristics, the Root Mean Squared Error (RMSE) and the correlation coefficient (R^2) are evaluated.

$$\mathrm{RMSE}[\mathrm{W}] = \sqrt{\frac{1}{N}\sum_{n=1}^{N}\left(P_{pv\_mea}(n) - P_{pv\_sim}(n)\right)^2} \qquad (2.3)$$

$$R^2[\%] = \left[1 - \frac{\sum_{n=1}^{N}\left(P_{pv\_mea}(n) - P_{pv\_sim}(n)\right)^2}{\sum_{n=1}^{N}\left(P_{pv\_mea}(n)\right)^2}\right].100 \quad (2.4)$$

Where $P_{pv\_mea}(n)$ [W] is the *nth* measured value of the PV output power, $P_{pv\_sim}(n)$ [W] is the *nth* simulated value of the PV output power, and N [ ] is the number of modelled or measured points.

Table 2. 1: Comparisons between simulated and measured P-V curves for different cases

	BP Solar MSX 120W		LORENTZ 75W		Sanyo HIT 200W	
Case	(A)	(B)	(C)	(D)	(E)	(F)
Shading patterns [W/m^2]	Module #1=120 Module #2=970 Module #3=970	Module #1=500 Module #2=940 Module #3=700	Module #1=975 Module #2=110 (50%) Module #3=110 (50%)	Module #1=985 Module #2=985 Module #3=115 (50%)	1 cell= 380 95 cells =950	24 cells= 362 72 cells=920
Temperature [°C]	27.5	30	48	48	51.5	52
RMSE [W]	2.80	2.43	4.01	6.11	3.94	2.06
R^2 [%]	99.95	99.97	99.49	99.56	99.84	99.91

With reference to the reported results in table (2.1), the RMSE values are relatively low (ranged between 2.06 W and 6.11 W) and the correlation coefficients are greater than 99% for all cases. These results indicate that the proposed Simscape-based PV model offers a good performance in predicting PV characteristics of partially shaded PVGs. Moreover, Simscape components (PV cells, bypass diodes, etc) can be easily used to model a large-scale PVG with different configuration wanted.

2.4. PV module technologies

Nowadays, solar cells with C-Si or thin film technologies are very familiar from use viewpoint. They comprise a wide portion of installations worldwide. However, both technologies face challenges and present merits and demerits. These challenges include materials optimization, efficiency improvement and cost reduction. Therefore, in the following, the C-Si and thin film technologies are compared in terms of conversion efficiency, durability and design flexibility, etc. they

are compared also in terms of cost and use of rare elements. Different PV modules using different technologies have been considered, Q.Pro 230Wp PV which is based on C-Si technology (Poly C-Si), Q.Smart 95Wp and FS-272 that both are based on thin film technology (CIGS and CdTe, respectively). Many technical performances of those PV modules have been provided in their datasheets as given in table (2.2).

Table (2.2) provides the efficiency of the conversion with respect to life span (i.e., long-term performance-durability) as well as the efficiency of light to electricity conversion at STC.

Table 2. 2: Linear performance warranty and rated efficiency provided by the manufacturer's specifications

Designation		First Solar FS-272	Q.Pro 230Wp	Q.Smart 95Wp
Technology		CdTe	Poly C-Si	CIGS
Long-term performance-durability	Min η [%] from nominal power within 1 year.	100	97	100
	Min η [%] from nominal power after 10 years.	90	92	96
	Min η [%] from nominal power after 25 years.	80	83	85
Efficiency at STC η [%]		≈ 10.07	≥ 13.8	13.4 ≥ η ≥12.5

Since the release of C-Si and thin film technologies to the market, research works seeking for better efficiency has never been stopped. Figure (2.9) shows the evolution of efficiency improvement for each PV technology since 2009.

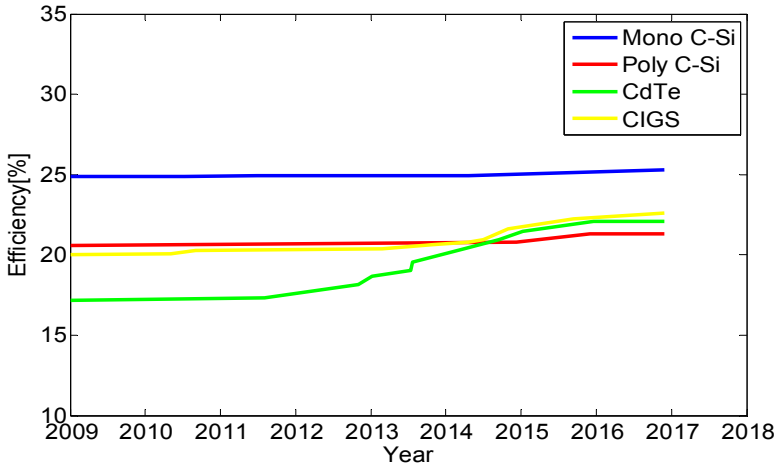

Figure 2. 9: The progress in efficiency improvement of Mono C-Si, Poly C-Si, CdTe and CIGS since 2009

2.4.1. Crystalline Silicon (C-Si) technologies

The leader in PV industry and applications is C-Si technology. Silicon is a material with gap energy of 1.1 eV which can be found in more than 90 % of PV production [114]. PV modules with C-Si solar cells have been the focus of research since the 1950s and currently they cover around 85% of the PV market [115]. Depending on the long-term field testing for reliability and the high volume manufacturing facilities, C-Si PV industry is regarded as the mature one. The theoretical maximum efficiency for this technology is about 29% [116], with world record efficiency of 25.3 % and 21.3% for Mono C-Si and Poly C-Si, respectively [117]. This technology is expected to survive for a multiple decades due to their significant merits in economic and technical aspects. Figure (2.9) shows the rise in efficiency since 2009 of C-Si, CIGS and CdTe. Mono C-Si technology retains the highest efficiency in comparison to thin film technologies (i.e., based on either CdTe or CIGS). Furthermore, the rise in efficiency for C-Si (Poly C-Si and Mono C-Si) and CIGS are low with respect to that of CdTe.

Poly C-Si solar cells are the next class of C-Si technologies. In fact, the major advantage of Poly C-Si is the cost reduction compared with Mono C-Si class, However, this cost reduction resulted in a low conversion efficiency compared with Mono C-Si class. Poly C-Si benefits from the maturity of the C-Si industry. Thereby, it is cheaper in the market as its fabrication process is faster and much easier than the other existing silicon technologies [118]. The Average price of PV modules with Poly C-Si technology is down about 14% per year (US$ 0.6/Watt achieved in 2014) [119]. In the last decade, the Poly C-Si and Mono C-Si account for most of the market shares in PV manufacturing industry. Furthermore, Poly C-Si PV modules are widely used in all kind of applications thanks to their tradeoff between the low cost and the average power efficiency [120]. However, it is worth noting that Poly C-Si and Mono C-Si suffer from some limitations; the relative high cost involved in the fabrication compared to thin films [114], the weight and rigidity of modules. Study presented in [121] has shown that solar cells with C-Si technologies have the best performance only in ambient or low temperatures, along with CIGS and CdTe. Therefore, C-Si can exhibit poor performance under high temperature. In addition, the low absorption coefficient and the shortage feedback of silicon results in low conversion efficiency under low irradiance levels. It is worth noting that during the

fabrication stage, a premium silicon quality is crucial for fabricating high performance PV cells. From table (2.2), its seems that Q.Pro 230Wp PV module has around 13.8 % efficiency at STC, and can retain about 83% of initial power over a 25 year period. Accordingly, it can retain over 3% more long-term-performance-durability compared to CdTe.

2.4.2. Thin Film technologies

Great interest has been devoted to the investigation of new alternative materials and device processing technologies in order to overcome some of the C-Si technology limitations. This has leaded to new technologies which expand rapidly, especially, thin film technologies.

As reported in [120], thin film technologies production in 2014 have been increased by an estimated 25%. Nowadays, these technologies are held the most remainder portion of the PV market after C-Si. The contributions of thin film lie in the no need for expensive semiconductor substrates and the reduced amount of active semiconducting material used in each solar cell, which allow a reduced cost of PV module while maintaining reasonable conversion efficiency. Thin film technologies are in progress to be a promising candidate in comparison to C-Si, for solar energy conversion delivering a vast scope in terms of device fabrication and design.

Solar cells based on thin film technologies have lower cost and efficiency compared to Mono C-Si technology. In manufacturing of thin film solar cells, the used film thicknesses are typically around hundreds of nanometers to a few micrometers to absorb most of the incident light. On the other hand, the thickness required in C-Si technology solar cells is about hundreds of micrometers; this resulted in the price advantage of thin film solar cells. Besides, the production of thin films does not require high temperature device processing. However, they are still unable to offset the advantages of the more established C-Si industry. Thin films can be deposited onto a variety of inexpensive supporting substrates such as: plastic, glass and foil. In addition, applying a flexible support substrate to CIGS thin-film during the deposition processes allows obtaining a large-scale flexible PV plant and opens new fields of applications (e.g., coated on existing surfaces or integrated with building components such as: roof tiles). Thin film technologies are commercially available on the PV market either CdTe, CIGS or amorphous silicon.

The latter is not sufficient to offset the advantages of the other thin film technology; therefore, it is rapidly receding. It is worth noting that CIGS and CdTe PV technologies have reached remarkable power conversion efficiencies. Knowing that CIGS has become the leader in efficiency of thin film technologies [122] and CdTe gaining importance through the fast increase in conversion efficiency [114].

2.4.2.1. Cadmium Telluride CdTe

CdTe regarded as one of the first semiconductor that was used in thin film technologies to improve the low efficiency experienced with amorphous silicon. Furthermore, the tremendous research targeting CdTe, is to create a balance between performances and cost making it essential in achieving high conversion efficiencies. The CdTe is a robust semiconducting material, this is because it has a remarkable tolerance towards the high processing temperatures [114]. At present, PV modules with CdTe-based thin-film technology are one of the fastest-growing segments of commercial module production [123]. Therefore, CdTe-based thin-film technologies now firmly established as the basis for the market-leading thin-film PV module technology, as well as, the most cost-effective to manufacture. As discussed in [124], the cost of CdTe PV modules has now been dropped below one US$-per-watt. As a result, the cost of power generation is rapidly approaching grid parity.

In CdTe and CIGS, the semiconductor layer can be utilized as very thin films (2 to 3 μm) to absorb nearly all the incoming insolation [122]. In addition, the glass substrate plate that layered the CdTe compound has a high optical absorption coefficient in order to enable light to reach the semiconductor layer more efficiently, as a result, only a low level of irradiance is needed to produce power. PV modules based on CdTe technology are commercially available nowadays with conversion efficiency ranged between 7% and 12% on average. However, the tremendous improvements of this technology have increased its cell efficiency record to 22.1% [117].

From figure (2.9), the path towards high-efficiency for CdTe has been quicker than the other considered technologies. Therefore, a remarkable progress has been made in the efficiency improvement with rate about 0.3% since 2009, which results in latest achieving efficiency higher than that of Poly C-Si one. However, it still exhibits a lower efficiency than CIGS. Moreover, from table (2.2), it can be noticed

that First Solar FS-272 PV module (i.e., with CdTe technology) presents the lowest efficiency and the poorest linear performance warranty compared to other considered technologies.

It is important to note that CdTe-based thin-film solar cells have a simple structure of the two-component absorber layer (i.e., contain only cadmium and tellurium) [124], However, Tellurium has a limited supply, which makes a CdTe-based thin-film PV modules not as a real solution for large-scale deployment. Likewise, the Cadmium is a toxic material which is dangerous to both industrial operators and outdoor applications. Therefore, it must be treated carefully in its handling and disposal. Consequently, further improvements in conversion efficiency as well as in material and interface properties of CdTe solar cells are needed.

2.4.2.2. Copper Indium Gallium Selenide, CIGS

CIGS technology is regarded among the most popular thin film technologies. It offers inherent advantages of thin-film for cost reduction and high absorption coefficients (i.e., with a band gap of 1.68 eV) [106]. Copper, Indium, Gallium and Selenium [Cu (In, Ga) Se_2] are the main materials that compose this semiconductor type.

Thin CIGS films can be deposited onto a variety of flexible (e.g., mostly metals, ceramic, plastics and special polymers, etc) and rigid (e.g., soda lime glass, etc) substrate materials. However, the used substrate material has to be chosen considering its availability in large quantities, the compatibility with the subsequent deposition steps (i.e., different chemical and physical properties have to be taken into consideration), cost effective, robustness and lightweight.

A key stage in the fabrication of CIGS solar cells is to choose the appropriate substrate in order to create a compromise between the desired performance and the processing conditions. Therefore, choosing a polymer as flexible substrate offers the advantage of being with a much lower roughness and density than metals flexible substrates. However, polymer materials cannot withstand high temperature levels (e.g., 500–600 °C). Therefore, using a low temperature process leads to significantly inferior absorber quality of solar cells [125]. On the other hand, the high temperature process leads to substantial improvements in the absorber quality which results in high efficiency solar cells. However, the chosen flexible substrate

should be able to withstand a high level of temperature (e.g., metals have the ability to withstand very high deposition temperature). Ceramic materials have also been used as flexible substrates. However, one of the major drawbacks of this type of flexible substrate is its brittle behavior which might be an issue for industrial fabrication on a large scale. Besides the materials related problems, it requires the use of an appropriate technique of manufacturing, equipment and tools should all be optimized to reduce the manufacturing cost and to gain in efficiency. The considered technique that still under way for the development to produce large commercialization of CIGS PV modules on flexible substrates, is Roll-to-Roll production technique. The latter enables the use of compact-size-deposition-equipment to further reduce the production cost.

From figure (2.9), and in comparison to Mono C-Si, CIGS-based thin-film technology still has a lower efficiency. However, CIGS solar cells perform greatly and prevent the waste of energy conversion when the irradiance over the whole PV module is non-uniform or low. Another advantage behind CIGS-based thin-film technology is that the CIGS's conversion efficiency is not affected much as the PV module temperature increases. Unlike C-Si that depends highly on the temperature level, that is, in locations where the temperature level is usually high (e.g., Sub-Saharan Africa, Arab states of the Persian Gulf), the efficiency of C-Si PV modules can be much affected. This makes the latter technology not suitable for hot places. The moderate efficiency associated with CIGS-based thin-film PV modules ranges from 10% to 15%, with record conversion efficiency of 22.6 % [117]. In other hand, transferring the technology from the laboratory environment into the large-scale industrial manufacturing field leads to a new challenges, mainly for CIGS deposition, interconnections of cells and long-term performance stability. As reported in table (2.2), Q.Smart 95Wp PV module (i.e., CIGS technology) has the highest linear performance warranty than First Solar FS-272 (i.e., CdTe technology) and Q.Pro 230Wp (i.e., Poly C-Si technology).

To recapitulate, C-Si technologies (Mono C-Si and Poly C-Si) are the most suitable for the large scale deployment considering their abundance and the ratio efficiency to price. Specifically, Mono C-Si PV technology is more efficient but relatively more expensive than Poly C-Si one.

Currently, the two key drivers in CdTe technology research are reducing the cost of production and to limiting the environmental impact (i.e., reducing the used toxic material amount or identifying an effective replacement for it with neither an environmental risk nor a high cost). Therefore, the cost decreasing with respect to the efficiency improvement of CdTe-based-thin-film technology continued to challenge many thin film companies. Consequently, this technology is projected to be more attractive in future life.

CIGS technology reveals that highly-efficient-flexible PV modules with performance close to rigid PV modules can be developed. However, several issues still need to be solved such as: finding the ideal manufacturing techniques to drive down the cost and improving efficiency. Actually, the trends in research works and development are intended for reducing electronic and optical losses (by optimizing the different types of interconnection, improving the antireflection layers, etc) and looking for the most efficient and inexpensive-flexible-substrate materials, etc. Nevertheless, the production capacities of CIGS PV modules deposited on flexible substrates still low compared to CIGS modules deposited on rigid substrates.

2.4.3. Experimental data analysis

The study presented in this sub-section is aimed to confirm some of the discussions given previously and to evaluate which PV technology is preferable in a specific location. A number of measurements have been carried out at the test facility of Trieste University, Italy. To this, the three PV modules namely Q.Pro 230Wp (Poly C-Si technology), Q.Smart 95Wp (CIGS technology) and First Solar FS-272 (CdTe technology) have been considered. The electrical specifications of these modules are reported in table (A.2-Appendix A). Different experiments are conducted at both STC and Actual Working Conditions (AWCs: where temperature and irradiance levels are different from STC) for each of the above modules. The I-V characteristic of each PV module is recorded by sweeping the output voltage from zero to V_{oc}.

The test facility is shown in figure (2.10) where three PV modules are made available. It comprises also two data-loggers (type E-Log, MW8024-02/10 produced by LSI Lastem S.r.l [126]) for climatic and electrical data, they are connected to a computer for the data to be collected and saved; DC-DC converter (type Solar Magic

produced by National Semiconductor Ltd) connected to a resistive load, one ISO9060 first class thermopile global radiometer type C100R DPA153 (produced by LSI Lastem S.r.l [126]) installed on the same frame carrying PV modules (the daily uncertainty for this device is less than 5%, the sensitivity is 30÷45 $\mu V.m^2/W$ and the flat spectral response range is (305-2800 nm)), three module temperature contact probes (type DLE 124 by LSI Lastem S.r.l) have an accuracy of ±0.15 °C and three shunts type SHP300A60-Compact (produced by Hobut Ltd [127]) calibrated with an accuracy better than 0.01%. Fast measurements of I-V characteristics are carried out by varying the duty cycle of the DC-DC converter from the minimum to its maximum value. At this time, both the climatic data (irradiance and temperature) and electrical data (PV current and voltage) are simultaneously acquired and stored in the computer.

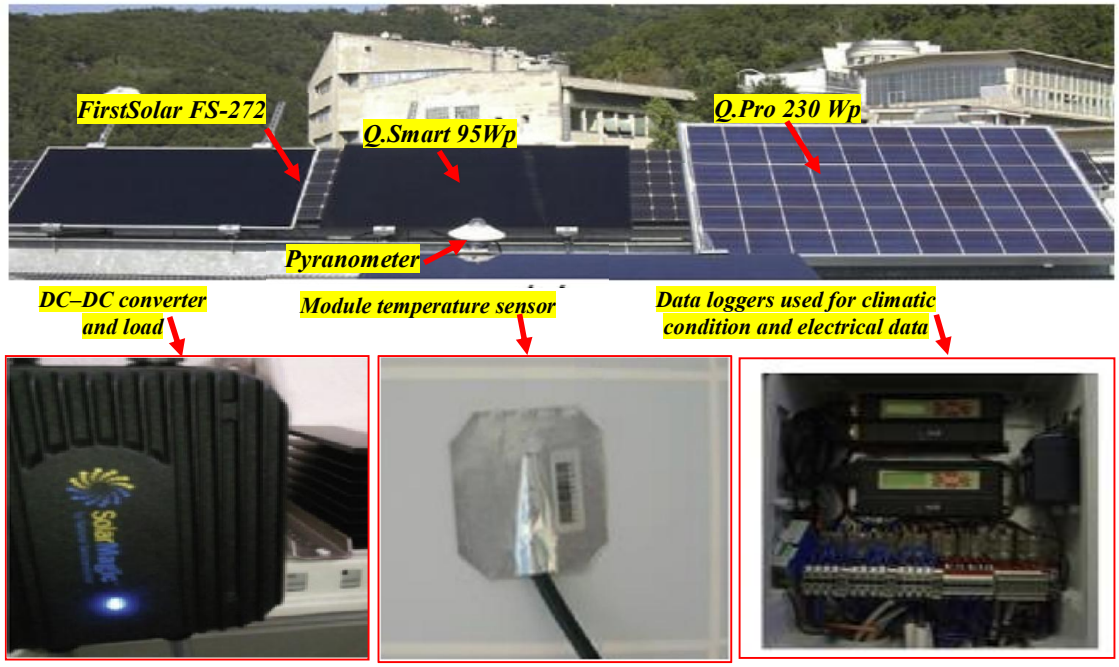

Figure 2. 10: Test facility to measure the electrical characteristics of the used PV modules

The fill factor (given by equation (2.8)) measures the square–like sharpness of the I-V curve. Therefore, it tests the degree of closeness of the voltage at the MPP (V_{MPP}) to the open circuit voltage (V_{oc}) and that of the current at the MPP (I_{MPP}) to the short-circuit current (I_{sc}). Thus, high fill factor value (i.e., near the unit) reveals a high efficiency of the module as the latter is the ratio of P_{MPP} to the product of V_{oc} and I_{sc}. In other words, it reveals that the solar cells are generally less affected by both resistive and recombination losses at the operating point.

The efficiency of light to electricity conversion (i.e., η_L [%]) of the PV module is the ratio of its maximum output power ($V_{MPP}.I_{MPP}$) by the amount of insolation falling on its surface. It measures how well the PV module can convert the insolation reaching its total surface area, into electric current. Therefore, higher value of efficiency leads to better conversion of light to electricity. This relation is given by

$$\eta_L\ [\%] = \frac{P_{MPP}}{S.G} \times 100 \tag{2.5}$$

Where, S [m^2] is the lighting area of the PV module; G [W/m^2] is the insolation level falling on the PV module.

Table (2.3) shows the results of computing the fill factor and the conversion efficiency at both STC and AWC. It can be seen that in most cases, CIGS technology achieves the best values of fill factor (ranging from 0.66 to 0.7251). Moreover, the conversion efficiency of both CdTe and CIGS are not affected as much as the conversion of Poly C-Si when the temperature increases or the irradiance on the module decreases. On the other hand, the greatest conversion efficiency under STC is achieved by Poly C-Si. However, under AWCs, when the temperature is high or the irradiance is relatively low, the performance of this technology is highly affected as the efficiency collapses from 14.08% to 9.70% when the temperature is increased to 55.5°C. This explains why Poly C-Si technology is not recommended to be employed in location with hot climate.

Table 2. 3: Experimental fill factors and efficiencies under different environmental condition

PV Module	Technology	Environmental condition		$V_{\_MPP\_PU}$ [p.u]	$I_{\_MPP\_PU}$ [p.u]	FF [ ]	η_L [%]
		G [W/m²]	T [°C]				
First Solar FS-272	CdTe	1000	25	0.7508	0.8862	0.6654	10.07
		920	56	0.7222	0.7553	0.5455	8.17
		470	30	0.7235	0.7827	0.5663	9.3
Q.Pro 230Wp	Poly C-Si	1000	25	0.7913	0.9255	0.7324	14.08
		980	55.5	0.6820	0.8483	0.5785	9.70
		480	36.5	0.7522	0.9132	0.6870	11.94
Q.Smart 95Wp	CIGS	1000	25	0.7962	0.9107	0.7251	12.48
		995	56	0.7552	0.8738	0.66	10.31
		347	30	0.7976	0.8877	0.708	11.53

2.5. An improved Simscape-based-model

2.5.1. Modeling of PVG

In the light of the previous analysis done in section 2.3, one can find that PV model should be at once efficient, accurate and easily to be applied by designers. Moreover, it is much better if the developed PV model is based only on the data provided by the manufacturer. For this purpose, the present work proposes an improved Matlab-Simscape-based model to characterize PV modules for different technologies. The developed model requires that data available in the module's datasheet. In addition, it offers the freedom to modify the configuration by playing on the physical connections of solar cells and bypass diodes.

As has already been discussed in sub-section (2.3.2) that the block-parameters solar-cell requires both the climatic conditions (irradiance and the temperature levels) and electrical parameters (V_{oc}, I_{sc}, A and R_S). The V_{oc} and I_{sc} values are obtained from PV module's datasheet. However, the series resistance R_S was tuned by trial-error approach. Which makes the determination of an appropriate R_S value a difficult task. Moreover, the ideality factor was not adapted to fit the modeled PV technology.

In the following, a contribution towards developing a PV model that depends only on the datasheet in order to predict P-V and I-V characteristics is made. In which, expression uses the available information in the manufacturer's datasheet to estimate the value of series resistance R_S has been adopted. Moreover, for each modelled technology (Poly C-Si, CdTe or CIGS), a specific ideality factor value is used. Mono C-Si, Poly C-Si, CdTe and CIGS ideality factors are given in table (2.4).

Table 2. 4: Ideality factor for different PV technologies [128]

Technology	Ideality factor
Mono C-Si	1.2
Poly C-Si	1.3
CdTe	1.5
CIGS	1.5

The series resistance R_S is not provided in the manufacturer's datasheet. Previous work on this subject obtained the series resistance value by using trial-

error method [129, 130]. However, to model a PV plant with different PV module classes, it is so difficult to find the accurate R_S for each PV module. In [131], R_S is determined by evaluating the derivative of the model equation at V_{oc} point, which leads to a significant computation efforts. An iterative algorithm is used in [132] that is based on the minimization of ($dP/dV_{MPP}=0$) to find an optimal value of the adjustment factor (α). Once the latter is reached, the R_S can be calculated. Another approach based on optimization is presented in [133] where the determination of R_S value is carried out by evaluating an expression based on unknown factor and the parameters reported in the datasheet. However, this approach is very sensitive to the initial solution as it uses the Newton-Raphson method for the determination of the unknown factor. In the same context, the authors in [134] has employed a binomial search routine to seek the optimal value of R_S within an estimated interval. However, the use of this optimization method made the determination of R_S a complex task. A complicated function of series resistance is solved iteratively in [135] by using a typical series resistance of the PV module as a starting point. However, the model needs additional information besides the standard data provided by the manufacturer's datasheet. For the aforementioned drawbacks, designers of PV systems often find difficulties in applying such models. To cope with this inconvenience, a more suitable empiric expression is presented in this work. The expression uses the available information in the manufacturer's datasheet to forwardly estimate the value of series resistance R_S.

This method is based on the computation of the fill factor which is determined as follows:

$$V_{\_MPP}[p.u] = \frac{V_{MPP}}{V_{oc}} \tag{2.6}$$

$$I_{\_MPP}[p.u] = \frac{I_{MPP}}{I_{sc}} \tag{2.7}$$

$$FF[\ ] = V_{\_MPP}[p.u].I_{\_MPP}[p.u] \tag{2.8}$$

Where V_{oc} [V] and I_{sc} [A] are the open circuit voltage and the short circuit current, respectively; $FF[\ ]$ is the PV module's fill factor at STC.

The solar cell's series resistance R_S [Ω] [136], is calculated as:

$$R_S = \frac{V_{OC}}{I_{SC}}.R_{SN} \tag{2.9}$$

R_{SN} [ ] is the normalized solar cell's series resistance that is determined as shown below [137]:

$$R_{SN} = 1 - \frac{FF}{FF_{N,25}} \tag{2.10}$$

Where $FF_{N,25}$ [ ] is the normalized fill factor when the solar cell temperature is 25° C and given as [137]:

$$FF_{N,25} = \frac{v_{OCN,25} - \ln(v_{OCN,25} - 0.72)}{v_{OCN,25} + 1} \tag{2.11}$$

Where, $V_{OCN,25}$ [ ] is the normalized open-circuit voltage at temperature of 25 °C which is calculated as [136]:

$$v_{OCN,25} = \frac{V_{OC}}{Vt_{,25}.n_S} \tag{2.12}$$

Where $V_{t,25}$ [V] is the junction thermal voltage of the solar cell at 25° C; n_s [ ] is the number cells of the PV module.

Finally, the junction thermal voltage of the solar cell at 25° C is given by:

$$Vt_{,25} = \frac{k.(25+273)}{q} \tag{2.13}$$

Where k [$J.K^{-1}$] and q [C] are the Boltzmann's constant and the electron charge, respectively.

2.5.2. Experimental validation of the improved Simscape-based-model

The validation of the improved Simscape-based model is carried out to show its effectiveness for predicting the I-V and P-V characteristics of the different technologies (i.e., Poly C-Si, CdTe and CIGS). Firstly, First Solar FS-272, Q.Pro 230Wp and Q.Smart 95Wp models are implemented by using physical-component-

blocks (such as: solar cell block, bypass diode block, etc) and physical-networks. Then, each PV module's solar cells have been characterized according to the electrical characteristics reported in table (A.2-Appendix A) as well as the ideality factor values reported in table (2.4). Moreover, equations (2.6–2.13) have been used to compute the series resistance of solar cells for each PV module. The obtained values (***Rs***_First Solar FS-272 is 0.1402 Ω, ***Rs***_Q.Pro 230Wp is 0.0094 Ω, ***Rs***_ Q.Smart 95Wp is 0.0565 Ω) are used to parameterize blocks of solar cells. Figure (2.11) shows the Simscape implementation of 'Q.Pro 230Wp' PV module that consists of 3 bypass diodes and 60 Poly C-Si solar cells. So as to sweep the I-V and P-V characteristics, the three implemented PV modules have been used with the same system for sweeping-acquiring I-V and P-V characteristics presented in figure (2.4). Simulation is done using the recorded climate condition. The obtained I-V and P-V characteristics of Simscape-based-model have been compared to those measured for the same weather conditions.

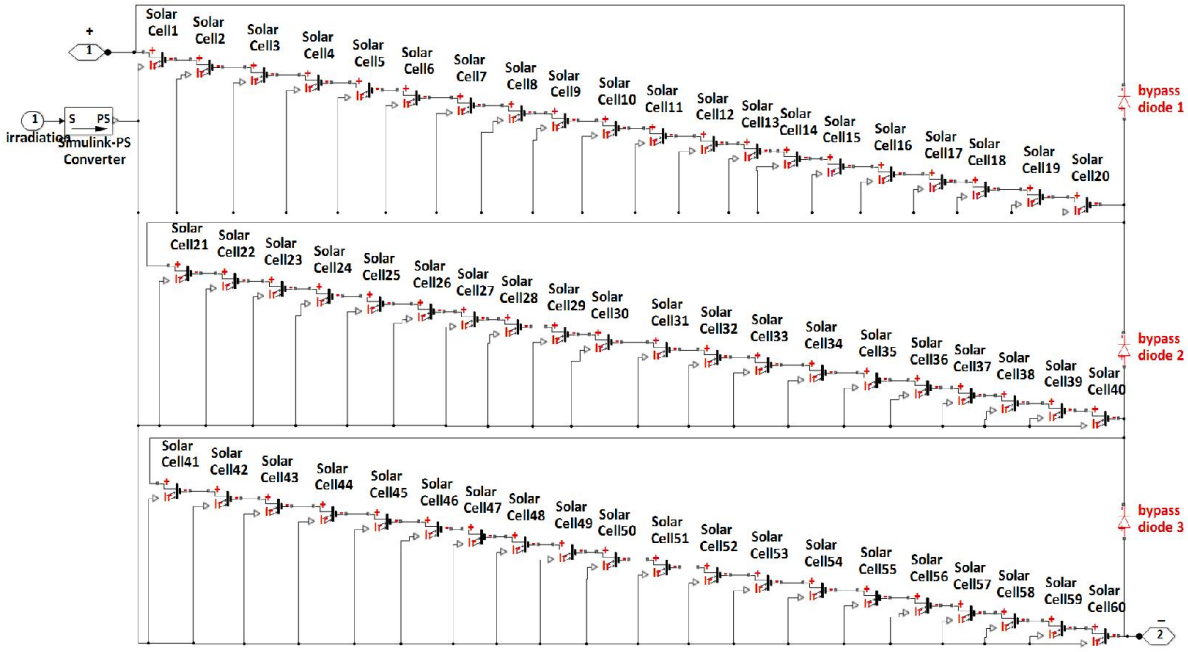

Figure 2. 11: Simscape implementation of 'Q.Pro 230Wp'

Figures (2.12)-(2.17) show the simulated versus the measured data of the I-V and P-V characteristics for each PV technology. It can be noticed that there is a good agreement between the simulated and the measured electrical characteristics.

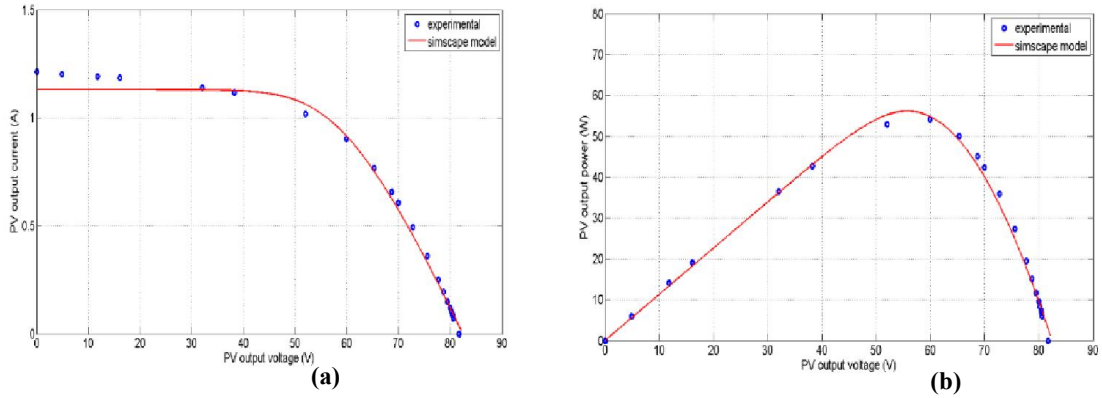

Figure 2. 12: Experimental data (dotted line), Simscape-model (solid line) for PV module FS-272 operating at G=920 W/m^2 and T=56 °C (a) I-V characteristic (b) P-V characteristic

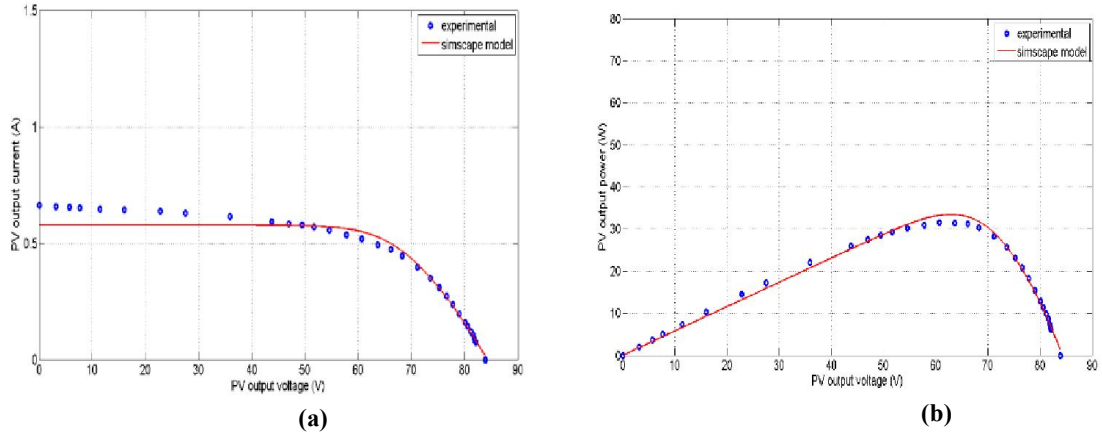

Figure 2. 13: Experimental data (dotted line), Simscape-model (solid line) for PV module FS-272 operating at G=470 W/m^2 and T=30 °C (a) I-V characteristic (b) P-V characteristic

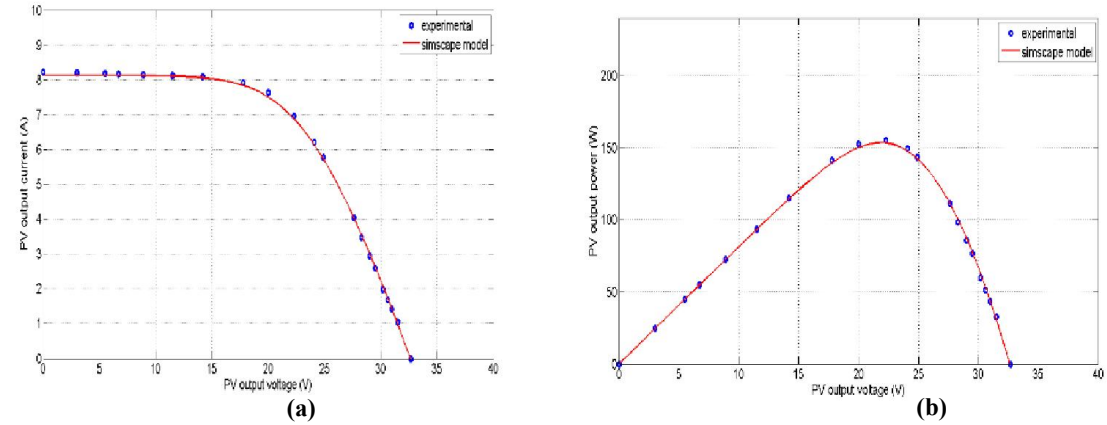

Figure 2. 14: Experimental data (dotted line), Simscape-model (solid line) for PV module Qpro operating at G=980 W/m^2 and T=55.5 °C (a) I-V characteristic (b) P-V characteristic

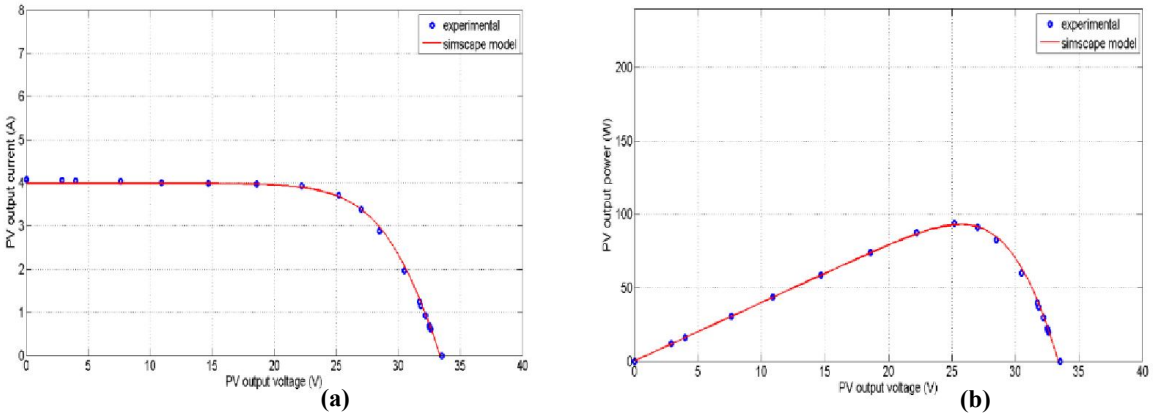

Figure 2. 15: Experimental data (dotted line), Simscape-model (solid line) for PV module Qpro operating at G=480 W/m^2 and T=36.5 °C (a) I-V characteristic (b) P-V characteristic

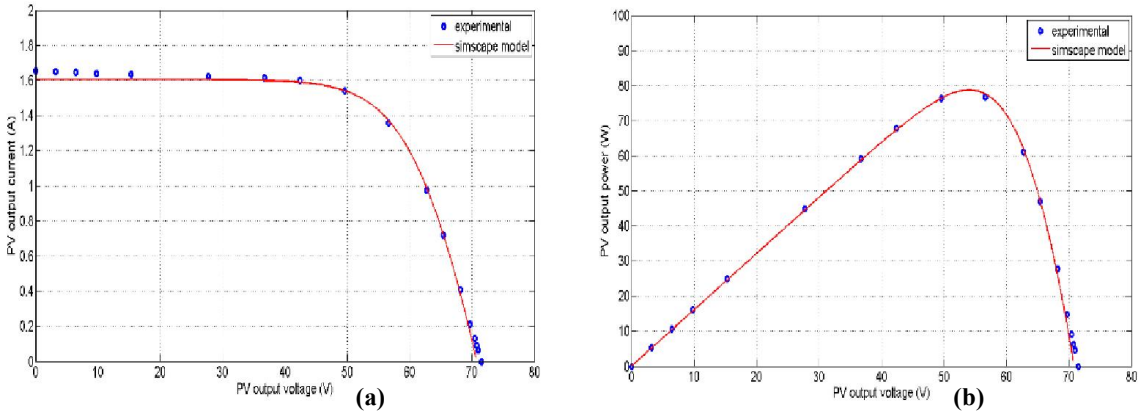

Figure 2. 16: Experimental data (dotted line), Simscape-model (solid line) for PV module Qsmart operating at G=995 W/m^2 and T=56 °C (a) I-V characteristic (b) P-V characteristic

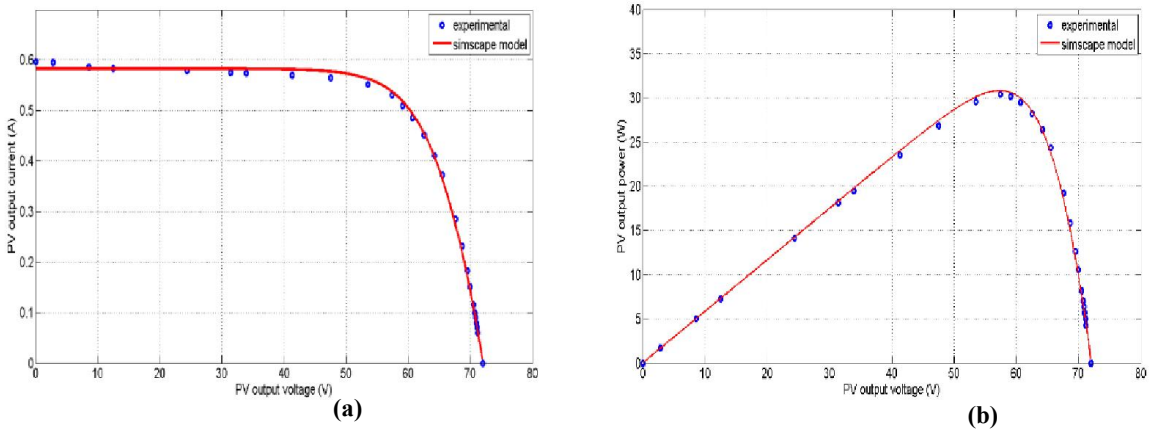

Figure 2. 17: Experimental data (dotted line), Simscape-model (solid line) for PV module Qsmart operating at G=347 W/m^2 and T=30 °C (a) I-V characteristic (b) P-V characteristic

In order to measure the accuracy of the developed Simscape-based-model in predicting the P-V and I-V characteristics of each technology under the considered environmental conditions, several statistical error tests are used to characterize the

degree of matching between simulated and measured characteristics. These statistical error tests are RMSE and R^2 (given by equations. (2.3) and (2.4), respectively) in addition to the Mean Percentage Error (MPE) and the Deviation from the measured values (Dev) given by the following equations:

The Mean Percentage Error (MPE)

$$\mathrm{MPE}[\%] = \frac{1}{N}\sum_{n=1}^{N}\left(\frac{P_{pv\_sim}(n) - P_{pv\_mea}(n)}{P_{pv\_mea}(n)}\right).100 \tag{2.14}$$

The Deviation from the measured values (Dev)

$$\mathrm{Dev}[\ ] = \frac{\sum_{n=1}^{N} P_{pv\_sim}(n) - \sum_{n=1}^{N} P_{pv\_mea}(n)}{\sum_{n=1}^{N} P_{pv\_mea}(n)} \tag{2.15}$$

Where $P_{pv\_mea}(n)$ [W] is the *nth* measured value of the PV output power, $P_{pv\_sim}(n)$ [W] is the *nth* simulated value of the PV output power, and N [ ] is the number of simulated or measured points.

Table (2.5) shows, for each PV module and for a given climate condition, the computed statistical errors. One can notice that the RMSE values are relatively low; ranging between 0.311W and 1.246W. Furthermore, the deviations from the measured values are the range that is [-0.0125, 0.0118]. The correlation coefficient values are greater than 99.8 % regardless the technology of the module and the weather conditions. Moreover, the absolute values of the MPE are always less or equal than 0.057 %. Upon the analysis of these results, it can be concluded that the proposed Simscape-based-model offers a good performance in predicting the electrical characteristics (i.e., current, voltage, power) of different PV technologies, particularly, a PV module having Poly C-Si technology. The latter has the highest correlation values (99.99%) and the lowest |MPE| and |Dev|, 0.0031 and 0.00064, respectively. Likewise, the obtained statistical errors of CIGS PV module lead to say that Simscape-based-model can offer satisfactory prediction for this technology. However, the predicted electrical characteristics of CdTe PV module present the poorest performances compared to the remaining. This has the lowest correlation (99.82%) and the highest |MPE| and |Dev| (0.057 and 0.0125, respectively).

Table 2. 5: Comparisons between simulated and measured P-V curves of each used PV technologies

PV module	technology	G [W/m²]	T [°C]	RMSE [W]	R^2[%]	MPE [%]	Dev [ ]
First Solar FS-272	CdTe	920	56	1.2462	99.82	-0.057	-0.0125
		470	30	0.7937	99.85	0.0357	0.0118
Q.Pro 230Wp	Poly C-Si	980	55.5	0.5976	99.99	0.0031	0.00064
		480	36.5	0.5762	99.99	0.0236	0.0045
Q.Smart 95Wp	CIGS	995	56	0.5767	99.98	-0.0123	-0.0022
		347	30	0.3118	99.97	0.0185	0.0050

2.6. Conclusions

A survey of the recent progress on the most common PV technologies (i.e., C-Si and thin film) has been presented. Mono C-Si the leader in PV industry has been highlighted. Furthermore, thin film technologies still to be considered as the most suitable for the large scale deployment. In the other hand, thin film technology suffers from the low conversion efficiency. However, it is expected to be increased quickly in the future. PV modules namely Q.Pro 230Wp (Poly C-Si-first generation), Q.Smart 95Wp (CIGS-second generation) and First Solar FS-272 (CdTe-second generation) have been experimentally tested under STC and AWCs. Subsequently, the fill factor and the efficiency have been experimentally evaluated. The results show that Poly C-Si PV module is not suitable to be employed in hot locations.

Turning now to the second part of this chapter where a PV model based on Simscape has been proposed to predict electrical characteristics of different PV technologies. Then, it has been experimentally tested under STC and AWCs. Test results show a good matching between recorded and simulated data. In addition to that, assessment criteria based on four statistical errors have been calculated to precisely evaluate the suggested Simscape-based PV model. Obtained results show that Simscape-based-model offers a satisfactory accuracy of prediction.

Having regard to the advantages of Simscape-based-model, it will be adopted in the following two chapters as a modelling approach of PVGs within the standalone PV system (PVG, a DC-DC converter, load and MPPT controller).

CHAPTER 3
A NEW GOLDEN SECTION MPPT FOR PV SYSTEMS

3.1. Overview

One way to improve the efficiency of solar powered systems is to maximize the energy harvesting from the PVG by using a MPPT algorithm. The latter must be simple for implementation, fast and accurate to cope with fast changing atmospheric conditions and PSCs. This chapter presents a new MPPT method based on Golden-Section Optimization (GSO) technique for PV systems. The proposed method converges to the MPP by interval shrinking. Initially, two points are selected from the search space whose boundaries are known, evaluated then a new point is accordingly generated. At given iteration the algorithm has a new narrowed interval bounded by the new point and one of the initial points according to the evaluation results. The algorithm stops iterating (interval shrinking) when the interval becomes small enough and the PVG is forced to operate at the average value of the last found interval without perturbing either the voltage or the duty cycle. This makes the PV system converges rapidly to the MPP without voltage or power oscillations, thereby lower energy waste. Comparison results with recently published work are provided to show the validity of the GSO-MPPT under fast changing conditions and PSCs.

3.2. MPPT using Golden Section Optimization technique

3.2.1. Golden Section Optimization (GSO) technique

The GSO is a technique for finding extremum (minimum or maximum) by repeatedly narrowing the width of the interval inside which extremum exists. The name “Golden Section” originates from a classical problem of dividing line segments in a particular way [138-140]. The line segment limited by the search space [a, b] of length L is divided into two sub-segments, the major length L_1 and the minor length L_2, such that

$$\frac{L}{L_1} = \frac{L_1}{L_2} \tag{3.1}$$

Equation (3.1) can be rewritten as

$$\frac{L_1 + L_2}{L_1} = \frac{L_1}{L_2} = \Phi \tag{3.2}$$

Where, ϕ is the Golden ratio that is the quotient of the major sub-segment to the minor sub-segment.

Equation (3.2) results in following quadratic equation in terms of ϕ

$$\Phi^2 - \Phi - 1 = 0 \tag{3.3}$$

One solution of the equation (3.3), for ϕ that must be positive results in

$$\Phi = \frac{1+\sqrt{5}}{2} = 1.618 \tag{3.4}$$

The Golden Section (α) being the ratio of the minor sub-segment and the major sub-segment is the reciprocal of the Golden ratio

$$\alpha = \frac{1}{\Phi} = \Phi - 1 = 0.618 \tag{3.5}$$

In line-search optimization, this method is known as GSO technique that uses the Golden Section to generate two points from the search space (line limited by the interval [a, b]).

$$X_1 = b - 0.618(b-a) \tag{3.6}$$

$$X_2 = a + 0.618(b-a) \tag{3.7}$$

The cost function to be maximized, $f(x)$, is evaluated at these two points X_1 and X_2.

- If $f(X_1) < f(X_2)$, the abscissa of the maximum point cannot be less than X_1 . Thus, one may conclude that the maximum is in the range of $[X_1, b]$ which is taken as the new interval for the next iteration.
- Else, if $f(X_1) > f(X_2)$, the maximum's abscissa must be less than X_2. Therefore the maximum must lie in the range $[a, X_2]$, the interval taken in the next iteration. The process is continuously repeated until the difference $|X_1 - X_2|$ is less than a certain chosen precision, the resultant maximum's abscissa is given at point $X_0 = 0.5(X_1 + X_2)$.

3.2.2. GSO-MPPT

The operation of MPPT cannot be achieved unless a tunable power stage (a DC-DC converter with its PWM generator) is used to interface the load. The choice of one of the existing converters (type; buck, boost or buck-boost) depends on the voltage required by the load. The boost converter is used to rise the low voltage provided by the PVG to a high voltage for the load. Whereas, the buck converter is

used to drive a low voltage load from a high voltage PVG. The control parameter provided by the MPPT controller is the duty cycle (D), it is used as an input of the PWM generator. The latter generates a PWM signal to control the switch of the DC-DC converter for maximum extraction of power. Figure (3.1) shows a block diagram of a standalone PV system.

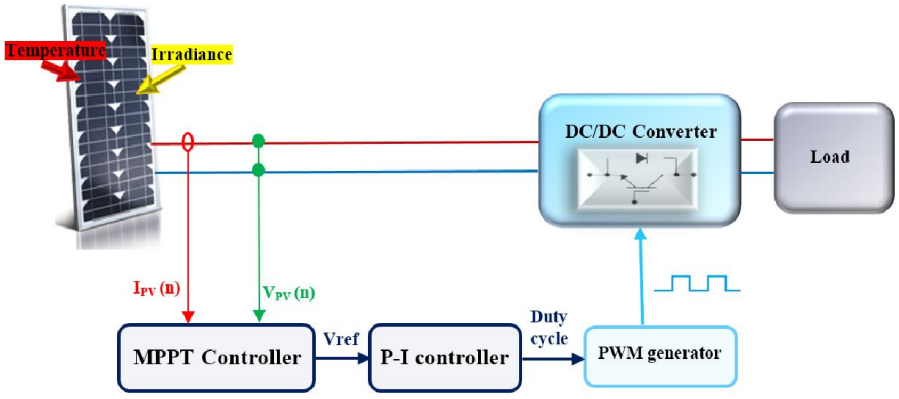

Figure 3. 1: Block diagram of the standalone PV system

It can be noticed from the previous sub-section that the evaluation needs the knowledge of the cost function, *f(X)* which is not available in PV system. However, for a given reference voltage, the power is evaluated by measuring first the output PV current (I_{pv}) and voltage (V_{pv}), and then multiply the two readings to obtain the power value (P_{pv}). Therefore, in GSO-based MPPT system, the searching variable is taken as voltage and the function to be optimized is represented by the P-V curve of the panel that must be on-line sampled. The searching interval could be as [0, V_{oc}] or slightly reduced from the left since the V_{MPP} is always closer to V_{oc}. Initially two reference voltage values V_1^*, V_2^* are generated from the starting interval [a, b] such that:

$$V_1^* = b - 0.618(b-a) \tag{3.8}$$

$$V_2^* = a + 0.618(b-a) \tag{3.9}$$

The length of the search space is L=b-a, therefore upon substituting b=L+a in equation (3.7), the same value of the reference could be written as

$$V_1^* = a + 0.382(b-a) \tag{3.10}$$

This makes the generation of the two values referred to the same point a. The power values corresponding to these reference voltage values, $P_{pv}(V_1^*)$ and $P_{pv}(V_2^*)$ are measured then compared and accordingly the search interval is shrunk from

either the right or the left. Three points are kept and the forth is taken away. The process is continued until the MPP is reached, that is

$$\left|V_2^* - V_1^*\right| \leq \varepsilon \tag{3.11}$$

Once the MPP is reached, the voltage reference is kept constant by the PI controller and the system is forced to operate at that point, unless a change in T or G occurs and the algorithm restarts the search of the new MPP. The flowchart depicted in figure (3.2) summarizes the entire proposed algorithm.

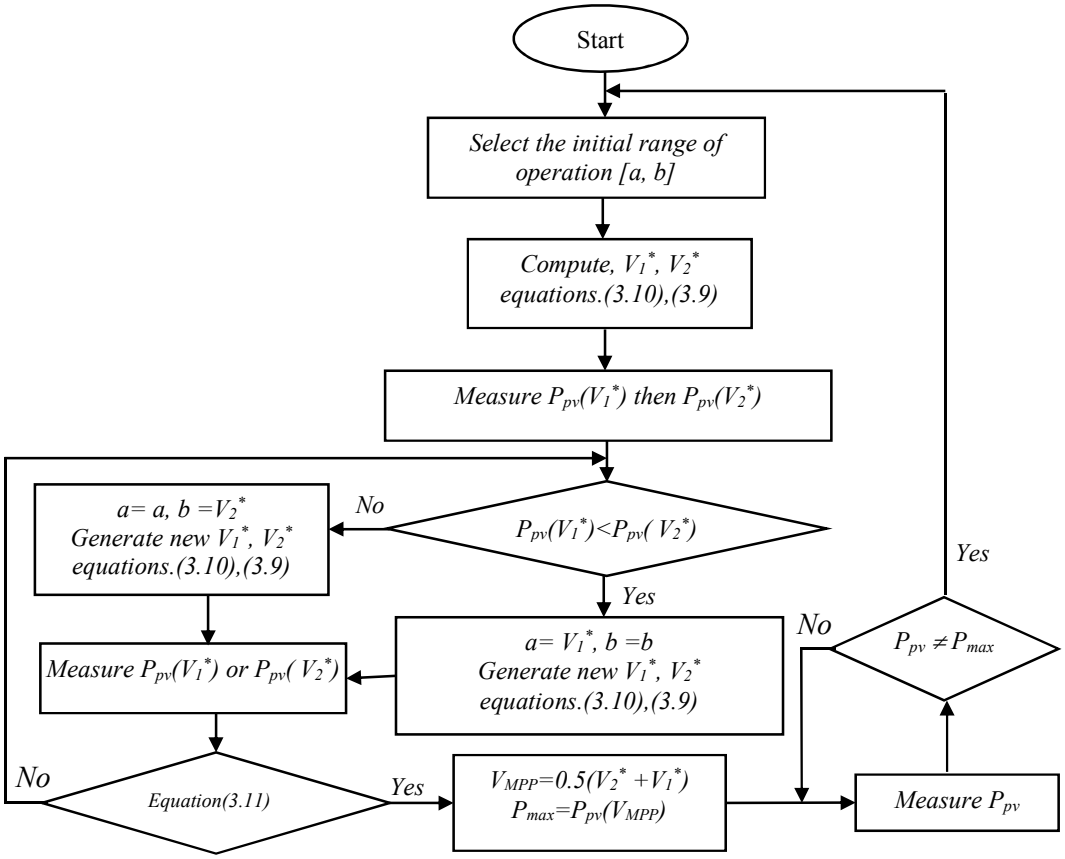

Figure 3. 2: Flowchart of the Proposed GSO-MPPT

3.3. Results and discussion

To verify the effectiveness of the proposed algorithm, different simulations have been carried out using Matlab/Simulink software and under different conditions namely: STC, fast varying atmospheric conditions and PSCs. Figure (3.3) shows Matlab/Simulink implementation of the whole standalone PV system shown in figure (3.1). The flowchart of GSO-MPPT depicted in figure (3.2), implemented using

embedded function available in the software's library. The PV generator, the used power stage (buck converter+ PWM generator) and a resistive load (of 1Ω) are implemented using 'Simscape' toolbox. Table (A.3-Appendix A) reports the specification of the PV module KC200GT at STC. The parameters of the buck DC-DC converter components are listed in table (3.1).

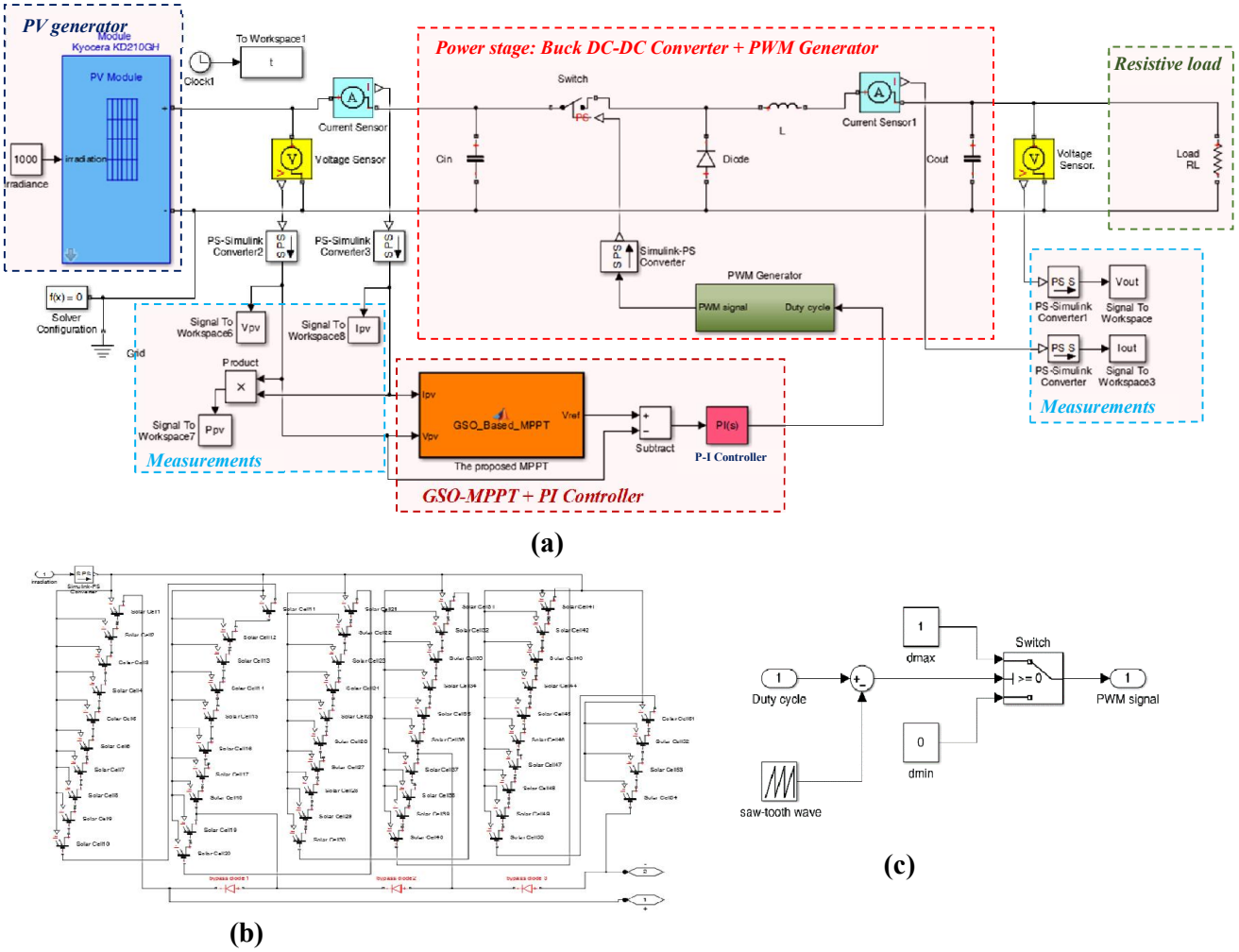

Figure 3. 3: Implementation of standalone PV system controlled by the proposed GSO-MPPT: (a) PVG + Power stage + load + GSO-MPPT + measurements, (b) PVG KC200 GT with 3 bypass diodes, (c) PWM generator circuit

Table 3. 1: Values of components of the buck DC-DC converter

Components	Values
Inductor, (L) [µH]	300
Input capacitor, (C_{in}) [µF]	100
Output capacitor, (C_{out}) [µF]	990
MOSFEt's Switching frequency, (f_s) [kHz]	100

3.3.1. Test under STC

Under STC, the PV module exhibits the same atmospheric conditions shown in the datasheet provided by the manufacturer, which are G=1000W/m², T=25°C. The simulation starts with a random operating point that is different from the maximum power operating point (V_{MPP}, I_{MPP}) and the initial maximum power chosen in the GSO-MPPT is zero. This makes the algorithm starts seeking the real MPP. Figure (3.4) depicts the variation of the reference voltage generated by the GSO-MPPT algorithm, the PV voltage (V_{pv}) and the output or the load voltage (V_{out}). Figure (3.5) illustrates the waveforms of the PV module current (I_{pv}) and the load current (I_{out}) and the power extracted from the PV module (P_{pv}). The process of shrinking the interval is clear in the curve of the reference voltage. The algorithm has made 7 iterations to reach the desired voltage or V_{MPP}= 26.3V according to the datasheet.

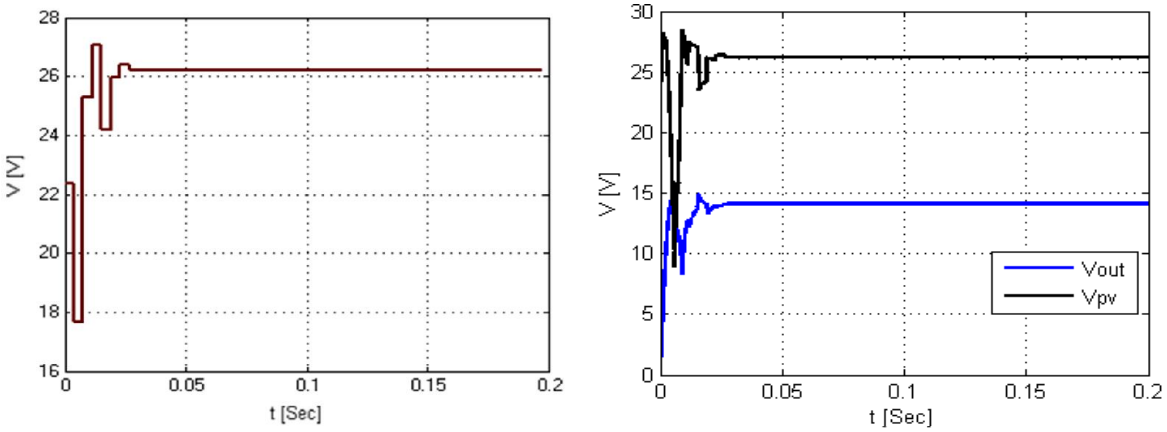

Figure 3. 4: MPP's seeking process by GSO-MPPT: (a) reference voltage, (b) PV and load voltages

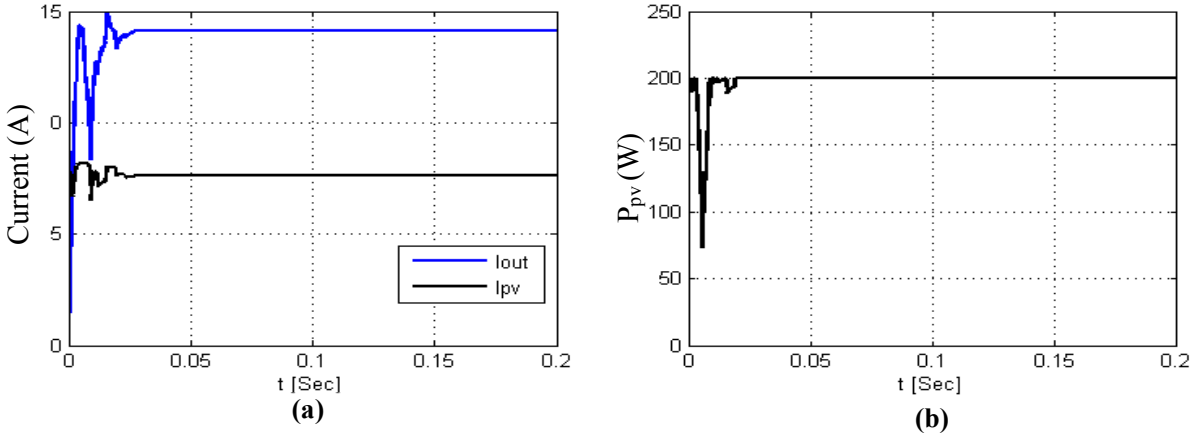

Figure 3. 5: MPP tracking: (a) Current waveforms, (b) PV panel output power

In figure (3.4-b), it can be noticed that once the algorithm converged to the MPP, the voltage of the PV module as well as the load voltage (chopper's output voltage) are maintained constant without any oscillations. The time response to reach the steady state operating point is about 0.02 seconds. The current of PV as well as the output current go through the dynamic of the same time to settle down to their maximum power values, as shown in figure (3.5-a).

The steady state output power is 200W (as shown in figure (3.5-b)), which is the maximum power that can be extracted from the PV module at G=1000W/m^2.

As shown in figure (3.4-b)-(3.5-a), when the GSO-MPPT algorithm seeks, the optimal voltage cause oscillations of PV voltage and current during P_{MPP} search. These oscillations of current and voltage result in power oscillations and take only 0.025 seconds, which is the convergence time of the algorithm.

3.3.2. Test under variable irradiance

In this test, the temperature is kept constant at $T=25°C$ and different step changes in the irradiance are introduced. The time step of irradiance change is set to 0.2 seconds that is a perturbation frequency of $5Hz$. The initial irradiance is G=400W/m², then stepped up to G=800W/m², and finally increased to G=1000W/m². The obtained results are shown in figure (3.6).

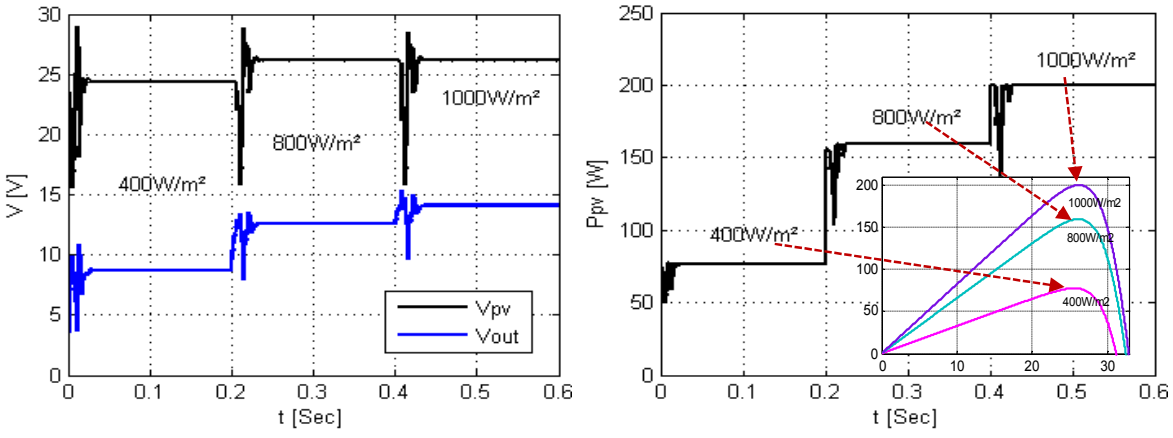

(a) **(b)**

Figure 3. 6: Results of changing in the irradiance level: (a) Voltage waveforms, (b) PV panel output power

Using the P-V characteristic of the PV module under study, it is easy to check the matching between the MPPs corresponding to the different irradiance levels and those obtained by the GSO-MPPT algorithm. Besides, oscillations of voltage do not exist at all which results in constant output power of the PV panel and thereby

avoiding waste of energy due to the oscillations. Except the oscillations due to the Golden-section search, the output power is almost very close to the maximum power produced by the PV module.

3.3.3. Test under variable temperature

In this test, the irradiance is kept constant at G=1000W/m² and a sequence of step change in temperature is introduced. The time step of temperature change is the same as that of the irradiance, 0.2 seconds. The temperature starts with 25°C stepped up to 50°C and finally to 70°C. The obtained results are depicted in figure (3.7).

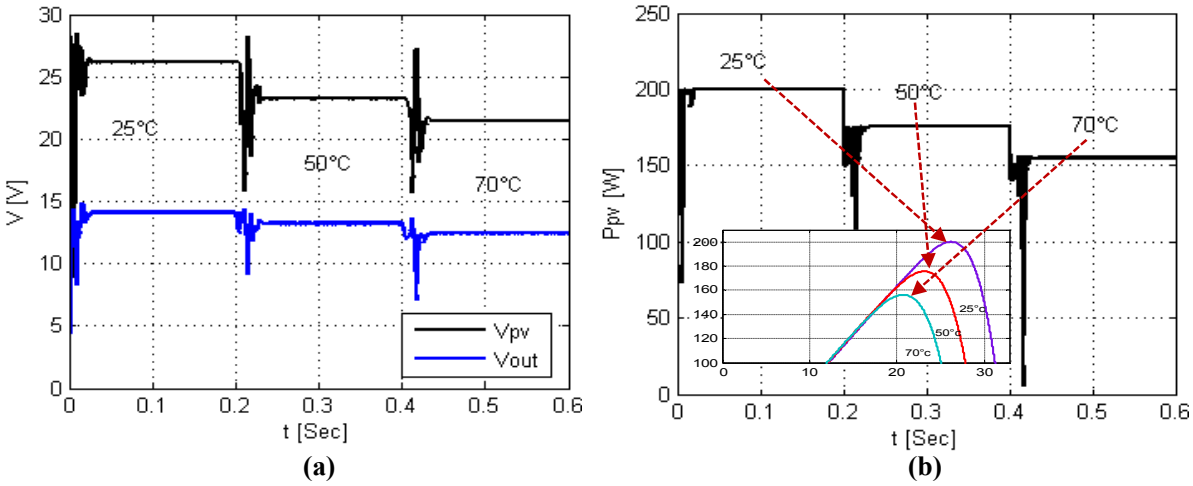

Figure 3. 7: Results of changing in the irradiance level: (a) Voltage waveforms, (b) PV panel output power

Upon comparison of the P-V characteristics at the above temperature values with those extracted by GSO-MPPT, the effectiveness of the latter and its accuracy in tracking the MPP when the PV panel undertakes variation of temperature can be checked.

3.3.4. Tests under PSCs

In this sub-section, the behavior of the proposed algorithm is investigated while the PV module undergoes PS. Two tests have been carried out on the PVG, whose P-V characteristics are shown in figure (3.8).

Figure (3.8) depicts I-V and P-V characteristics of a partially shaded PVG composed of two series connected KC200GT PV modules. The red line represents the characteristic of the PVG with uniform solar irradiance (1 kW/m²). The blue

characteristics are obtained by varying the irradiance of only one module from 0.8 kW/m^2 to 0.4 kW/m^2 with a step of 0.2 kW/m^2.

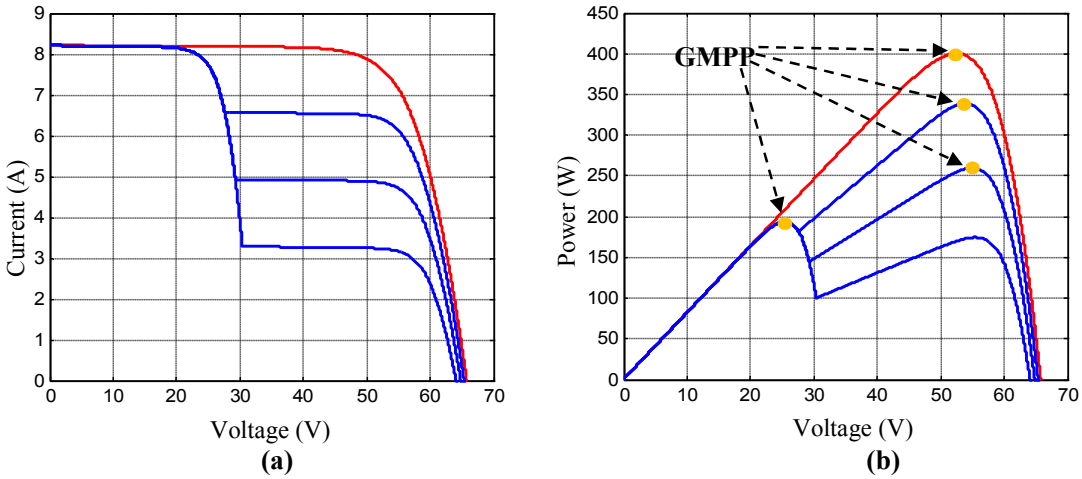

Figure 3. 8: PVG characteristics under PS, (a) I–V curve, (b) P–V curve

- **Test 1**

Initially, the PVG is operated under UICs where the irradiance and temperature levels are those of STC, G=1 KW/m² and T=25°C, respectively. At t=0.2 seconds the PS occurs when the irradiance of one module is reduced to 800 W/m² such that the resulting P-V characteristic curve is the one given on figure (3.8-b) and the GMPP available is 340W. Figure (3.9) shows the simulation results of the PVG under these conditions by using the developed GSO-MPPT.

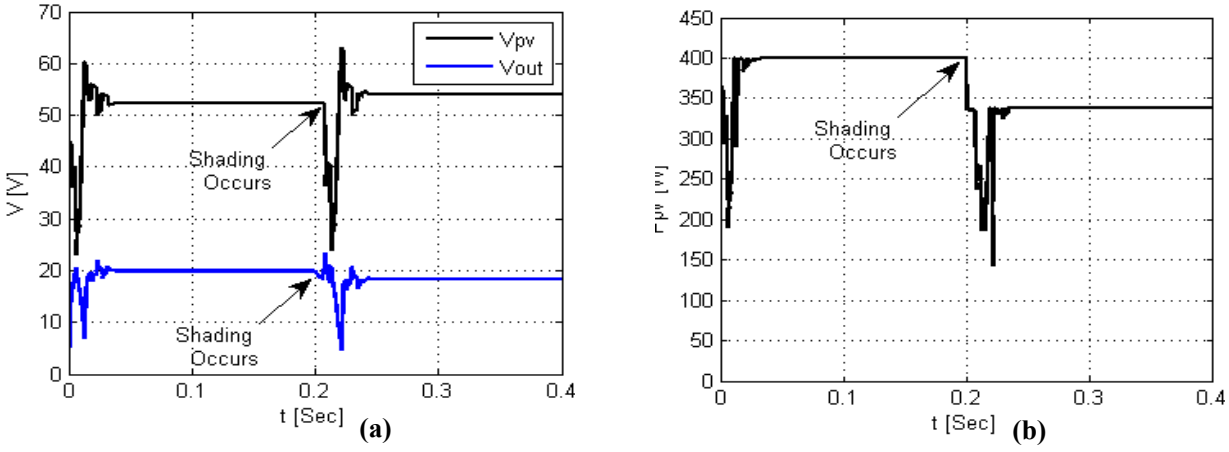

Figure 3. 9: Operation under PSCs, (a) Voltage waveforms, (b) PVG output power

Under UICs, the PVG generates 400 W along the interval from 0 to 0.2 seconds, see figure (3.9-b). This value is the result of the sum of two identical series connected PV modules operating at their MPP thanks to the GSO-MPPT.

At t=0.2s, one of the modules receives an irradiance of 800W/m^2 which makes the PV panel undergoes PS and the P-V characteristic of the PVG has two peaks with the GMPP being 340W. Figure (3.9-a) and figure (3.9-b) show that the proposed algorithm converged rapidly to the appropriate voltage leading to the GMPP of 340W.

- **Test 2**

To assess the robustness of the proposed algorithm in seeking the GMPP, the PVG has been subjected to non-uniform irradiance from the starting. PV module 1 receives an irradiance of 800W/m² and the other one receives 1000W/m², the temperature is kept constant at 25°C. The obtained results are shown in figure (3.10). It is clearly observed, that the GSO-MPPT is not trapped by the LMPP of the P-V characteristic and has converged accurately to the GMPP.

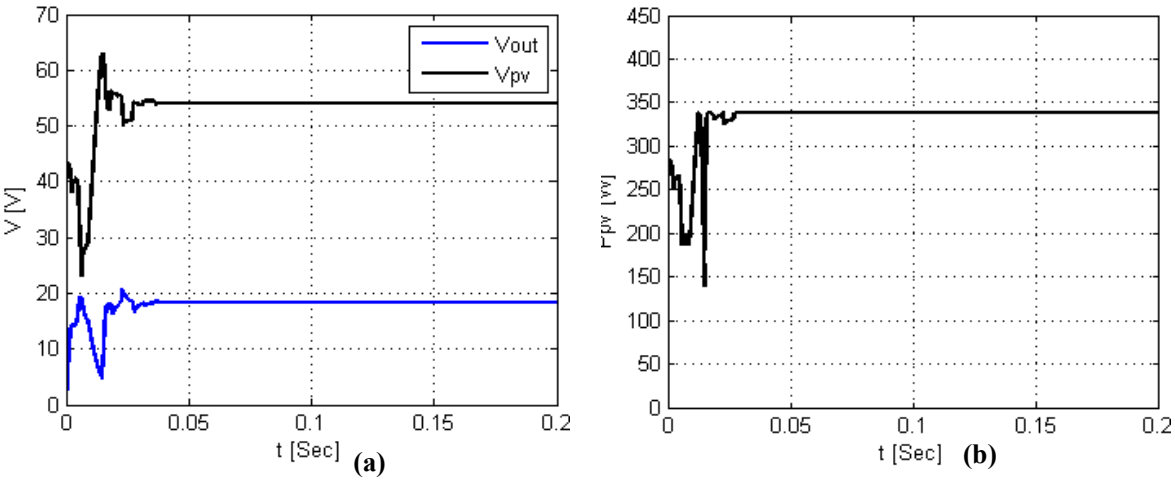

Figure 3. 10: Operation under PSCs, test2 (a) Voltage waveforms, (b) PVG output power

Besides the two successful tests under PSCs, performed previously, GSO-MPPT has been tested with many other shading patterns. The results indicate that GSO-MPPT cannot track accurately the GMPP when the shading pattern applied to the PVG is complicated. In other words, when the P-V characteristic curve exhibits power peaks more than two, GSO-MPPT will be not able to track accurately the GMPP.

3.4. Comparison with other MPPT methods

In this section, a performance comparison between the proposed method and others recently published MPPTs is undertaken by employing the most used assessment criteria such as: convergence time, MPPT efficiency, required sensors,

algorithm's complexity, etc. One should differentiate between the conversion efficiency of PV modules (given by equation (2.5)) and the MPPT efficiency. Conversion efficiency, being difficult to estimate as a parameter since it requires the knowledge of the amount of insolation falling on the PVG surface, its value is very low compared to MPPT efficiency. In the present comparison, the latter efficiency is the only parameter of interest. As discussed in [141], the MPPT efficiency (static or dynamic efficiency) is an important parameter for assessing the performance of MPPT methods. The static efficiency describes the ability of a MPPT to find and hold the desired MPP under constant environmental conditions (i.e. constant irradiance and temperature). Before evaluating the static efficiency, a stabilization period is necessary. When the steady state is achieved, it can be defined as:

$$\eta_{MPPT}(t) = \frac{P_{pv}(t)}{P_{max}(t)} \times 100 \tag{3.12}$$

Where, $P_{pv}(t)$ represents the measured output power of the PVG under the control of the MPPT, whereas $P_{max}(t)$ is the output power at the true MPP. In the case of discrete time calculations, the static efficiency is calculated as follows:

$$\eta_{MPPT} = \frac{P_{pv}(n)}{P_{max}(n)} \times 100 \tag{3.13}$$

In order for the static efficiency to be evaluated more accurately, it can be averaged over a multiple number of samples when the steady state is achieved.

In the case of fast varying atmospheric conditions, the static efficiency cannot provide a sufficient degree of precision about the MPPT performance. Therefore, the dynamic efficiency has to be considered. The latter efficiency describes the ability of a MPPT method to track the desired MPP in the case when the irradiance and temperature change frequently. It can be determined as the average ratio between $P_{pv}(t)$ (i.e. the measured PV output power under the control of MPPT) and $P_{max}(t)$ (i.e. the output power at the true MPP) over a desired time interval. The latter takes into account the transient and the steady state conditions. It is defined as:

$$\eta_{MPPT} = 100 \times \frac{\int_0^T P_{pv}(t)\,dt}{\int_0^T P_{max}(t)\,dt} \tag{3.14}$$

In the case of discrete time calculations and by considering a sampling period T_s, the dynamic efficiency is calculated as follows:

$$\eta_{MPPT} = 100 \times \frac{\sum_{n=1}^{N} P_{pv}(n).T_s}{\sum_{n=1}^{N} P_{max}(n).T_s} = 100 \times \frac{\sum_{n=1}^{N} P_{pv}(n)}{\sum_{n=1}^{N} P_{max}(n)} \quad (3.15)$$

With the purpose of demonstrating the effectiveness of the proposed GSO-MPPT in tracking the MPP under static and dynamic conditions. It is compared with six MPPT methods, where different indices are adopted and employed for the evaluation of each technique. Some MPPT techniques are validated under static tracking condition only and some of them have been validated even under dynamic tracking conditions. Because of this, two different comparison studies will be investigated in this section. The first study, which regards static tracking, compares the proposed MPPT with others based on some performance indices such as: convergence time, static error, power production, static efficiency, required sensors, algorithm's complexity, etc. The second study, which regards dynamic tracking, compares the proposed the MPPT with others based on the dynamic efficiency, convergence time and complexity level.

3.4.1. Regarding static tracking

In this test, the proposed method is compared with conventional P&O and two recently published MPPT methods which are based on FLC. The FL based MPPT [78] was called Hill-Climbing FLC (HC-FLC). This technique uses 16 fuzzy control rules which have been derived from the principle of conventional HC MPPT. Therefore, this technique aims to take advantage of conventional HC MPPT search and overcome its three drawbacks, such as: the slow convergence, the considerable steady state oscillations and the large deviation from the MPP under fast variations of irradiance level. The second MPPT is known as adaptive P&O-FLC method [36]. This method is inspired from the principle of conventional P&O MPPT algorithm. It uses the same inputs of conventional P&O and replaces the comparison, switching and voltage reference updating by FLC. The universe of discourse of the two inputs has been covered by 5 fuzzy sets which results in 25 fuzzy rules. The two above methods as well as conventional P&O have been reprogrammed using

Matlab/Simulink software package and applied to the same PV module associated with GSO-MPPT being presented in this chapter.

Figure (3.11) shows the simulation results of the above two FL-MPPT techniques, the conventional P&O MPPT and the GSO-MPPT. Simulation has been done at STC in order to compute the static efficiency. It can be noticed that all the MPPT techniques have converged to the right MPP but with different performance indices that are shown in table (3.2).

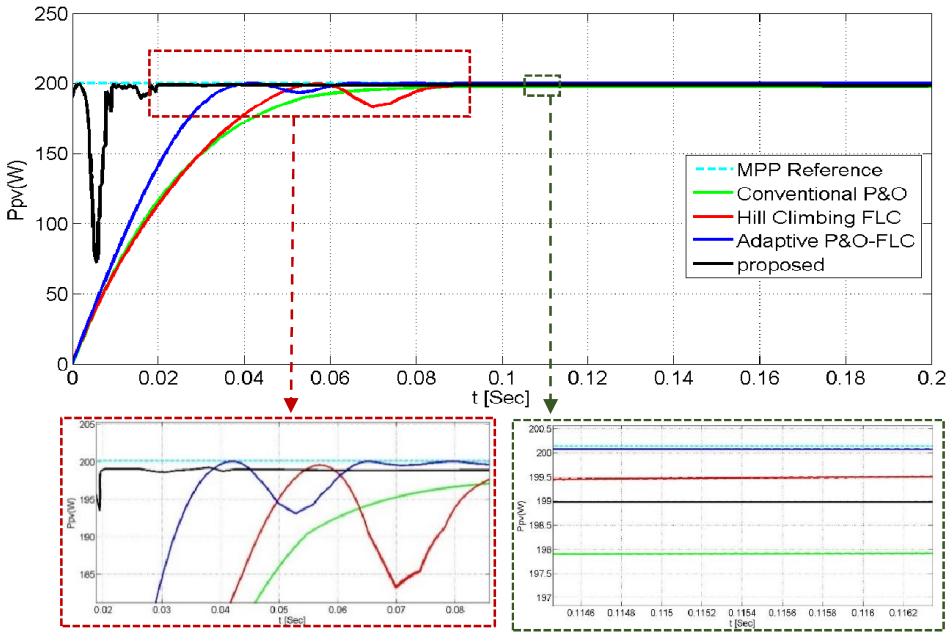

Figure 3. 11: The PV output power of the compared methods at STC

Table 3. 2: Performances of the four MPPT methods

Evaluated parameters	GSO (proposed)	Conventional P&O	HC-FLC [78] (2011)	Adaptive P&O-FLC [36] (2014)
Convergence time [s]	0.025	0.069	0.055	0.04
Static error [W]	1.143	2.343	0.643	negligible
Power production [W]	199	197.8	199.5	200.1
Static efficiency [%]	99.43	98.83	99.68	99.98
Sensors used	(current, voltage)	(current, voltage)	(current, voltage)	(current, voltage)
Tracking method	GSO	P&O	FLC with 16 rules	FLC with 25 rules
Algorithm's complexity	Very low	Very low	Medium	High
Direct duty cycle control	No	No	Yes	Yes
Robustness	Yes	yes	yes	yes

It can be observed that conventional P&O method has low complexity but it presents the highest static error (2.343W) and the lowest efficiency (98.83%). It is obvious that HC-FLC presents less complexity with only 16 rules as compared to the adaptive P&O-FLC and outperforms the conventional P&O. However, the static efficiency is lower as compared to that of the adaptive P&O-FLC that provides the highest static efficiency but at the expense of using 25 rules making it the most complex in terms of implementation.

The proposed method performs better control in terms of convergence time and presents an algorithm as simple as that of the P&O. In addition, the proposed method has no parameter to tune and it uses two conventional sensors. The static error of the proposed GSO-MPPT is higher than those of FLC based-MPPTs but lower than that of the conventional P&O MPPT that is still used.

3.4.2. Regarding dynamic tracking

In the previous sub-sections, it has been shown that the proposed GSO-MPPT tracks accurately the MPP irrespective of the climate conditions. In fact, to verify the dynamic tracking of the proposed algorithm, the PV module must exhibits a special variation of the irradiance according to the European Standard EN50530 [142].

The test sequence starts with 30% of G_{STC} (1 KW/m^2) that takes some initial setting time, and then the irradiance is linearly increased with a given slope during a raise time t_1 to standard G_{STC}. The irradiance is kept constant during a period of time t_2 (dwell time of the high irradiance level) then linearly dropped to its initial value for a period of time t_3 after which the irradiance will be kept constant lasting t_4 (dwell time of the low irradiance level). This pattern is repeated as much as required by the different tests. Once the test is over, the dynamic MPPT efficiency is calculated by using equation (3.14) as follows:

$$\eta_{MPPT} = 100.\frac{\int_{0}^{44} P_{pv}(t)dt}{\int_{0}^{44} P_{max}(t)dt} \tag{3.16}$$

Figure (3.12) depicts the simulated tracking waveforms and the tracking error respectively. The peaks of P_{pv} in figure (3.12-a) that result each time the irradiance level is changed come from the fact that GSO-MPPT generates two voltage

references from the search space (from the left and from the right). It is obvious that one is closer to the MPP but other is far from it. Therefore, the later causes the biggest peak. After that, power peaks decline as the search space around the MPP narrows till the algorithm converges to the real MPP. By evaluating equation (3.14), the dynamic efficiency has been found to be 99.602%.

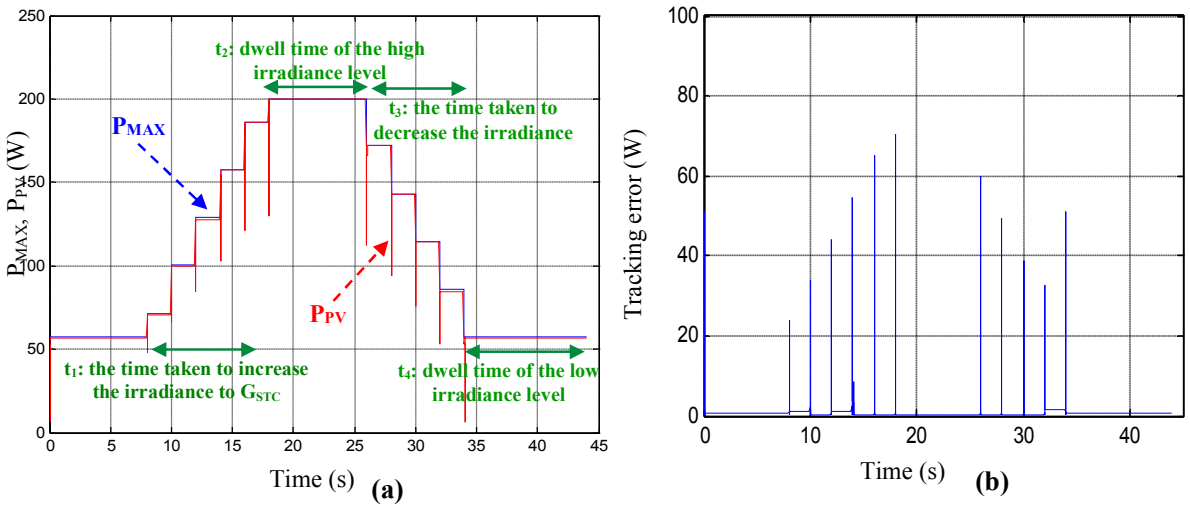

Figure 3. 12: Dynamic tracking results: (a) Power waveforms, (b) Tracking error

Table (3.3) depicts a comparison in terms of dynamic MPPT efficiency and convergence time between the GSO-MPPT and the ANFIS proposed in [143] as well as the two Emulated MPP Locus (EML)-based MPPTs proposed in [144]. As can be seen from table (3.3), the dynamic efficiency of the proposed GSO-MPPT is comparable with the efficiency of the methods proposed in [144], but the convergence to MPP is slower. Obviously, EML-based MPPTs are very fast because both methods piecewise line segments (PLS) and cubic equation (CE) use an emulator of MPP locus (EML). Using either a PLS or CE to model the MPP locus makes the process of seeking the MPP as simple as a forward computation of first order or polynomial single variable equation respectively.

Table 3. 3: Dynamic MPPT efficiency and complexity level

Evaluated parameters	GSO (proposed)	ANFIS [143] (2014)	PLS [144] (2013)	CE [144] (2013)
Convergence time [Sec]	0.025	0.25	0.007	0.007
Dynamic efficiency [%]	99.602	--	99,67	99.85
Complexity level	Low	Medium	Medium	Medium

The parameters of these equations are obtained by an off-line trained ANN using the PV characteristics of the investigated PVG. As results, both MPPT methods are model-based techniques that are expected to be very fast. However, besides the lack of robustness of model- based MPPTs, both techniques [144] are trained using data obtained by varying only the irradiance level. To take into account the effect of the temperature, a compensation circuit is used to shift left /right if the operating temperature increases /decreases, however, shifting the operating point is not as accurate as seeking the MPP using an MPPT algorithm. As reported in [66] the main drawback of ANNs or ANFIS-based MPPT is that it could fail when the PV modules start to be degraded, in this situation, training with new data should be carried out periodically. Finally, upon comparison with the aforementioned methods, the proposed GSO-MPPT's can easily track the GMPP with fast convergence time.

3.5. Conclusions

In order to improve the efficiency of PV systems, the PV module is associated to a chopper whose voltage or duty cycle is controlled by a MPPT algorithm. In this chapter, a new MPPT algorithm which is based on GSO technique has been presented. First, the chapter presents the principle of the GSO technique and then derives the flowchart of the MPPT based on this new investigated technique. Several tests have been conducted to verify the performances of the algorithm under STC conditions, fast changing conditions and PSCs. The main advantages are:

1. The GSO-MPPT does not require any derivatives. Therefore, only addition/subtraction and multiplications are used in the algorithm which employs a few arithmetic operations to compute the reference voltage. Moreover, the algorithm has no parameter to tune.
2. The convergence of the algorithm is very fast as the MPP is reached approximately within seven (7) steps.
3. Once the MPP is reached, the PV module operates with constant voltage and current without any steady state oscillations avoiding hence waste of energy due to oscillations.
4. Under fast changing atmospheric conditions, the algorithm exhibits high dynamic efficiency with very low tracking error.

However, it must be underlined that GSO-MPPT suffers from dependence on the PV parameters since it requires the knowledge of the value of the open circuit-voltage of the PVG. This value constitutes the upper value while zero is the lower value of the search space used by the GSO-MPPT. Moreover, GSO-MPPT may be trapped at LMPP when the PV characteristic curve has more than two peaks. This explains the need to develop a new MPPT method which is able to identify and track the GMPP under any complicated shading pattern and without any dependence on the PV system parameters.

CHAPTER 4
A NEW INTELLIGENT MPPT FOR PV SYSTEMS OPERATING UNDER FAST TRANSIENT VARIATIONS OF SHADING PATTERNS

4.1. Overview

This chapter introduces a novel method to track the GMPP under PSCs, for PV systems. The method combines two loops, a new scanning-storing loop as well as a tracking loop which is based on FLC.

Simulation results indicate that the developed MPPT performs better and guarantees an accurate convergence to the GMPP under complicated shading patterns. Furthermore, it provides a fast convergence to the GMPP in rapid transient variation of shading.

To evaluate the effectiveness of the developed MPPT, a comparison study with three recently published MPPTs has been carried out. The obtained results show that the developed MPPT has greatly enhanced the tracking efficiency under PSCs. Fast convergence, negligible oscillations and system-independent are the main advantages of the proposed MPPT.

4.2. PV interface configurations for standalone PV systems

4.2.1. Standalone PV systems

Off-grid PV systems can be categorized as either standalone or building integrated. Standalone PV system-design assumes that the system is not embedded in the building, unlike the building integrated design [145].

Standalone PV systems can be defined as systems with one or more distributed generation source, power-conditioning circuits, controllers, associated loads, storage systems and may operate independently from a utility grid [146]. Standalone PV systems are regarded as an effective solution to provide electricity to the places where connection to the local grid is impossible or would require very high costs to develop electricity grid. Therefore, they represent a key solution for population living in remote areas and having no access to grid utility while solar radiation is abundantly available.

4.2.2. PV interface configurations

PV Interface Configuration (PVIC) pertains to the way the chopper/inverter is connected. Different structures of PVIC for standalone PV systems have been presented in [28]. Figures (4.1-a) and (4.1-b) display a string and centralized PVICs that have been extensively used, due to their high power conversion efficiency. As well as, their low-cost design that consists of only one DC-DC converter, two sensors (current and voltage sensors) and MPPT controller to extract the MPP from the PVG [147]. However, the main disadvantage of string and centralized PVICs appears under PSCs when the MPPT fails to track the GMPP and gets trapped in one of the existing LMPPs, which results in the total efficiency decrease [148]. Therefore, using a suitable MPPT that is able to cope with PS problems is necessary. In multi-string PVIC shown in Figures (4.1-c), each string is connected to its own converter, sensors and MPPT controller. The latter connections allow tracking the MPP of individual PV string and hence improving the overall efficiency of the PV system. However, this PVIC requires using many converters, sensors and controllers, which in turn increases the initial cost of the PV installation. In addition to the higher switching losses that result from using many converters.

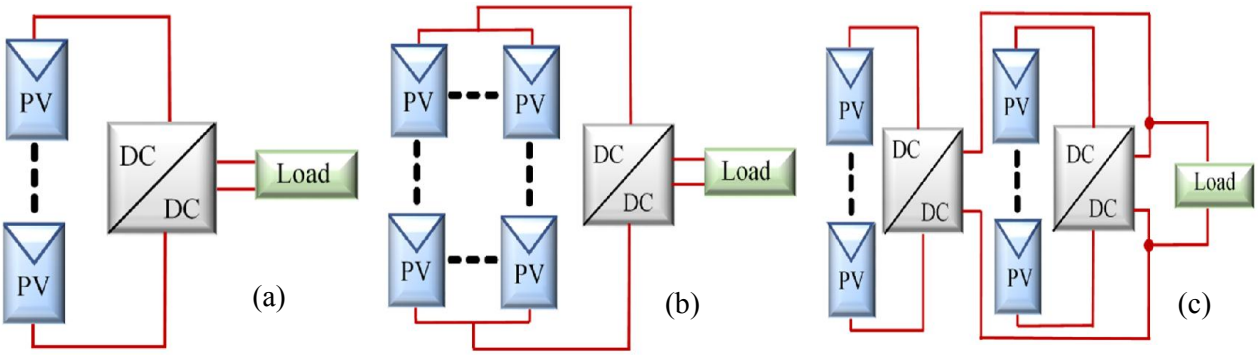

Figure 4. 1: PV interface configurations: (a) string, (b) centralized and (c) multistring

4.3. The proposed MPPT

This section presents a new MPPT technique that has been developed to track the GMPP of PV systems operating under uniform and non-uniform irradiance conditions. It combines a scanning-storing procedure with FLC-based MPPT. The block diagram of a standalone PV system with the proposed MPPT is depicted in figure (4.2). The scanning-storing procedure aims to identify the GMPP and its corresponding duty cycle $D_{GMPP,}$ then, the tracking loop based-FLC is activated to

track the identified GMPP. The major purpose of the proposed MPPT is to increase the tracking response and improve the efficiency of the PV system under PSCs.

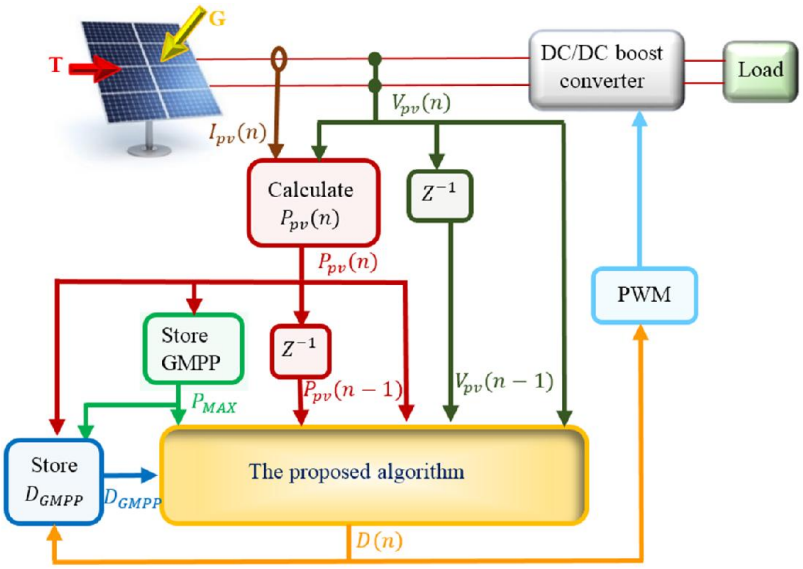

Figure 4. 2: The block diagram of the PV system with the proposed MPPT.

4.3.1. MPPT algorithm

The proposed MPPT algorithm is presented in the flowchart shown in figure (4.3).

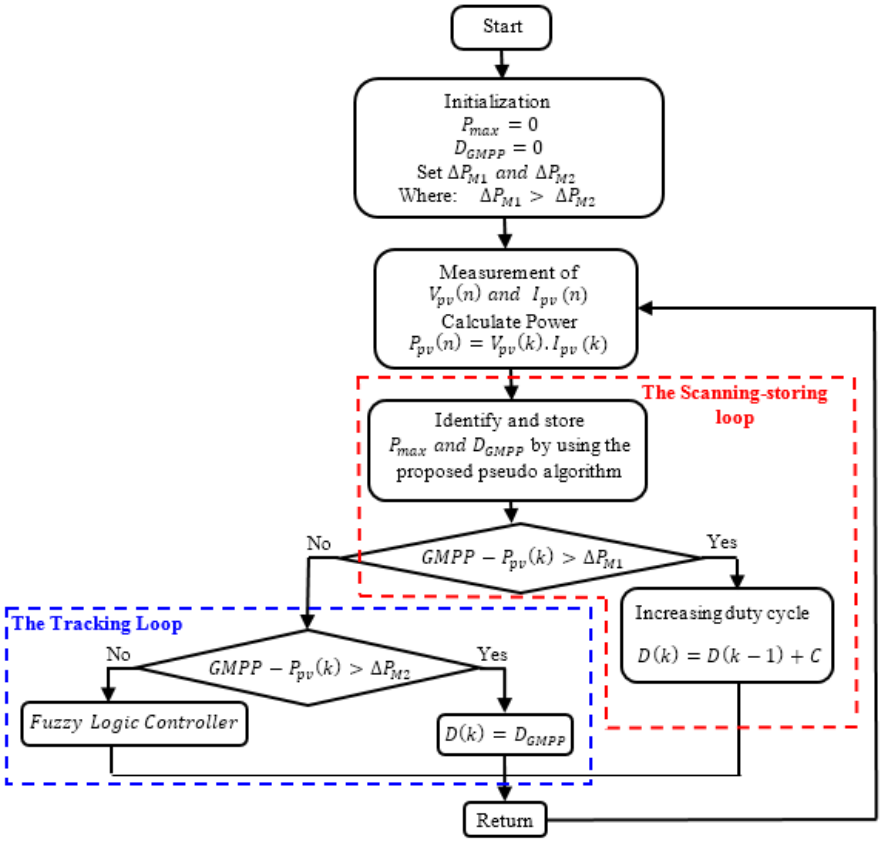

Figure 4. 3: Flowchart of the new MPPT algorithm.

As shown in the flowchart of figure (4.3), at the beginning, the MPPT's initial parameters are initialized by assigning 0 W to the maximum power (P_{max}), and 0 to the duty cycle corresponding to the GMPP (D_{GMPP}). ΔP_{M1} and ΔP_{M2} are two prefixed values which represent the allowable power difference between the GMPP and $P_{pv}(n)$. ΔP_{M1} must be chosen greater than ΔP_{M2}.

Then, the PVG output current $I_{pv}(n)$ and voltage $V_{pv}(n)$ for the *nth* instant are measured. Thus, the instantaneous power $P_{pv}(n)$ is calculated by multiplying $I_{pv}(n)$ by $V_{pv}(n)$.

During initial condition or varying weather conditions, the scanning-storing procedure is carried out by scanning the PV power output to identify and store the GMPP and D_{GMPP}. The scanning-storing loop is based on an observation that has been resulted by investigating different P-V characteristic curves under different shading patterns [149]. The study reveals that the amplitudes of power peaks of any P-V characteristic curve, are increasing before the GMPP and display the trend of decreasing as the peaks are longer away from the GMPP.

During the operation of the scanning-storing loop, the duty cycle is increased from its minimum value D_{min} until its maximum value D_{max} with a fixed step size C. Meanwhile, the output power $P_{pv}(n)$ must be analysed by executing the pseudo algorithm presented in sub-section (4.3.2), to identify the GMPP and D_{GMPP}.

A comparison between the GMPP and the instantaneous power $P_{pv}(n)$ is made to conclude the scanning-storing loop and start the tracking loop. Therefore, if the difference $GMPP\text{-}P_{pv}(n)$ is greater than the prefixed value ΔP_{M1}, the scanning-storing loop continues increasing the duty cycle, looking for other greater peak. On the contrary, the tracking loop is carried out by examining if the difference $GMPP\text{-}P_{pv}(n)$ is greater than the prefixed value ΔP_{M2}. If the last condition is satisfied, D_{GMPP} is applied to move the operating point rapidly near the GMPP. Otherwise, the FLC is carried out to reach the GMPP with minimum power ripples.

4.3.2. The scanning-storing procedure

As explained before, the scanning-storing procedure carried out by increasing the duty cycle from its minimum value D_{min} until reaching its maximum D_{max} with a fixed step size C in order to sweep the PV power. Meanwhile, GMPP and D_{GMPP} are identified and stored. D_{max} is the duty cycle corresponding to the instantaneous measured power that meet the condition $GMPP\text{-}P_{pv}(n) \leq \Delta P_{M1}$. Figure (4.4) shows the

process of the scanning-storing procedure, while the pseudo algorithm of the procedure is reported below.

To identify the GMPP, the stored maximum power P_{max} must be compared with the instantaneous measured power $P_{pv}(n)$, where the GMPP is identified as the maximum value of P_{max} (As shown in figure 4.4)

$P_{max}(n) = \max(P_{pv}(n), P_{max}(n-1))$.

$GMPP = \max(P_{max}(n))$.

To identify the D_{GMPP}, the power variation ΔP_{pv} and the variation between the P_{max} and P_{pv} are calculated,

$\Delta P_{pv}(n) = P_{pv}(n) - P_{pv}(n-1)$.

$\Delta P_{max}(n) = P_{max}(n) - P_{pv}(n)$.

The following conditions should be verified, knowing that D(n) is the actual duty cycle.

If $\Delta P_{max}(n) \leq 0$ and $\Delta P_{pv}(n) \geq 0$

Then $d_{GMPP}(n) = D(n)$

Else $d_{GMPP}(n) = d_{GMPP}(n-1)$

End $D_{GMPP} = d_{GMPP}(n)$

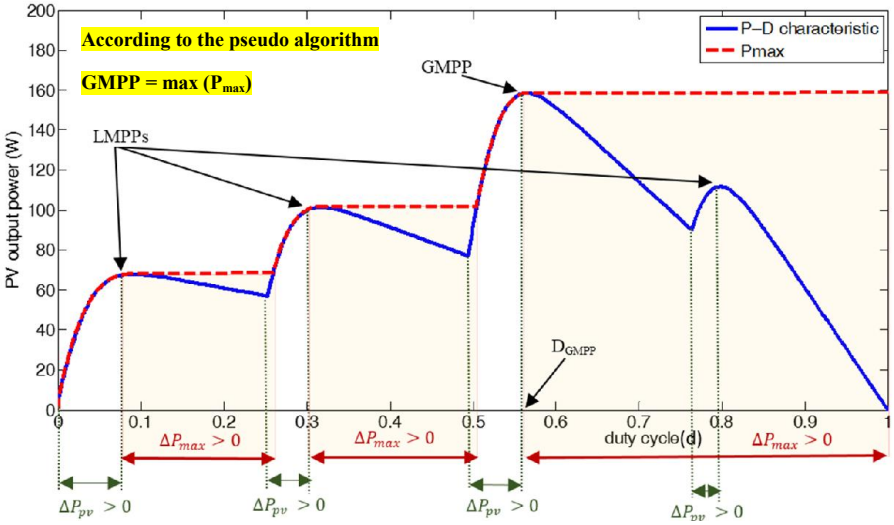

Figure 4. 4: The scanning-storing procedure to identify the GMPP and D_{GMPP} according to the pseudo algorithm.

4.3.3. FLC design

The main role of the FLC is to control the PVG outputs (current and voltage) by means of a DC-DC converter. The FLC inputs are E and ΔE at the sampling time n, which are defined by equations (4.1) and (4.2) [80]:

$$E(n) = \frac{P_{pv}(n) - P_{pv}(n-1)}{V_{pv}(n) - V_{pv}(n-1)} \tag{4.1}$$

$$\Delta E(n) = E(n) - E(n-1) \tag{4.2}$$

Where E(n) is the instantaneous error that indicates if the operating point is located on the left or the right side of the MPP. ΔE(n) is the instantaneous error-change that indicates the moving direction of the operating point.

As figure (4.5) illustrates, the FLC generally consists of three stages: Fuzzification, Inference (i.e. including the rules based) and Defuzzification. Those stages are involved in tracking the desired MPP.

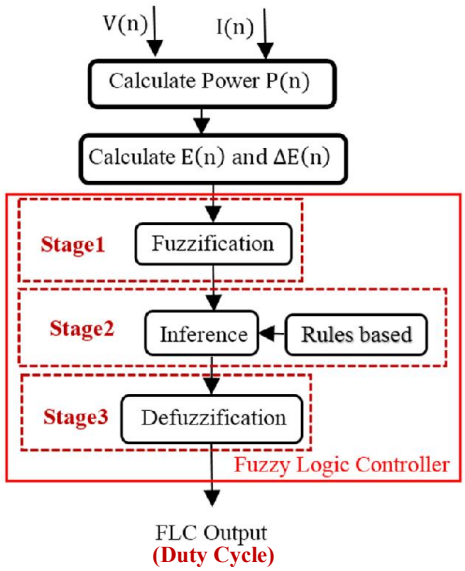

Figure 4. 5: Block diagram of FLC algorithm

According to the block diagram shown in figure (4.5), the inputs E(n) and ΔE(n) are calculated by using equations (4.1) and (4.2), respectively. Then, each numerical input is converted by means of membership-functions into linguistic values (stage1).

With reference to figure (4.6), the universe of discourse for each input membership-function is divided into five fuzzy sets described as follows: NB (Negative Big), NS (Negative Small), ZE (Zero), Ps (Positive Small) and PB (Positive Big).The same number of partitions is used for the FLC output (change in duty cycle).

The fuzzy inference employs Mamdani's max-min inference system, managed by the research in the fuzzy rules (stage 2). After the rules application, a defuzzifier based on the center of gravity technique is employed to adjust and generate the control signal, which is the instantaneous duty cycle (stage 3). This output is transmitted to the DC-DC converter switch (MOSFET or IGBT) by means of a PWM generator in order to achieve the GMPP.

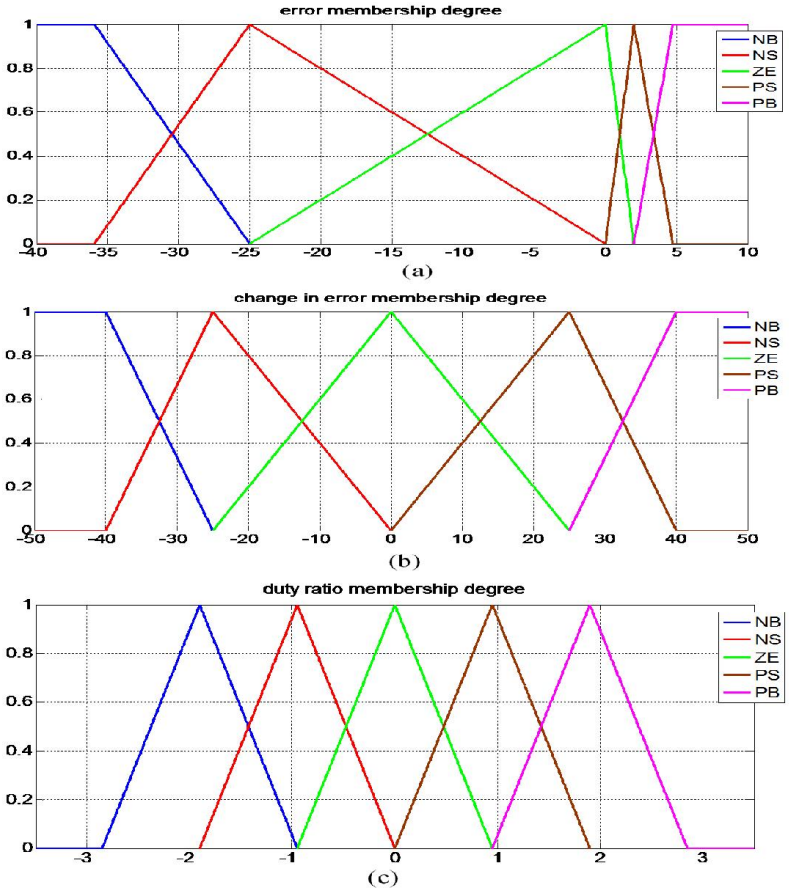

Figure 4. 6: Membership-functions related to the input and the output of FLC (a) error, (b) error change, (c) duty cycle change (output)

The fuzzy rules are reported in table (4.1). They are adapted to control a PV system that uses a boost converter as power-conditioning circuit.

Table 4. 1: Fuzzy rules

E \ ΔE	*NB*	*NS*	*ZE*	*PS*	*PB*
NB	*PB*	*PB*	*PS*	*PB*	*PB*
NS	*PB*	*PS*	*PS*	*PS*	*PB*
ZE	*NS*	*NS*	*ZE*	*PS*	*PS*
PS	*NB*	*NS*	*NS*	*NS*	*NB*
PB	*NB*	*NB*	*NS*	*NB*	*NB*

4.3.4. DC-DC boost converter

To fully utilize the PV generated energy, a PV power-conditioning circuit is required to interface the PVG and the load. The proposed MPPT has been used with a DC-DC boost converter regarding its advantages (such as: low cost, simple design and easily controlled). It is worth noting that the use of a single DC-DC boost converter to control the whole PV system results in mitigating the switching losses and the implementation cost. The output voltage V_{out} is expressed by the following equation:

$$\frac{V_{out}}{V_{pv}} = \frac{1}{1-D} \tag{4.3}$$

Where, D is the duty cycle provided by the MPPT, V_{out} is the output voltage of the DC-DC converter and V_{pv} is at the same time the PVG output voltage and the input of the DC-DC converter.

Table (4.2) reports the boost DC-DC specifications, while figure (4.7) shows its implementation using Simscape libraries.

Table 4. 2: DC-DC boost converter specifications

Designation	Values
Capacitance (C_{out})	50 µF
Capacitance (C_{in})	10 µF
Inductance (L)	2.6 mH
Frequency (f)	40 kHz

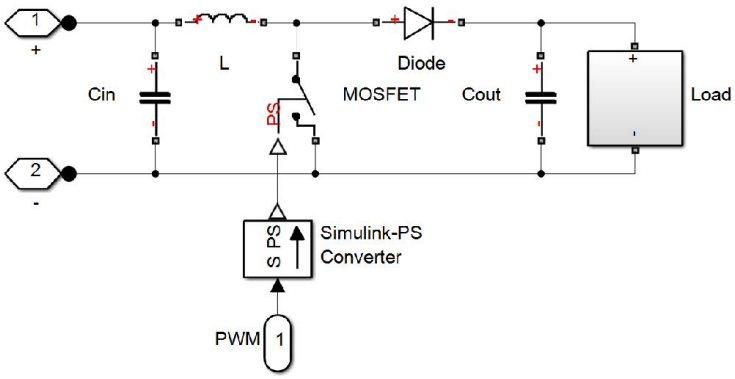

Figure 4. 7: Implementation of a DC-DC boost converter using Simscape.

4.4. Simulation results

In order to evaluate the performance of the proposed MPPT under different weather conditions, different tests were conducted on the standalone PV system that has been implemented by using Matlab/Simulink-Simscape libraries. Moreover, the tracking ability of the proposed MPPT is checked by employing different PVICs (string and centralized configurations). Figure (4.8) shows the main subsystems constituting the implemented standalone PV system.

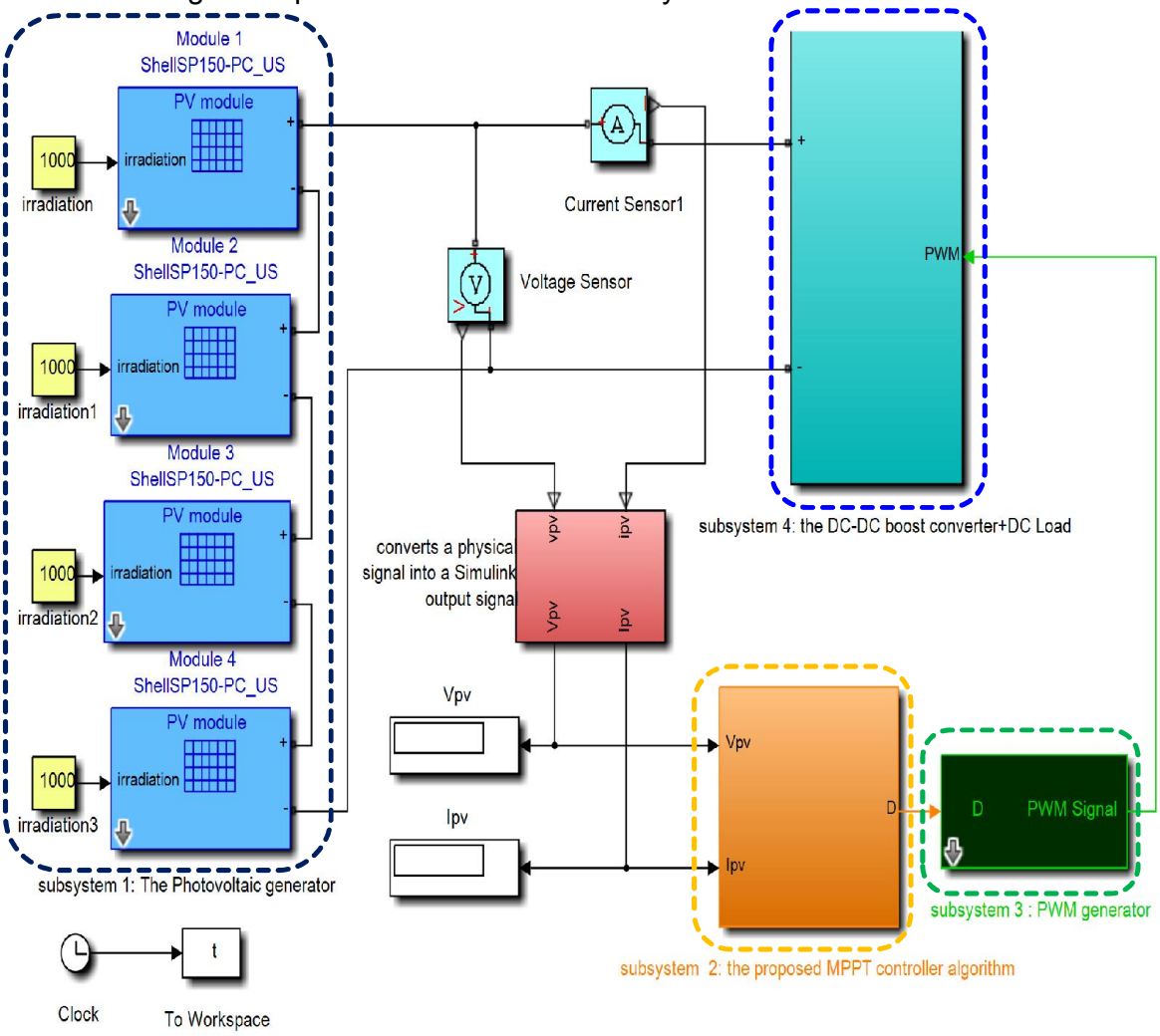

Figure 4. 8: Different blocks of standalone PV system, including the proposed MPPT.

- ***Subsystem 1***: contains the Simscape implementation of the PVG, it is composed of four series-connected PV modules type '' Shell SP150-PC ''with a rated maximum power of 600 W. Each PV module has 72 Mono C-Si solar cells connected in series, in addition to 3 bypass diodes. Table (A.4-Appendix A) gives the electrical specifications of ''Shell SP150-PC'' PV module.

- ***Subsystem 2***: contains the proposed MPPT, implemented by Matlab-Simulink libraries.
- ***Subsystem 3***: includes a PWM generator that has been used to control the DC-DC boost converter (its implementation is illustrated in figure (3.3-c)).
- ***Subsystem 4:*** consists of a DC-DC boost converter associated with a DC load (its implementation is shown in figure (4.7)). The load being connected at the output of the DC-DC converter is a resistive load having the values of 30 ohm.

4.4.1. Test under UICs

In this test, the temperature is kept constant at T=25°C and different step changes in the irradiance are introduced in order to check the performance of the proposed MPPT under fast transient variations of uniform irradiance levels.

According to figure (4.9), the irradiance starts with 500 W/m^2, stepped up to 1000 W/m^2 at 0.5s, then stepped down to 500 W/m^2 at 1s, and finally stepped up to G=700 W/m² at 1.5s.

The scanning-storing procedure causes some power loss during start up condition as well as when irradiance level changes. Nevertheless, the proposed MPPT tracks the MPP after each step of irradiance variation with relatively fast convergence time, negligible steady state oscillations and small static error (0.5 W). Moreover, by using equation (3.14), a dynamic MPPT efficiency of 98.79% has been achieved.

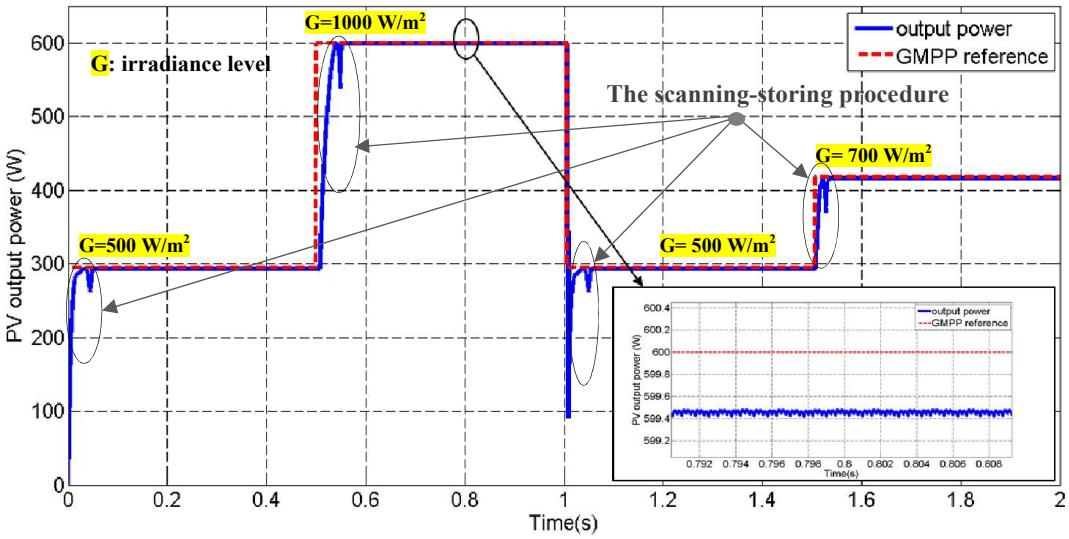

Figure 4. 9: The PV output power under fast transient variations in equally distributed irradiance levels.

4.4.2. Tests under PSCs

- **Test 1**

To evaluate the performance of the proposed MPPT under PSCs, three unshaded PV modules receive 1000 W/m^2 whereas the fourth one receives an irradiance of 525 W/m^2 which makes the PV panel undergoes PS. As shown in figure (4.10), the P-V characteristic curve exhibits two peaks, one of them represents the GMPP (443W) and the other, is the LMPP (369W). Furthermore, it is clearly observed that the proposed MPPT is able to identify and track the GMPP with success, knowing that the dynamic efficiency achieved is 99.91 %.

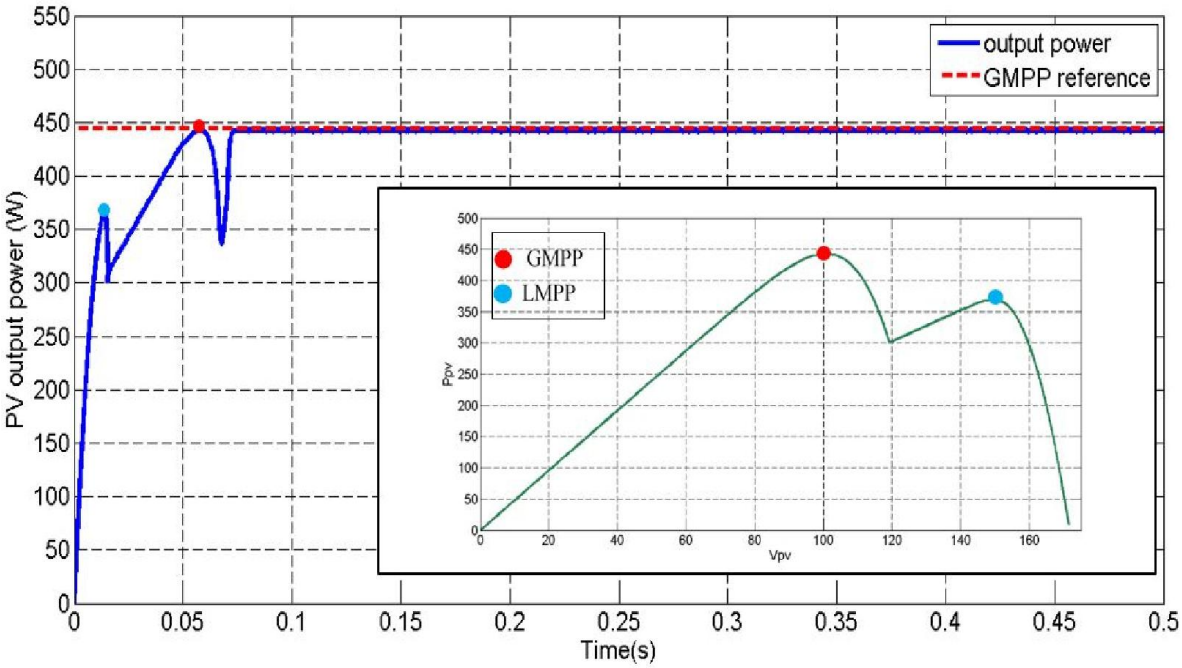

Figure 4. 10:The PV output power during PSCs along with the corresponding P-V characteristic curve.

- **Test 2**

For an extensive verification, the tracking ability of the proposed MPPT is checked against fast variation of shading patterns. Firstly, four different irradiance levels are applied to the PVG, which are set to 1000 W/m^2, 850 W/m^2, 450 W/m^2 and 100 W/m^2. Secondly, another shading pattern is applied at 0.5s, where three PV modules are fully illuminated (1000 W/m^2) and the fourth one has an irradiance of 525 W/m^2. The P-V characteristic curves resulted from each shading pattern are shown in figure (4.11).

Figure (4.11) clearly shows that the GMPP has been successfully identified among the existing LMPPs, thanks to the scanning-storing procedure. Moreover, the proposed MPPT achieves a dynamic efficiency of 97.28% thanks to the tracking loop.

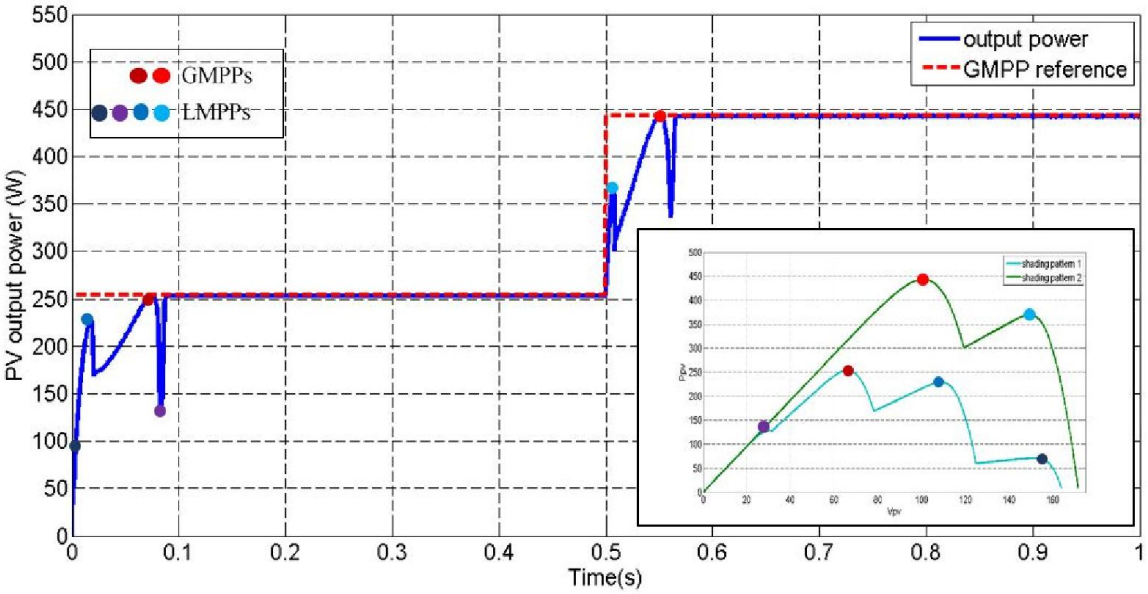

Figure 4. 11: The PV output power under fast transient variations of shading patterns, along with the corresponding P-V characteristic curve.

- **Test 3**

According to the flowchart of figure (4.3), it can be clearly seen that the proposed MPPT requires only the measured current and voltage delivered by the PVG, and does not have any dependence on the PVG parameters.

Based on previous tests using a string configuration, it can be clearly concluded that the GMPP has been well identified and tracked by the proposed MPPT. The upcoming test is devoted to verify whether the proposed MPPT has no dependence on PVICs, and hence can be used with any configuration of modules constituting the PV array. For this aim, the proposed MPPT will be associated with a centralized PVIC and tested under PSCs. The PVG is composed of two parallel strings, each string is composed of four series connected PV modules, as illustrated in figure (4.12). Each string has three fully illuminated PV modules (1000 W/m^2), while the forth one receives an irradiance of 525 W/m^2.

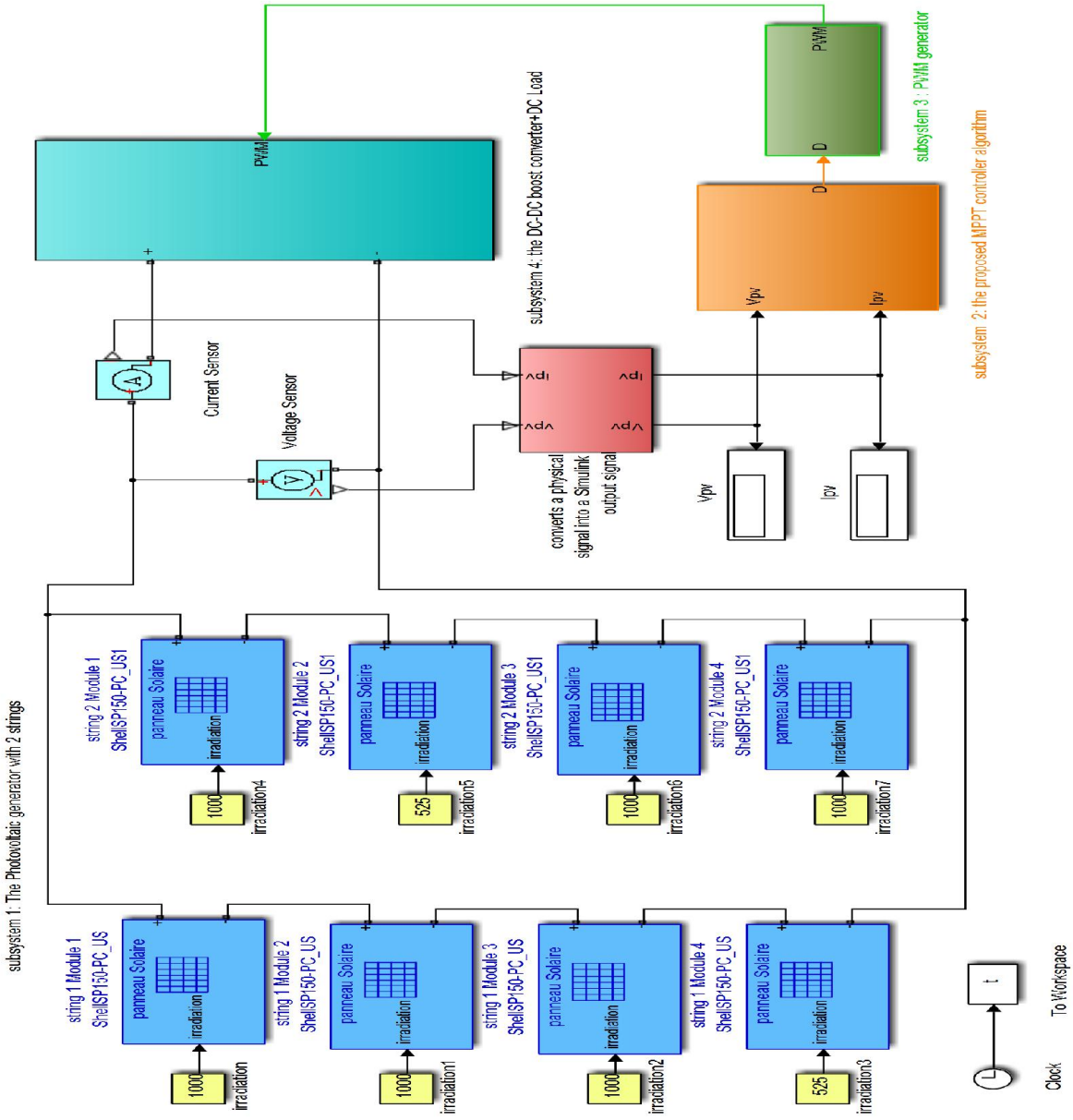

Figure 4. 12: The implementation of standalone PV system with centralized PVIC

Figure (4.13) depicts waveforms of the PV output power extracted by the proposed MPPT, along with the P-V characteristic curve. As it can be seen, the P-V curve exhibits two power peaks, one of them represents the GMPP (885 W) and the other is a LMPP (737 W). One can easily notice the ability of the proposed MPPT in identifying and tracking the GMPP (885 W) in the case where a centralized configuration is used. Therefore, it can be confirmed that the proposed MPPT has no dependence on the PVG parameters nor on the PVIC used.

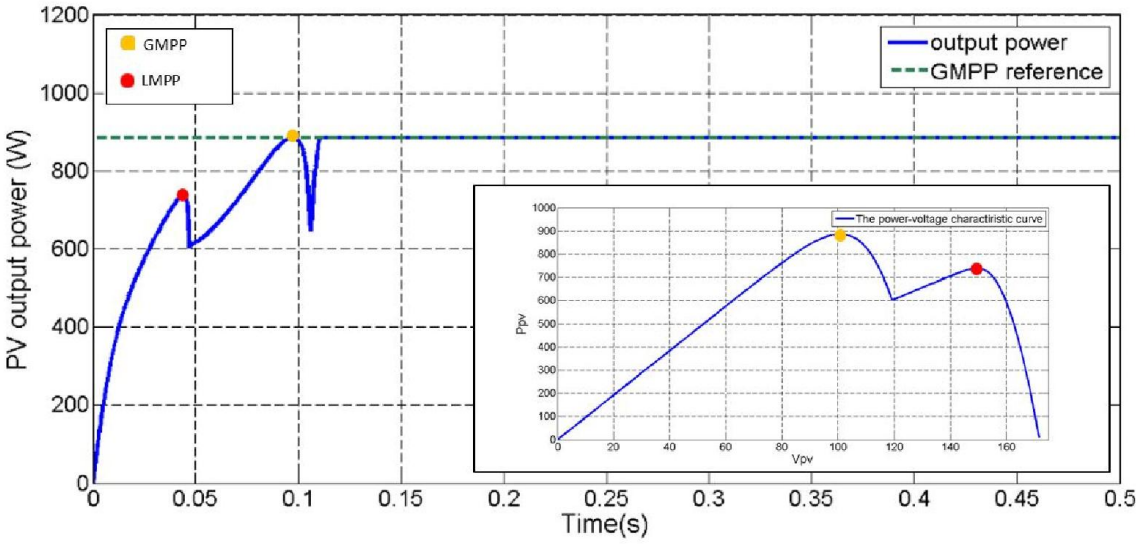

Figure 4. 13: The PV output power under PSCs using centralized PVIC, along with the corresponding P-V characteristic curve.

4.5. Comparative study

To show the effectiveness of the developed MPPT over other available MPPTs, a performance comparison between the proposed one and three MPPTs published by Alajmi *et al.* [37], Ishaque *et al.* [87] and Ji *et al.* [101] is undertaken in this part.

The MPPTs proposed by Alajmi *et al.* [37], Ishaque *et al.* [87] and Ji *et al.* [101] have been presented and discussed in chapter (1), sub-sections (1.4.1) and (1.4.2).

- **Test 1**

In this comparison, the four PV modules constituting the PVG shown in figure (4.8) receive respectively the following levels of irradiance, 980 W/m^2, 850 W/m^2, 500 W/m^2 and 100 W/m^2. The resulting P-V characteristic curve is the one given in figure (4.15-b), four power peaks have been observed and the GMPP is 253W. Under the aforementioned conditions, waveforms of the power extracted by the investigated MPPTs are depicted in figure (4.14). It can be clearly seen that the MPPT proposed by Ji *et al.* [101] has failed to track the GMPP because of the incapability of the linear function to change the voltage reference near the GMPP. On the other hand, the three other MPPTs track the GMPP with success but with different performance indices. It is worth mentioning that the proposed MPPT has the fastest response with a small static error (figure (4.14)).

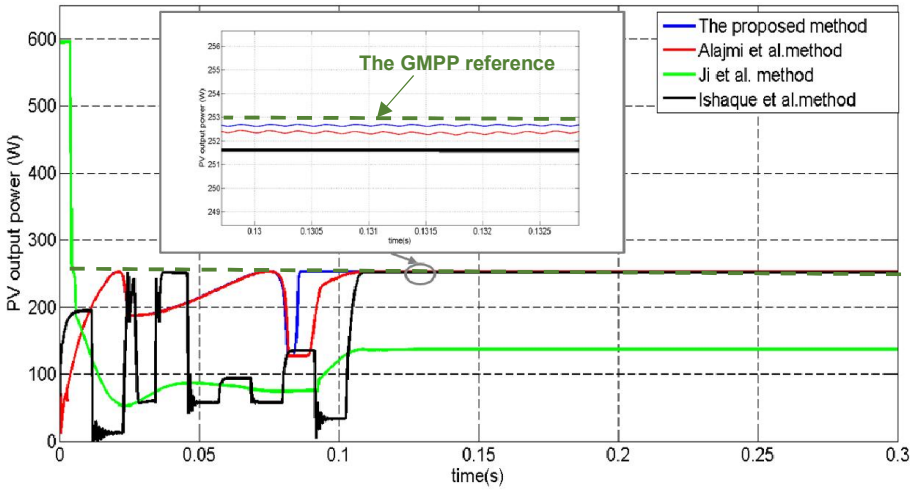

Figure 4. 14: Waveforms of the power extracted by the investigated MPPTs under PSCs (the shading pattern was 980 W/m², 850 W/m², 500 W/m² and 100 W/m²)

Figure (4.15) depicts the reason for the tracking failure of Ji *et al*. [101] MPPT.

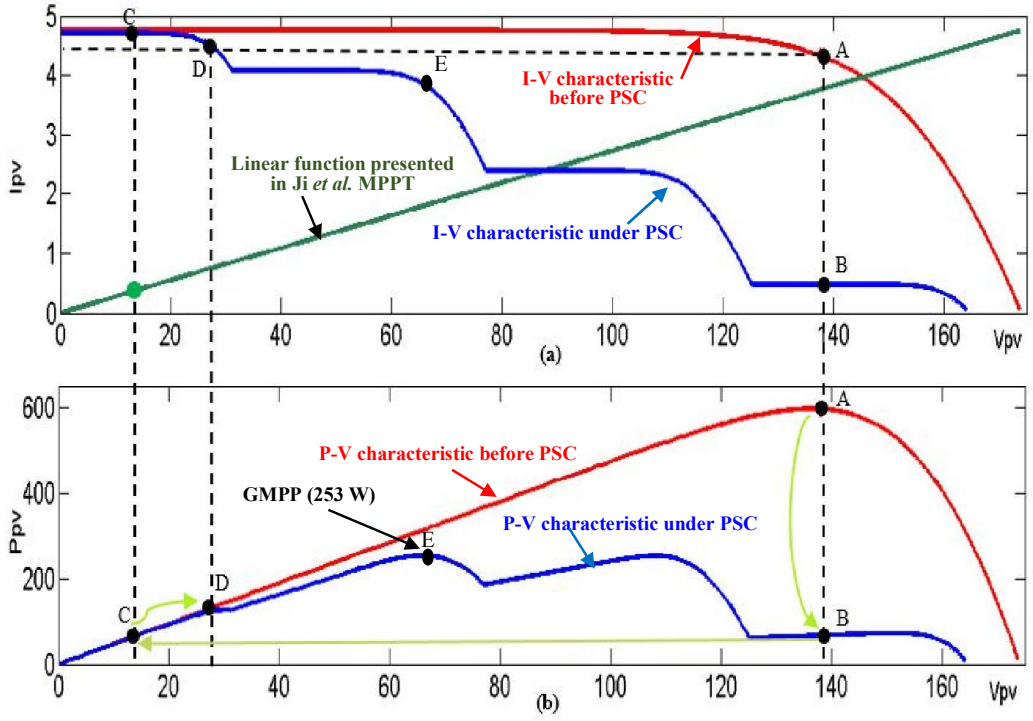

Figure 4. 15: I-V and P-V characteristics of the PV string before and under PSC along with the tracking steps performed by Ji *et al* MPPT (the movement of the operating point is from A to D (LMPP), whereas, the GMPP is located at E).

According to figures (4.15-a) and (4.15-b), initially, the irradiance has been uniform over the entire surface of the PVG. In this condition, the operating point is at the point A (MPP). Then, it has moved to the vicinity of the point B when the PVG undergoes PS. The linear function presented in Ji *et al.* [101] has been used to move the operating point from B to the lower voltage range located at the vicinity of the point C. Finally, a variable step size InCond is carried out to track the nearest peak, which is the local peak D. Therefore, the method proposed by Ji *et al.* [101] fails to perform the GMPP located at the point E as shown in figure (4.16). As a matter of fact, the linear function may fail to determine a true location near the GMPP when P-V characteristic has a number of peaks greater than three.

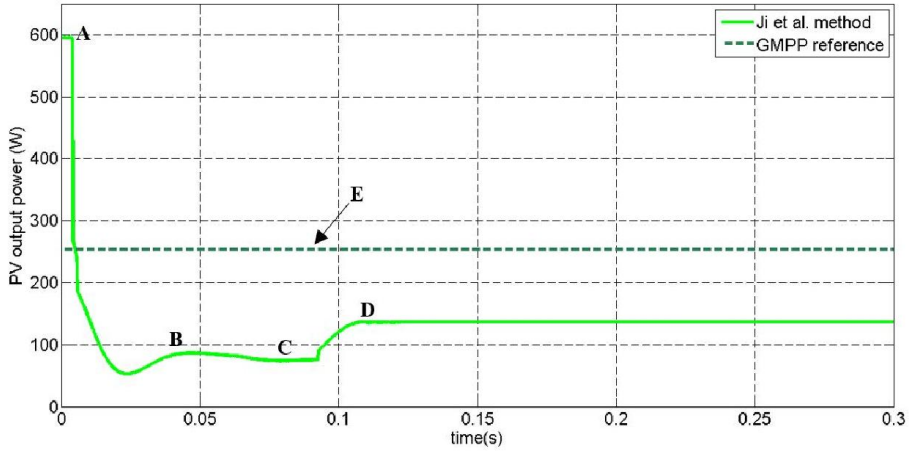

Figure 4. 16: Real time simulation of the tracking failure performed by Ji et al MPPT under 980 W/m^2, 850W/m^2, 500W/m^2 and 100 W/m^2.

- **Test 2**

Figure (4.17) shows waveforms of the power extracted by the investigated MPPT and the proposed one. In the following comparison, the PVG is composed of three series connected PV modules, two of them are fully illuminated (by 1000W/m^2) and the third one receives an irradiance of 525W/m^2.The P-V characteristic curve shown in figure (4.17-b) exhibits two peaks with a GMPP of 295 W. From the power waveforms shown in figure (4.17-a), it can be noticed that all the investigated MPPTs have converged to the GMPP but with different performance indices that are shown in Table (4.3).

According the Table (4.3), it can be observed that Ishaque *et al.* MPPT takes a long time (138 ms) to converge to the GMPP. Ji *et al.* MPPT has a low complexity.

However, it presents the highest static error (10.6 W) and high power ripples when the GMPP is achieved. The FLC used by the proposed MPPT has only 25 rules compared to that of Alajmi *et al.* [37] (32 rules). Moreover, when the P-V characteristic curve exhibits two successive peaks that have almost the same amplitude (i.e. one of them is the GMPP), the FLC employed by Alajmi *et al.* [37] may fail to track the global peak. As a result, lower probability of successfully finding the GMPP (91/100) as compared to the proposed MPPT.

Based on the results of this comparison, it can be concluded that the proposed MPPT is a good candidate for PV systems. Since it gives the possibility of improving the tracking performance in terms of different parameters such as: high tracking efficiency (99.66%), short convergence time (94 ms), no dependence on the PV system and high probability of finding the GMPP.

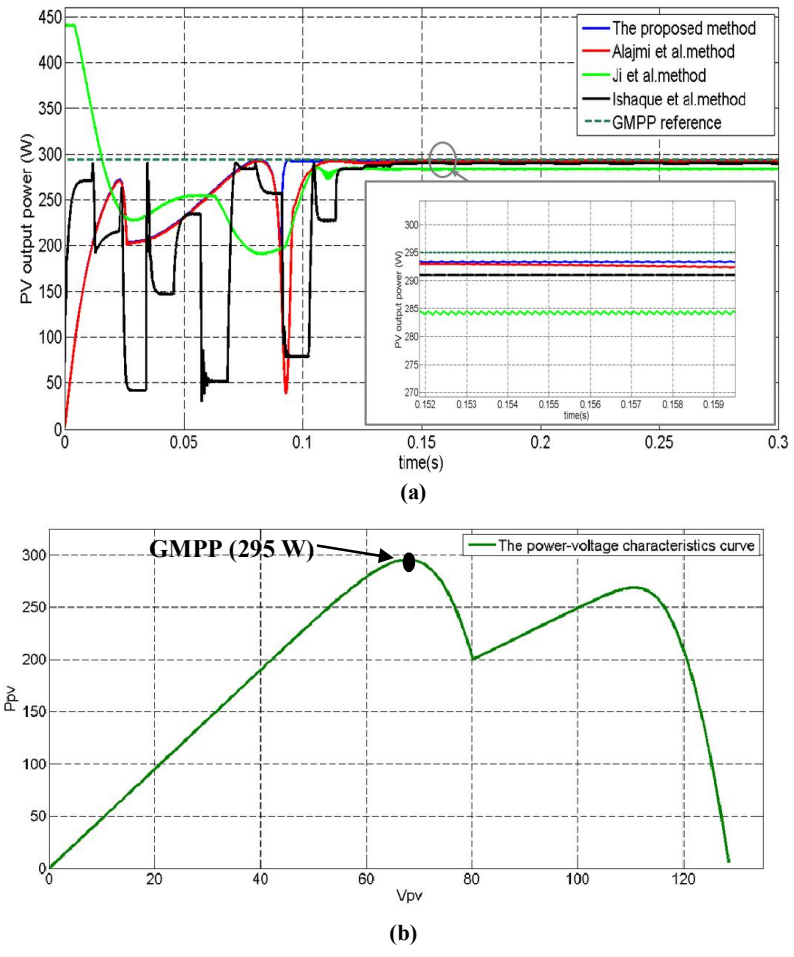

Figure 4. 17: (a) waveforms of the power extracted by the investigated MPPTs under PSCs (the shading pattern was 1000 W/m^2, 1000 W/m^2 and 525 W/m^2) (b) the P-V characteristic curve under the aforementioned shading pattern.

Table 4. 3: Comparison of three GMPPTs with the proposed one under PSCs.

Evaluated parameters	Proposed MPPT	Ji *et al.* [101] (2011)	Alajmi *et al.* [37] (2013)	Ishaque *et al.* [87] (2012)
Response time (ms)	94	106	113	138
Static error (W)	1	10.6	2.3	4
Power production (W)	294	284.4	292.7	291
Efficiency (%)	99,66	96,41	99,22	98,64
Probability of successfully finding the GMPP under PSC for 100 shading patterns	High 100/100	Low 69/100	High 91/100	Medium to High 83/100
Practical implementation	Yes	Yes	Yes	Yes
sensors	(current, voltage)	(current, voltage)	(current, voltage)	(current, voltage)
Tracking method	FLC with 25 rules	InCond	FLC with 32 rules	PSO
Algorithm's complexity	High	Low	Medium to high	High
Dependence on the PV system	No	Yes	No	No

4.6. Conclusions

A new intelligent MPPT has been proposed to track the GMPP under complicated shading patterns. Simulation results have been carried out to validate the proposed MPPT. Based on the obtained results, it can be concluded that the proposed MPPT avoids LMPPs by using the scanning-storing procedure. Moreover, a rapid convergence to the GMPP under transient variation of shading patterns has been ensured by using the tracking loop. The proposed MPPT method boasts other advantages such as: high efficiency, neither dependence on the PV system parameters nor on the PVIC used.

A comparative study with previous works has been carried out and the results revealed that the investigated MPPTs have some advantages and disadvantages. Moreover, the proposed MPPT outperforms the others in terms of convergence time and efficiency. However, it has a high complexity level. The last disadvantage is explained by the fact that the tracking loop is based on FLC with 25 rules making it complex in terms of implementation. The next chapter presents an experimental evaluation of a new MPPT method that has a low complexity and many other advantages.

CHAPTER 5
EXPERIMENTAL ASSESSMENT OF NEW FAST MPPT FOR PV SYSTEMS UNDER PSCs

5.1. Overview

The chapter carries presents experimental investigation of a new MPPT method for PV systems. The originality of this MPPT consists in the usage of a novel mechanism of global maximum power point identifying loop when the system undergoes multiple MPPs and the use of adaptive variable step HC technique to track the identified GMPP. It is worth mentioning the complexity level of this MPPT is significantly reduced compared to the one presented in the previous chapter, since the novel identifying loop is simplified compared to the scanning-storing procedure. Moreover, the tracking loop complexity is reduced by using an adaptive variable step size HC instead of FLC. This adaptive variable step HC MPPT adjusts the value of the duty cycle's step size according to the values of the identified GMPP and the measured PV power. The adjustment targets to select an appropriate step size satisfying the tradeoff between fast tracking dynamics and minimum energy loss due to power oscillations around the GMPP. To figure out the advantages of the proposed MPPT, it is implemented together with three LMPPTs (e.g., two conventional MPPTs and FL-based one) and compared with six recently developed GMPPTs. Obtained experimental results as well as comparison outcomes show that the proposed MPPT technique is fast while tracking GMPP (around 2.4 s) and resilient against perturbations that may occur during the operation of the PV system. Moreover, the proposed MPPT boasts other advantages such as: ease of implementation, no dependence on the PV system and requires only two conventional sensors of voltage and current respectively.

5.2. The Proposed MPPT method

Extracting maximum power from a PV source under any given distribution of insolation levels, as well, for any ambient temperature is a central task in PV-fed applications. Therefore, it is imperative to develop a MPPT control strategy that is simple, fast, robust, and accurate in identifying and tracking the appropriate MPP, leading to enhanced performances of the PV system, especially under PSCs. In order to satisfy the aforementioned criteria, the proposed MPPT is developed to

track the desired MPP for PV systems under both UICs and PSCs. The algorithm combines two loops, the first one is a novel identifying-loop that aims to discriminate the GMPP from the LMPPs. Identifying the GMPP allows the determination of the corresponding duty cycle (D_{GMPP}) at the same time. The second loop is the tracking loop that aims to track with accuracy the pre-identified GMPP. The block diagram of figure (5.1) shows the main components constituting the whole PV system while figure (5.2) depicts the flowchart of the proposed MPPT.

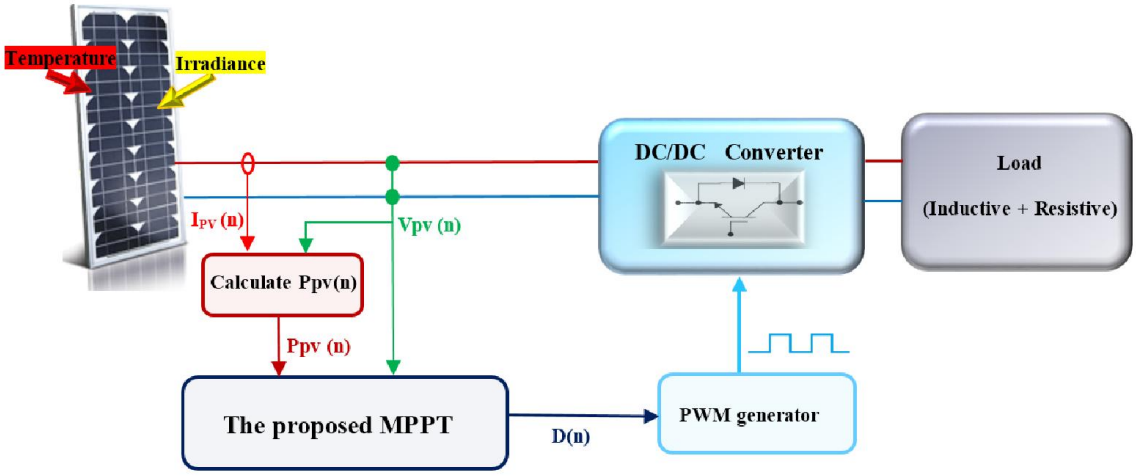

Figure 5. 1: The block diagram of the PV system, including the proposed MPPT

As shown in the flowchart of figure (5.2), the maximum power (P_{max}) is firstly initialized by assigning 0 W to it, and the duty cycle $D(n)$ is set to d_{min}. The latter is the minimum acceptable value of duty cycle. $PM1$, $PM2$ and $PM3$ are three threshold values that represent the allowable power difference between the identified GMPP and the measured instantaneous power $Ppv\ (n)$. They must be chosen as to satisfy the following criterion, $PM1 > PM2 > PM3$.

After that, the algorithm acquires the values of voltage $V_{pv}\ (n)$ and current $I_{pv}\ (n)$ at the output of the PVG (e.g., PV module/string/array). These measurements will be used to compute the instantaneous power output $Ppv\ (n)$ that is simply the product of $V_{pv}\ (n)$ and $I_{pv}\ (n)$. This value is the key parameter in the algorithm, as it will be compared with the aforementioned three thresholds levels in order to first identify then to track the GMPP.

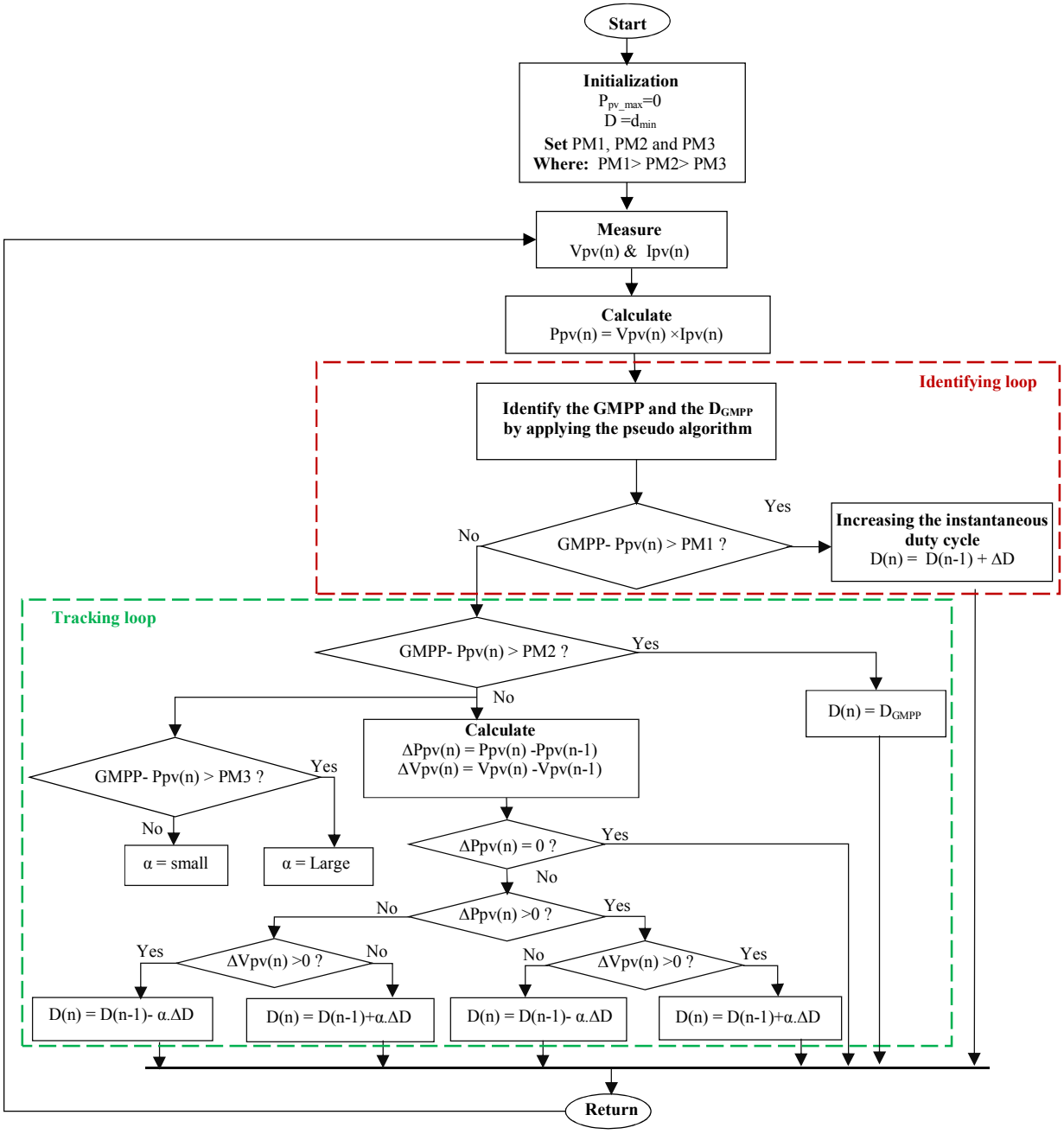

Figure 5. 2: Flowchart of the proposed MPPT

During start up condition as well as when climate parameters change, the identifying loop increases the instantaneous duty cycle $D(n)$ with a fixed step size ΔD, by starting from its minimum predefined value d_{min} to its maximum value d_{max}. This operation allows to sweep the PV output power to identify the GMPP, as well as, its corresponding duty cycle D_{GMPP}. The identification is carried out by executing the pseudo algorithm shown in the flowchart of figure (5.2) and which generates the appropriate GMPP and its corresponding D_{GMPP}. It is worth mentioning that this pseudo algorithm has more simplicity compared to that of sub-section (4.3.2), as it

employs only the variation ΔP_{pv_max} to identify the optimal duty cycle (D_{GMPP}). Whereas, the scanning-storing procedure presented in sub-section (4.3.2), uses both the power variation ΔP_{pv} and the variation between the P_{max} and P_{pv}.

Identify the GMPP and the D_{GMPP}:

To identify the GMPP among the LMPPs. Therefore, the *n-1*th stored-maximum-power ($P_{pv\_max}(n-1)$) should be compared with the actual power ($P_{pv}(n)$)

$P_{pv\_max}(n)$ is considered the maximum value between $P_{pv\_max}(n-1)$ and $P_{pv}(n)$

$P_{pv\_max}(n) = \max (P_{pv}(n), P_{pv\_max}(n-1))$

Figure (5.3) presents more illustrations about the pseudo algorithm. Where the GMPP, LMPPs, ΔP_{pv_max} and P_{pv_max} are depicted in the Power–Duty cycle (Ppv–D) characteristic curve.

The GMPP is considered the maximum value of $P_{pv\_max}(n)$

GMPP = $\max (P_{pv\_max}(n))$

At the same time while seeking GMPP, the loop identifies the optimal duty cycle (D_{GMPP}) corresponding to the GMPP (see figure (5.3)). Therefore, $\Delta P_{pv\_max}(n)$ is calculated as

$\Delta P_{pv\_max}(n) = P_{pv\_max}(n) - P_{pv\_max}(n-1)$

Knowing that D (n) is the actual duty cycle. D_{GMPP} can be identified as follows:

If $\Delta P_{pv\_max}(n) > 0$ $d_{GMPP}(n) = D(n)$

Else $d_{GMPP}(n) = d_{GMPP}(n-1)$

End

$\mathbf{D_{GMPP}} = d_{GMPP}(n)$

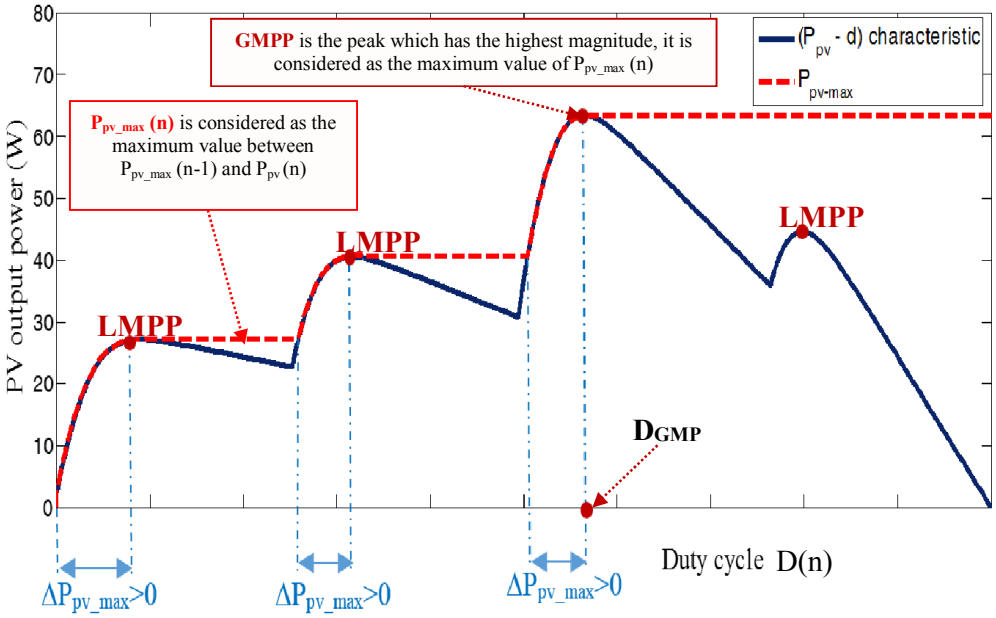

Figure 5. 3: The output Power–Duty cycle (P_{pv}–D) illustrating the two stages of the pseudo algorithm.

It is worth noting that the search range of the identifying loop is based on the study presented in [149] where different P-V characteristic curves subjected to different shading patterns are analyzed. The study concluded that amplitudes of peaks of any analyzed P-V characteristic curve increase before the GMPP and display the trend of decreasing when moving away after the GMPP. That is, the curve of peaks is unimodal and once the peak is reached from one side, the processes of seeking the GMPP is terminated to avoid sweeping the whole search space. In addition, the power peaks occur roughly at the multiple of 80% of open circuit voltage. For this reason, the PV curve was swept in an interval bounded by d_{min} and d_{max}. Where d_{max} is the maximum value of duty cycle that can be reached by the identifying loop in which the condition $GMPP - P_{pv}(n) < PM1$ is satisfied (e.g., $PM1$ has been chosen 40% of the maximum value of $P_{pv\_max}(n)$). According to the analysis done in [41], the values d_{min} can be taken as 10% of the whole variation range and d_{max} shall not exceed 90%.

In order to check that the proposed MPPT will not be trapped on a LMPP while searching for the GMPP, the identifying loop continues increasing the duty cycle till the difference $GMPP - P_{pv}(n)$ will be lower than $PM1$. Once the last condition is achieved, the last value of GMPP and D_{GMPP} are saved. Meanwhile, the MPPT is activated and the tracking loop seeks the recorded point by applying the pre-identified D_{GMPP} as the output of the MPPT. This means that the operating point will move quickly near the desired GMPP. Then, the algorithm proceeds to check whether the operating point is near the desired GMPP by evaluating whether the difference $GMPP - P_{pv}(n)$ is lower than $PM2$ (e.g., $PM2$ has been chosen 20% of the identified GMPP). If now the last conditions is satisfied, a variable step size HC takes over and moves the operating point rapidly and accurately to the exact GMPP. The value of α is chosen according to the difference $GMPP - P_{pv}(n)$ with respect to $PM3$. Therefore, if this difference is greater than $PM3$ (e.g., $PM3$ has been chosen 10% of the identified GMPP), the value of α is chosen to be large leading to large perturbation step size ($\alpha.\Delta D$) and subsequently fast convergence to the GMPP. As the PV operating power gets close to the GMPP, the difference $GMPP - P_{pv}(n)$ will be lower than $PM3$. Therefore, the value of α is going to be smaller which leads to a small perturbation step size ($\alpha.\Delta D$). The latter allows minimizing the energy losses due to oscillations in steady-state conditions.

5.3. Experimental Setup

Figure (5.4) shows the hardware implementation platform to be employed for the experimental assessment and validation of the proposed MPPT technique. Conventional P&O, VSS-InCond [35] and adaptive P&O-FLC [36] are implemented on the same platform as to compare them with the proposed one. The test bench includes a single DC-DC chopper, Pulse-Width Modulation (PWM) generator, resistive-inductive loads, current and voltage sensors, Tektronix digital oscilloscope BTS 1102B-ED, acquisition-unit, computer for displaying results and a dSPACE–1103 platform for MPPTs implementation.

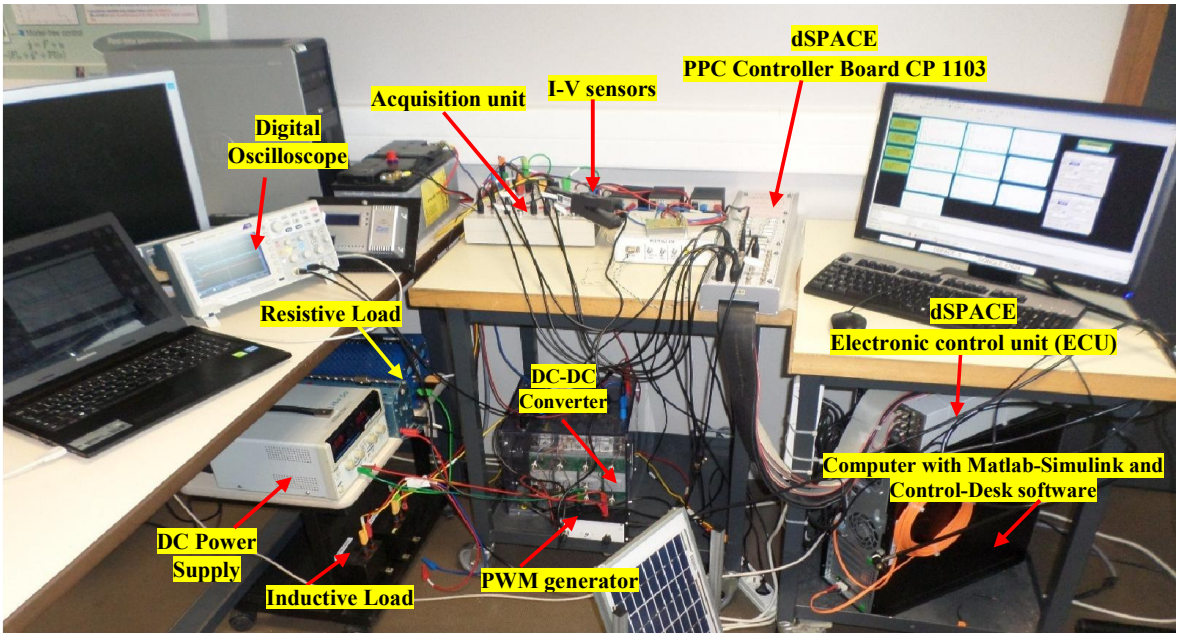

Figure 5. 4: Components of PV system under test

During UICs, the PV module receives a uniform irradiance with given intensity; therefore, a single MPP should appear in the P-V characteristic curve. In this case, a real PV module type P.A.Hilton Ltd 10M of 10 W peak power receives irradiance from a lamp as shown in figure (5.5).

To test the algorithm under PSCs, two PV modules ET-M536 20M having 20W peak power each are used. One of them is partially shaded and the other receives full irradiance from the lamp as shown in figure (5.6-a). Each PV module is equipped with its own parallel-connected bypass diode as depicted in figure (5.6-b).

Specifications and ratings at STC of irradiance and temperature of these modules are given in table (A.5-Appendix A).

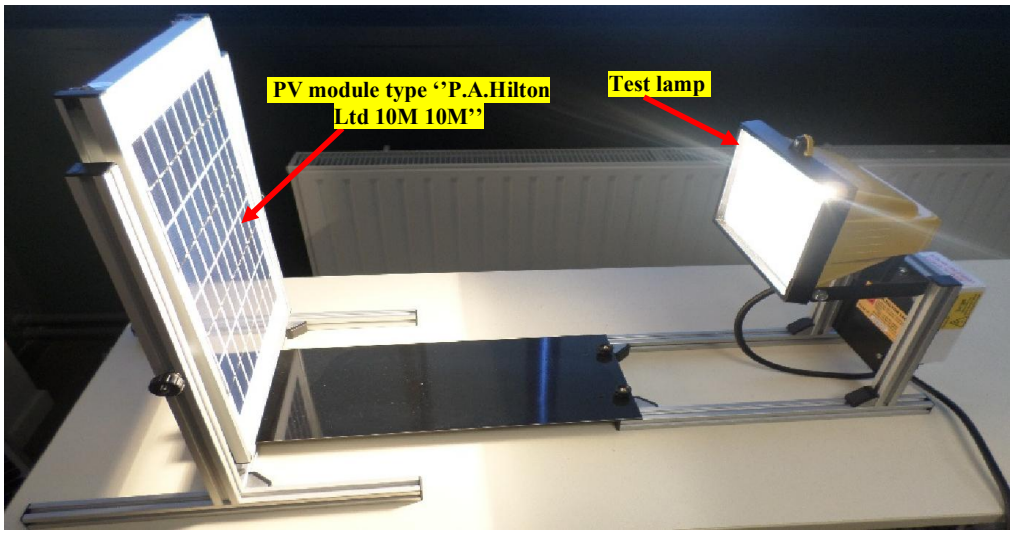

Figure 5. 5: PV module (P.A.Hilton Ltd 10M) and the test lamp as a source of light.

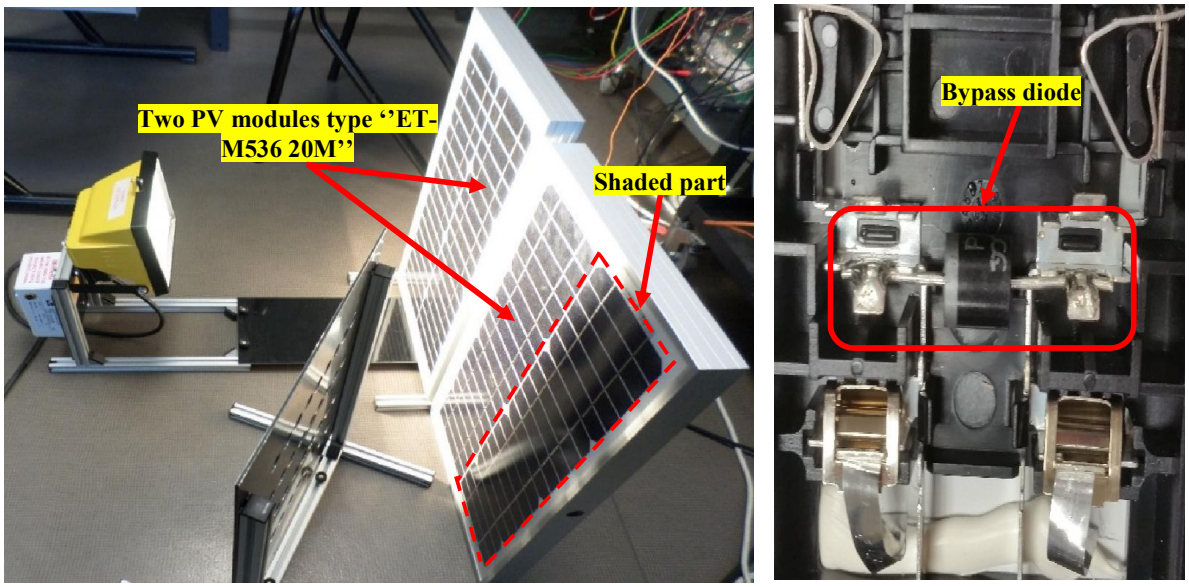

Figure 5. 6: (a) Two series-connected PV modules (ET-M536 20M), one of the modules is partially shaded (b) bypass diode connection.

Figure (5.7) depicts the simplified schematic diagram of the hardware implementation platform. The power stage interface between the PVG and the load is composed of a single DC-DC converter with 25 kHz switching frequency which together with its PWM generator. According to the measured I_{pv} and P_{pv}, the MPPT

controller computes the required duty cycle and sends it to the PWM generator. The latter converts the MPPT's duty cycle to a PWM signal which turns on and off the DC-DC converter's power switch. Varying the on/off time of switch allows varying the output voltage and hence the operating point of the whole PV system.

The load being connected at the output of the DC-DC converter is a series-connected inductive and resistive load having the values of 16 mH and 5 ohm, respectively. Voltage and current are measured then normalized and their values are acquired by the acquisition-unit at a sampling time of 1ms. The values of currents and voltage will be used to compute the power being needed by the MPPT algorithm.

The Simulink model of the implemented MPPTs with the hardware equipment for MPPT's real-time processing is made visible through the use of the Real Time Interface (RTI) block available in Simulink library. On the other hand, Control-Desk experiment software is considered as an acquisition manager system which is intended to facilitate the real time analysis of the system performance parameters. As well as, to perform real time measurements, to collect and save the measured data, in addition to provide access for visualization of different waveforms.

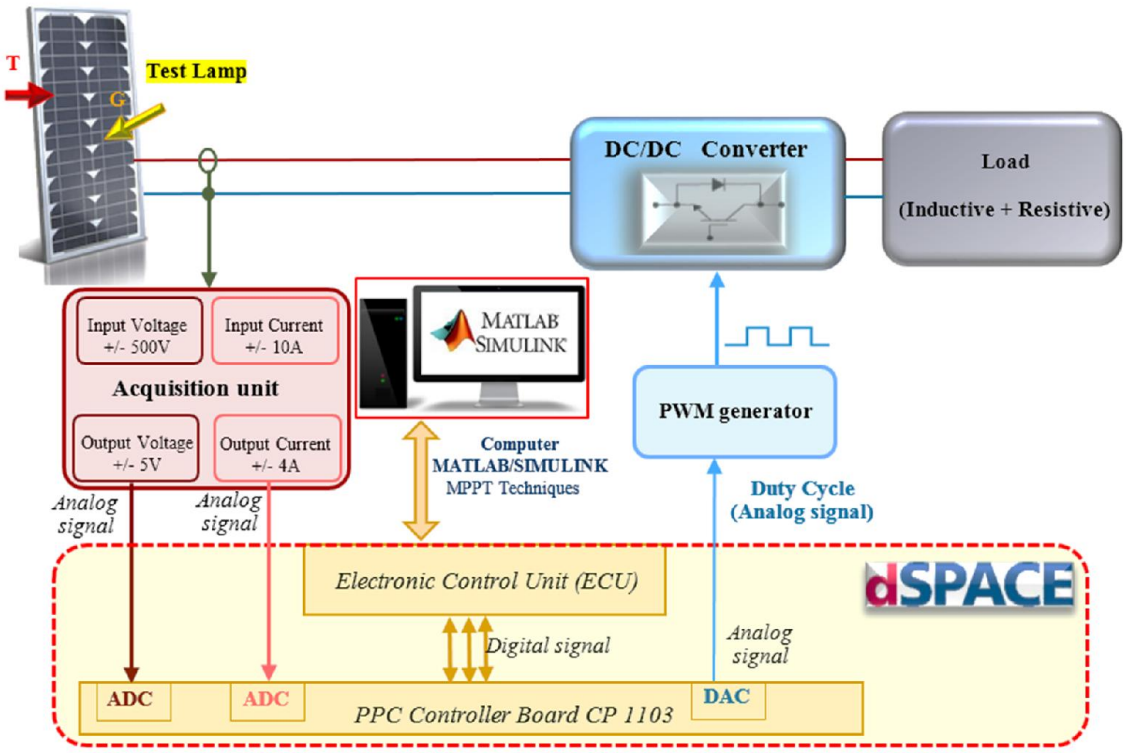

Figure 5. 7: Schematic of the overall system configuration

5.4. Experimental results

5.4.1. Test under UICs

To test the proposed MPPT under UICs, experiments were conducted on a 10 W PV module type P.A.Hilton Ltd 10M. As shown in figure (5.5) and during test, the PV module is brought so that it faces the test lamp and the illumination would be uniform. Under such UICs, the P-V characteristic curve of the PV module is swept by varying the duty cycle to identify the exact MPP. The measured PV voltage, current and power characteristics with respect to the variation of the duty cycle are given in figure (5.8-a). By analyzing these figures, one can easily notice the single peak characteristic of the power curve. Furthermore, the power peak that is the MPP is about 6 W.

Under the same irradiance condition, figure (5.8-b) shows that the proposed MPPT converges to the appropriate MPP obtained in figure (5.8-a). In other words, the proposed MPPT method starts with the first loop that is identifying the desired power which took around 2.5s. Then after that, the tracking loop takes over to impose the obtained desired power on the PV system. The total convergence time is obtained by summing the identification and the tracking times that is 2.4s.

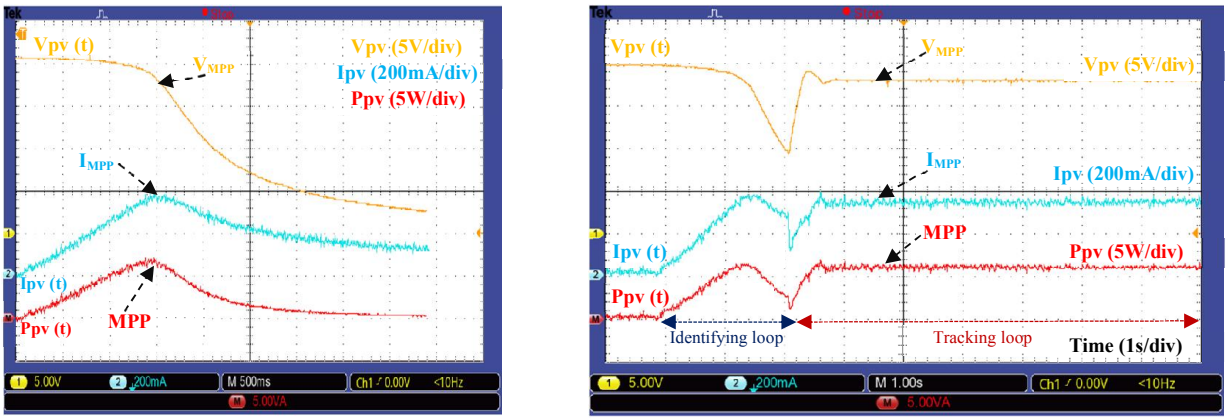

(a) (b)

Figure 5. 8: Experimental waveforms under UICs. (a) The swept PV characteristics (current, voltage and power). (b) The PV output current, voltage and power extracted by the proposed MPPT.

5.4.2. Test under PSCs

To show the effectiveness of the proposed MPPT under PSCs, experiments are conducted now on the two series-connected 20 W PV modules of type ET-M536

20M. As shown in figure (5.6-a), during test, one of the two PV modules is partially shaded by an opaque-test-plate, while the other is fully illuminated. Under this shading pattern, the PV current, voltage and power characteristic are swept and the obtained experimental waveforms are given in figure (5.9-a). It can be clearly seen that the power characteristic curve exhibits two power peaks where the lower is the LMPP and the greater must be GMPP. In terms of quantities, at GMPP the PV delivers 17 W and at LMPP only 10 W can be obtained from the PVG. Under these conditions, the proposed MPPT is lunched, and the obtained experimental waveforms of the PV current, voltage and power are shown in figure (5.9-b). By inspecting these waveforms, one can notice that the MPPT algorithm starts by identifying the GMPP that has been successfully found then starts the tracking loop to bring the PV system to this point. At the end of the convergence and in steady state operation, the power extracted is about 17W which is the GMPP obtained by the previous experiment. Total time of identification and tracking is about 2.5s.

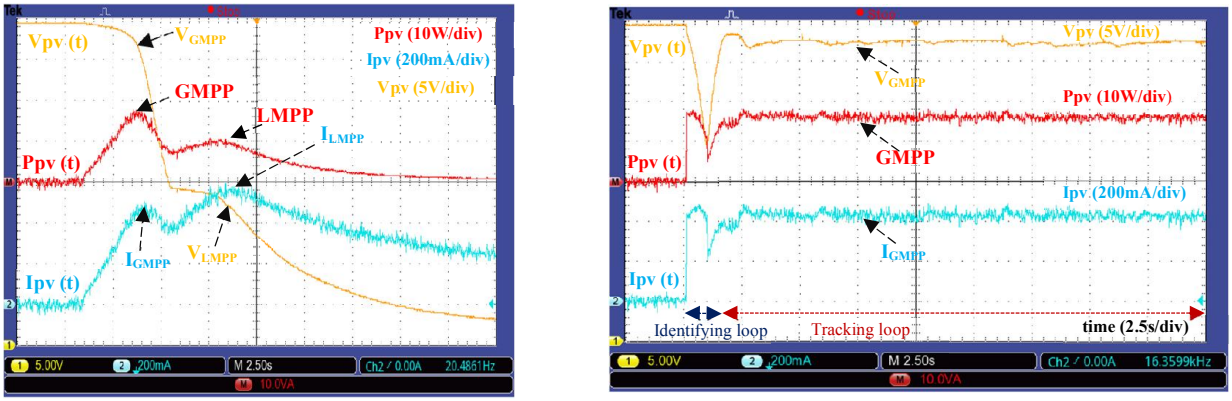

(a) (b)

Figure 5. 9: Experimental waveforms under PSC. (a) The swept PV characteristics (current, voltage and power). (b) Behavior of PVG being controlled by the proposed MPPT.

Based on the obtained results in both UICs and PSCs, one can draw the following outcome: the proposed MPPT is independent from the parameters of the PVG and hence can be used with any type of modules constituting the PV array. It can be justified by the fact that PV modules being employed in the two tests are different and have different electrical specifications (P.A.Hilton Ltd 10M and ET-M536 20M).

5.4.3. Test under fast variations of irradiance

In this sub-section, the tracking ability of the proposed MPPT is checked against fast variations of irradiance. This has been accomplished by varying the irradiance three times within few seconds. In the first time, the shading pattern of the last test has been reproduced where one PV module is partially shaded and the other is fully illuminated. The PV current, voltage and power characteristic are swept and the experimental waveforms are given in figure (5.10-a). The power characteristic curve exhibits two power peaks where the GMPP is 20 W and the LMPP is 9 W. As long as the proposed MPPT is activated, identification of the GMPP is started then once found it is tracked. The experimental waveforms of the PV current, voltage and power, extracted by the proposed MPPT are shown in figure (5.10-b).

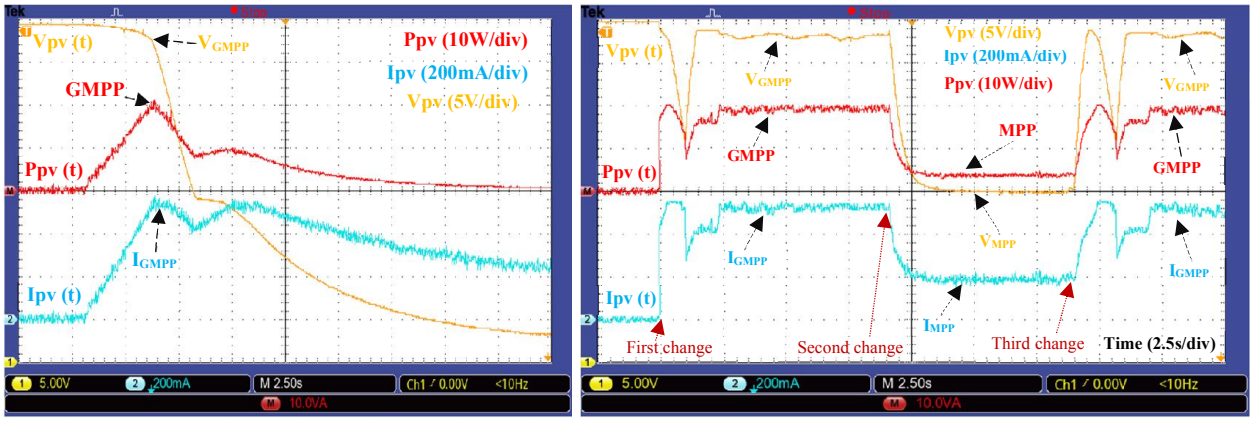

(a) (b)

Figure 5. 10: Experimental results under fast variation of irradiance. (a) The swept PV characteristics (current, voltage and power). (b) The behavior of PVG being controlled by the proposed MPPT.

Results clearly show that the GMPP has been successfully tracked. In the second time, variation of irradiance is performed by turning off the lamp. Under this condition, the irradiance applied on the two-series-connected PV modules is that of the room light. It is subsequently low and uniform for both PV modules. Since the irradiance is uniform, one MPP can be found on P-V characteristic curve. Results from figure (5.10-b), confirm the well tracking of this 5W MPP by the proposed MPPT. In the third and last time, another change of irradiance is carried out by turning on the lamp while the second PV module is still partially shaded. Under this

condition, it is known that GMPP is 20W and LMPP is about 9W. The change of irradiance has been detected by the MPPT algorithm, thus the identifying loop is started to find the appropriate GMPP then after that the tracking loop will ensure that the operating point matches the point just found by the identifying loop. The recorded graphs of voltage, current and power shown in Figure (5.10-b) confirm the effectiveness of the proposed MPPT technique as the GMPP is successfully re-identified and imposed.

5.5. Comparative study

In this section, the proposed MPPT technique is compared with local as well as global MPPT techniques. On the same test rig, three LMPPT techniques have been implemented and compared with the proposed one. This comparison allows validating the global searching feature of the proposed technique as those LMPPT techniques are not able to identify the GMPP. The other comparison with GMPPT methods shall allow appreciating the performance of the proposed method in terms of convergence time, required sensors, number of tuned parameters, algorithm's complexity and dependence on system parameters, etc.

5.5.1. Comparison with LMPPTs

Three well-known classical MPPT techniques, namely conventional P&O, VSS-InCond [35] and adaptive P&O-FLC are employed in the present comparison.

The adaptive P&O-FLC MPPT has already been employed in the comparison study presented in section (3.4.1). This method is an intelligent MPPT technique recently proposed by Zainuri *et al.*[36], where it employs fuzzy reasoning to improve the performance of classical P&O MPPT algorithm.

The previous PS pattern presented in sub-section (5.4.2) has been used for the test. Under such PSC, the output electrical characteristic of the two-series connected PV modules has two peaks, the GMPP is 17W and the LMPP is about 10W, as found previously. The three LMPPT techniques as well as the proposed one have been implemented for the same load and irradiance conditions. Experimental results showing the waveforms of PV output current, voltage and power obtained by the proposed MPPT, P&O, VSS-InCond and adaptive P&O-FLC are depicted in figure (5.11-a, b, c and d), respectively.

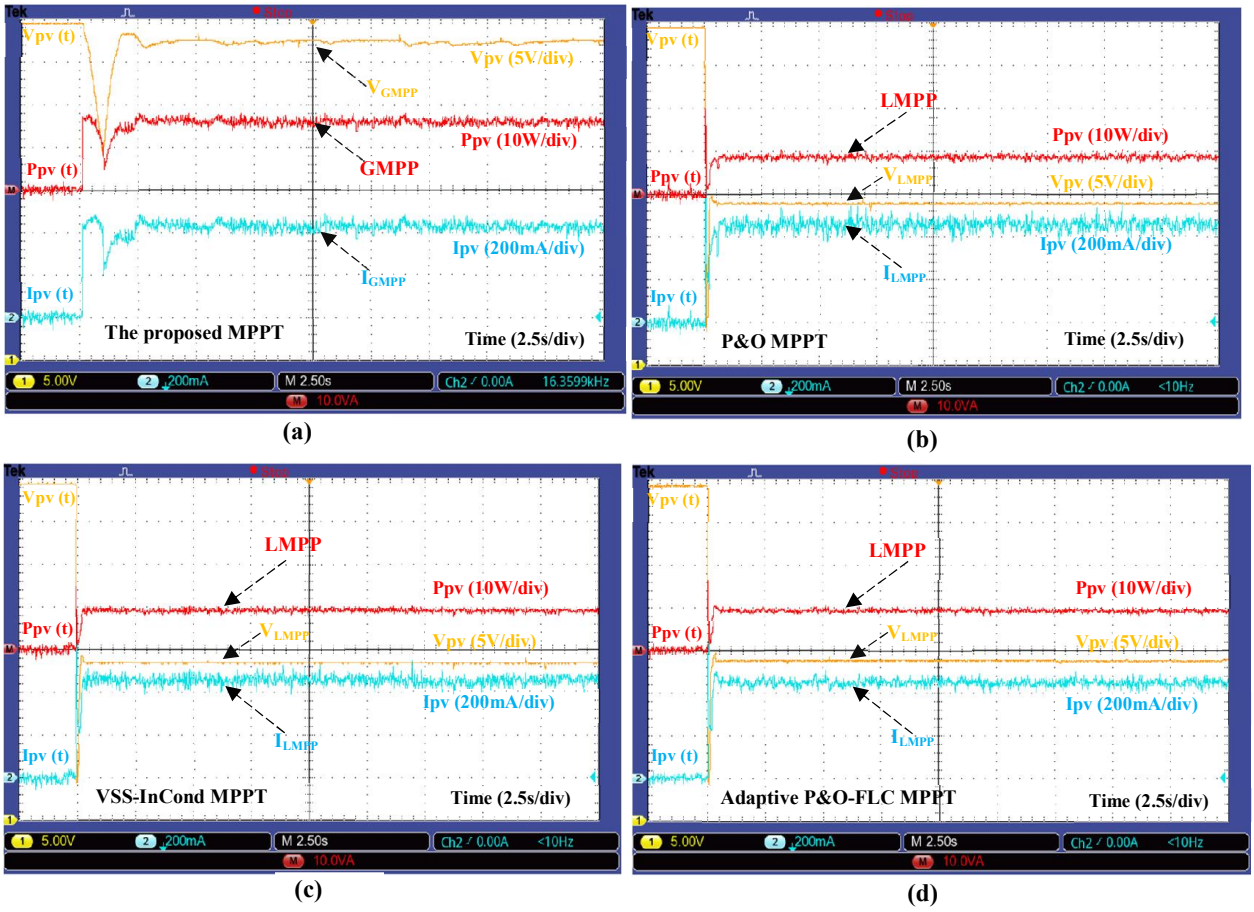

Figure 5. 11: Experimental waveforms of the PV output current, voltage and power under PSC obtained by: (a) the proposed MPPT, (b) P&O MPPT, (c) VSS-InCond MPPT (d) Adaptive P&O-FLC MPPT.

Upon comparison of waveforms shown in figure (5.9-a) to these results of figure (5.11-a, b, c and d), one can easily notice the ability of the proposed MPPT method in identifying and tracking the appropriate GMPP and the inability of the LMPPT methods to do so. In other words, the waveforms of figure (5.11-b, c and d) show that these methods are very fast but easily can be trapped to LMPP which is 10W in our case. Therefore, they fail to converge to the appropriate MPP when the PV system undergoes PS. Unlike P&O, VSS-InCond and adaptive P&O-FLC, the proposed MPPT offers guaranteed convergence to the GMPP. Consequently better operating efficiency of the whole PV system is obtained particularly during PSCs.

In order to highlight the advantages of the proposed MPPT with respect to P&O, VSS-InCond and adaptive P&O-FLC, other assessment criteria have been considered as reported in table (5.1). These criteria include ability to track the MPP under UICs, tracking performance under UICs, ability to track the GMPP under

PSCs, extracted power under PSCs, control variable, required sensors, initial setting parameters, control strategy, algorithm's complexity and dependence on the PVG parameters.

Table 5. 1: Comparison of LMPPT methods with proposed one under UICs and PSCs

Evaluated parameters	Proposed method	P&O	VSS-InCond [35] (2008)	Adaptive P&O-FLC [36] (2014)
Convergence ability to the MPP under UICs	Yes	Yes	Yes	Yes
Tracking performance under UICs	High	Medium	Medium to high	High
Ability to track the GMPP under PSCs	Yes	Poor tracking performance	Poor tracking performance	Poor tracking performance
Extracted power under PSCs (fig. 11)	Around 17 W (Convergence to the GMPP)	Around 10 W (Convergence to LMPP)	Around 10 W (Convergence to LMPP)	Around 10 W (Convergence to LMPP)
Control variable	Duty cycle	Voltage	Duty cycle	Duty cycle
Required sensors	1 current sensor 1 voltage sensor	1 current sensor 1 voltage sensor	1 current sensor 1 voltage sensor	1 current sensor 1 voltage sensor
Initial parameter settings	3 parameters (PM1, PM2 and PM3)	1 parameter (ΔVref the perturbation step size)	1 parameter (N the scaling factor which is tuned at the design time to adjust the perturbation step size)	3 parameters (two scaling factors of the two FLC inputs, one scaling factor of the FLC output)
Control strategy	New identifying and tracking loops	Sampling method based on P&O	Sampling method based on variable step size InCond	Intelligent control based on FLC
Algorithm's complexity	Low	Very low	Low	High
Dependence on system parameters	No	No	Yes Needs the knowledge of Voc	No

As can be seen from table (5.1), under UICs, all the investigated MPPTs are able to track the MPP, while only the proposed MPPT can track the GMPP (17W) under PSCs. Moreover, it can be observed that all the investigated MPPTs are independent from the PV system except the VSS-InCond that suffers from dependence and requires the knowledge of open circuit-voltage. From the initial settings point of view, both proposed MPPT and Adaptive P&O-FLC require tuning of three initial parameters, whereas both P&O and VSS-InCond MPPTs need the tuning of a single initial parameter. It is worth mentioning that scaling factors of Adaptive P&O-FLC are central for the convergence. That is, their adjustment directly affect its effectiveness in tracking the MPP. These factors are tuned by trial-error method, which makes the determination of their appropriate values a difficult task.

The MPPT methods under study vary in complexity. Thus, P&O is the simplest one while the Adaptive P&O-FLC is the most complex algorithm. This complexity is the result of using fuzzy sets and rules to decide whether increasing or decreasing the duty cycle. For each input variable which are two (ΔP and ΔV), five fuzzy subsets are used (N: Negative, ZE: Zero, Ps: Positive Small, P: Positive, PB: Positive Big). The same number of subsets is used for the output variable that is the duty cycle change (ΔD). Therefore, 25 fuzzy control rules are processed by this MPPT. Moreover, Mamdani's max-min inference system has been selected for the computation of fuzzy decision and center of gravity for the conversion of this decision into crisp value. Consequently, processing all these stages along with the 25 fuzzy rules makes the fuzzy logic based MPPT the most cumbersome and complex MPPT algorithm. The proposed MPPT algorithm is comparable to that of VSS-InCond except that an extra calculation is needed to implement the identifying loop.

5.5.2. Comparison with GMPPT techniques

A performance comparison between the proposed MPPT and other GMPPTs recently published [32, 37-41] is undertaken in this part. It is worth mentioning that these techniques have been well presented in chapter 1. The comparison with previous works has been done based on using some evaluation criteria such as: convergence time, required sensors, tracking method, algorithm's complexity, initial setting parameters and dependence on the PVG parameters. Table (5.2) shows the comparison of the proposed technique with the above-mentioned MPPTs.

All the investigated MPPTs need current and voltage sensors except the MPPT proposed by Lian *et al*. [40] that needs four sensors (i.e., 2 current sensors and 2 voltage sensors) which increases the implementation cost.

Furthermore, it can be observed that these MPPT methods vary in complexity. Thus, global search based algorithms and hybrid methods that employ, PSO, ACO or ABC to track the GMPP, have a high algorithm complexity level, as they need to test a population of duty cycles or voltages. This fact result in a considerable computational effort to ensure accurate tracking of GMPP during PSCs. Unlike

those algorithms, SA-based MPPT algorithm has a mediate complexity compared to other optimization algorithms under study.

From the viewpoint of required initial parameter settings, the proposed MPPT required an initial setting of three parameters. However, some of them need only one parameter to be tuned as in [32, 38], whereas in [37, 39, 40] four parameters are required to be tuned. It is worth mentioning that the initial setting parameters need to be correctly tuned, otherwise, the algorithm may be stuck to one of the LMPPs or its performance can be highly affected.

As far as the implementation is concerned, the proposed MPPT and those proposed in [32, 39] can be easily implemented since they have a low algorithm complexity. However, the MPPTs presented in [32, 40] depend on the PV system parameters. In other words, an accurate knowledge of parameters is necessary to get a high performance in tracking the GMPP. Therefore, this MPPT cannot be applied to PV module/array with unknown electrical characteristic or with indeterminate interconnection type of PV modules.

As stated in [41], the convergence time is an important parameter and central criterion in the evaluation of a MPPT methods. This time response is directly related to the amount of the extracted energy. Therefore, lesser the convergence time to achieve the GMPP, higher is the energy extracted from the PV system. The numerical values of convergence time given in table (5.2) illustrate superior tracking performance of the proposed MPPT, as well as of those presented in [39] and [37]. Based on the whole experimental results and the comparative study, It can be concluded that the proposed MPPT is a strong candidate for PV control application in PV systems under UICs and PSCs. Since it presents the possibility of enhancing the tracking performance in terms of different parameters such as: fast convergence, capability to reach the GMPP, no dependence on system, low complexity and the requirement of only the two conventional sensors.

Table 5. 2: Comparison of some recently developed GMPPTs with the proposed one

Evaluated parameters	Proposed method	Alajmi *et al.* [37] (2013)	Lian *et al.*[40] (2014)	Elserougi *et al.* [32] (2015)	Sundareswaran *et al.* [38] (2015)	Sundareswaran *et al.* [41] (2016)	Lyden *et al.* [39] (2016)
Convergence time	Around 2.4 s	Around 4.5 s	From 6.59 s to 9.69 s	From 11.6 s to 16.8 s	From 5.01 to 5.63 s	From 2.55 s to 3.75 s	Around 2.9 s
Required sensors	1 current sensor 1 voltage sensor	1 current sensor 1 voltage sensor	2 current sensor 2 voltage sensor	1 current sensor 1 voltage sensor	1 current sensor 1 voltage sensor	1 current sensor 1 voltage sensor	1 current sensor 1 voltage sensor
Tracking method	New identifying and tracking loops	Scan and Store + FLC with 32 rules	Combines P&O and PSO	Switched PV approach	ABC	Combines ACO and P&O	Simulated Annealing (SA)
Initial parameter settings	3 parameters (PM1, PM2 and PM3)	4 parameters (ΔPm constant, three constant used for tuning the universe of discourse of input/output membership function ΔP, VI, ΔP_M)	4 parameters (number of particles, the inertia weight and the two acceleration coefficients)	1 parameter (k is a constant which is ranged from 1< k <2)	1 parameter (the initial number of bees N_P)	2 parameters (ant population size, step size of ant Movement)	4 parameters (initial temperature, cooling rate, neighbor-hood size and final temperature)
Algorithm's complexity	Low	Medium	High	Low	High	High	Medium
Dependence on system parameters	No	No	Yes Needs the knowledge of Voc to initiate the 3 first particles	Yes Needs the knowledge of Isc to verify the condition (Ioref ≥ n.k.Isc)	No	No	No

5.6. Conclusions

The chapter develops a new MPPT method that can handle the problem of PS in PV systems. The method is based on the identification of the GMPP then its tracking. Experimental results have shown the effectiveness in tracking the appropriate MPP of the PVG whether under uniform or non-uniform irradiance conditions. The novelty of the method lies in the fast identification of the GMPP without sweeping the whole range of the duty cycle. Once the latter is identified, variable step size HC MPPT is activated to make the whole system operating at this GMPP. Experimental comparison with LMPPTs have emphasized the simplicity and the accurate convergence to the appropriate GMPP. Employing the most used assessment criteria, the method has been compared also with some recently developed GMPPT techniques. It can be concluded that the proposed MPPT is fast, accurate and robust which could make it a good candidate for the control of PV systems. The proposed MPPT method may be used as an alternative to conventional MPPTs in hybrid solar systems too such as: building integrated PV installations. For this application, it is used to cope with the non-uniformity of irradiance that is not avoidable in one hand, and in the other hand, to keep the conversion efficiency always at its maximum level.

GENERAL CONCLUSION

In this research work, a clean and sustainable source of energy based on PV systems has been presented. The PV system efficiency depends on how effectively the MPP is tracked, especially under PSCs. The main focuses of this work was how to improve the total PV system efficiency by developing and implementing efficient MPPT techniques. The techniques can extract and transfer the maximum available power from the PVG to the load, especially under rapid changing atmospheric conditions and PSCs.

The thesis has presented and discussed various existing MPPT methods for PV systems, which have been grouped into two main classes, LMPPTs and GMPPTs. LMPPTs are devoted to extract the MPP only when the irradiance striking the PVG is uniform. Whereas, GMPPTs can extract the maximum power under both uniform and non-uniform irradiance conditions. However, the complexity of the control scheme and the excessive amount of calculation are the main limitations of GMPPTs, due to the use soft computing or hybrid techniques.

A review of the recent developments on the most common PV technologies (i.e., C-Si and thin film) has been discussed. It has been highlighted that Mono C-Si technology still the leader in PV industry and applications compared to poly C-Si, CIGS and CdTe. PV modules namely Q.Pro 230Wp (Poly C-Si- first generation), Q.Smart 95Wp (CIGS- second generation) and First Solar FS-272 (CdTe- second generation) have been experimentally tested under STC and AWCs. Under the same conditions, the fill factor and the efficiency have been experimentally evaluated. The obtained results show that Poly C-Si is not suitable to be employed as PVG in hot locations.

Simscape-based-model has been proposed to predict electrical characteristics of C-Si and thin film technologies and subsequently different experimental tests have been carried out under STC and AWCs for validation purpose. The obtained results have proved a good agreement between experimental and simulated data using the proposed PV model. In addition, assessment criteria based on four statistical errors have been applied to precisely evaluate the suggested Simscape-

based PV model. The obtained results have shown a satisfactory accuracy of the Simscape-based-model in predicting the electrical characteristics of PV modules.

In order to improve the efficiency of PV systems, a new MPPT algorithm based on GSO technique has been developed. Several tests have been conducted to verify the performance of the algorithm under STC conditions, fast changing irradiance conditions and PSCs. The main advantages of GSO-MPPT are: (1) derivatives are not required (only addition/subtraction and multiplications are used in the algorithm), (2) no initial parameters are needed for tuning, (3) fast convergence to the MPP (the MPP is reached approximately within seven steps), (4) lack of oscillations under steady state oscillations, (5) high dynamic efficiency under fast changing atmospheric conditions. However, GSO-MPPT has dependence on the PV system parameters and it may be trapped at LMPP when the P-V characteristic curve exhibits more than two power peaks (PSCs).

A new MPPT based on artificial intelligence has been proposed to track the GMPP under complicated shading patterns. Simulation results have been carried out to validate the proposed MPPT. The obtained results show that the proposed MPPT avoids LMPPs by using the scanning-storing procedure. Moreover, a rapid convergence to the GMPP under transient variation of shading patterns has been ensured by using the tracking loop (FLC). The proposed MPPT boasts other advantages such as: high efficiency, no dependence on neither the PV system parameters nor on the used PVIC. However, this MPPT has a high complexity level, which can be explained by the fact that the tracking loop based on FLC with 25 fuzzy rules makes it complex in terms of implementation.

The last issue has been addressed by introducing a new MPPT that has a low complexity and many other advantages. The originality of our solution to reduce complexity lies in reducing the tracking loop complexity by developing an adaptive variable step size HC to use it instead of FLC, Moreover, the scanning-storing procedure has been replaced by another simple loop (identifying loop). Experimental results have shown the effectiveness of this MPPT in tracking the appropriate MPP under uniform or non-uniform irradiance conditions. The obtained results from comparison with LMPPTs have emphasized the simplicity and the accurate convergence to the GMPP. For more evaluation, the method has been compared with six recently published GMPPT techniques. It can be concluded that

the proposed MPPT is fast, accurate and robust which could make it a good candidate for the control of PV systems to cope with the non-uniformity of irradiance that is not avoidable in one hand, and in the other hand, to keep the conversion efficiency always at its maximum level.

On the basis of the promising findings presented in this thesis, the next stage of our research will be looking for new techniques to optimize and control hybrid Smart grids.

APPENDICES

APPENDIX A: ELECTRICAL CHARACTERISTICS OF THE USED PV MODULES

Table A.1

Designation	BP Solar MSX 120W	LORENTZ 75W	Sanyo HIT 200W
Maximum power (P_{MPP}) [W]	120	75	200
Voltage at P_{max}(V_{MPP}) [V]	33.7	16.5	55.8
Current at P_{max} (I_{MPP}) [A]	3.56	4.6	3.59
Open circuit voltage (V_{oc}) [V]	42.1	21	68.7
Short circuit current (I_{sc}) [A]	3.87	5.4	3.83
cells number	72 cells	32cells	96 cells
bypass diodes number	2	4	4

Table A.2

Designation	First Solar FS-272	Q.Pro 230Wp	Q.Smart 95Wp
Maximum power (P_{MPP}) [W]	72.5	230	95
Voltage at P_{max}(V_{MPP}) [V]	66.6	29.24	62.1
Current at P_{max} (I_{MPP}) [A]	1.09	7.95	1.53
Open circuit voltage (V_{oc}) [V]	88.7	36.95	78
Short circuit current (I_{sc}) [A]	1.23	8.59	1.68
Cells number	116 cells	60 cells	116 cells
Bypass diodes number	None	3	1
Technology of cells	CdTe	Poly C-Si	CIGS

Table A.3

Designation	KC200GT
Maximum power (P_{MPP}) [W]	200
Voltage at P_{max}(V_{MPP}) [V]	32.9
Current at P_{max} (I_{MPP}) [A]	8.21
Open circuit voltage (V_{oc}) [V]	26.3
Short circuit current (I_{sc}) [A]	7.61
Cells number	54 cells
Bypass diodes number	3
Technology of cells	Poly C-Si

Table A.4

Designation	Shell SP150-PC
Maximum power (P_{max}) [W]	150
Voltage at P_{max} (V_{MPP}) [V]	34
Current at P_{max}(I_{MPP}) [A]	4.4
Open circuit voltage (V_{oc}) [V]	43.4
Short circuit current (I_{sc}) [A]	4.8
Number of cells	72 cells
Technology of cells	Mono C-Si

Table A.5

Designation	P.A.Hilton Ltd 10M	ET-M536 20M
Maximum power (P_{max}) [W]	10	20
Voltage at P_{max} (V_{MPP}) [V]	17.9	17.82
Current at P_{max}(I_{MPP}) [A]	0.56	1.14
Open circuit voltage (V_{oc}) [V]	22.1	21.96
Short circuit current (I_{sc}) [A]	0.58	1.27
Bypass diode	None	1

APPENDIX B: LIST OF ABBREVIATIONS

ABC	Artificial Bee Colony
ACO	Ant Colony Optimization
ANFIS	Adaptive Neuro-Fuzzy Inference System
ANN	Artificial Neural Network
AWCs	Actual Working Conditions
CdTe	Cadmium Telluride
CF	Curve-Fitting
CIGS	Copper Indium Gallium Selenide
CS	Cuckoo Search
C-Si	Crystalline Silicon
Dev	Deviation from the measured values
EML	Emulated MPP Locus
FL	Fuzzy Logic
FLC	Fuzzy Logic Controller
FOCV	Fractional Open-Circuit Voltage
FSCI	Fractional Short-Circuit Current
GA	Genetic Algorithm
GMPP	Global Maximum Power Point
GMPPT	Global Maximum Power Point tracking
GSO	Golden Section Optimization
HC	Hill-Climbing
HC-FLC	Hill-Climbing Fuzzy logic controller
InCond	Incremental Conductance
I-V	Current–Voltage characteristic curve
LMPP	Local Maximum Power Point
LMPPT	Local Maximum Power Point tracking
LT	Look-up Table
Mono C-Si	Mono-Crystalline Silicon
MPE	Mean Percentage Error
MPP	Maximum Power Point
MPPT	Maximum Power Point Tracking

N	Negative
P	Positive
P&O	Perturb & Observe
PB	Positive Big
P-I	Proportional-Integral controller
Poly C-Si	Poly-Crystalline Silicon
PS	Partial Shading
Ps	Positive Small
PSCs	Partial Shading Conditions
PSO	Particle Swarm Optimization
PV	Photovoltaic
P-V	Power–Voltage characteristic curve
PVG	Photovoltaic Generator
PVIC	PV Interface Configuration
PWM	Pulse Width Modulation
R^2	Correlation coefficient
RMSE	Root Mean Squared Error
RTI	Real Time Interface
SA	Simulated Annealing
SC	Soft Computing
SEPIC	Single Ended Primary Inductor Converter
SMC	Sliding Mode Controller
STC	Standard Test Condition (STC: 1000 W/m^2 and 25 °C)
UICs	Uniform Irradiance Conditions
VSS-InCond	Variable Step Size Incremental Conductance
ZE	Zero

APPENDIX C: LIST OF SYMBOLS

A	The diode ideality factor [ ]
FF	The PV module's fill factor [ ]
$FF_{N,25}$	The normalized fill factor when the solar cell temperature is 25° C [ ]
G	The irradiance level [W/m^2]
I_0	The PV cell saturation current [A]
I_{MPP}	Current at Pmax [A]
I_{ph}	The PV cell light current [A]
I_{pv}	The photovoltaic generator output current [A]
I_{sc}	The short circuit current [A]
k	The Boltzmann's constant (1.38×10^{-23} [J/K])
K_{oc}	The value of the voltage factor [ ]
K_{sc}	The value of the current factor [ ]
N	The number of simulated or measured points [ ]
n_p	The number of PV cells connected together in parallel [ ]
n_s	The number of PV cells connected together in series [ ]
P_{MPP}	Maximum power [W]
P_{pv}	The photovoltaic generator output power [W]
$P_{pv\_mea}(n)$	The *nth* measured value of the PV output power [W]
$P_{pv\_sim}(n)$	The *nth* simulated value of the PV output power [W]
q	The charge of an electron (1.602×10^{-19} [C])
R_p	The PV cell shunt resistance [A]
R_s	The PV cell series resistance [Ω]
R_{SN}	The normalized solar cell's series resistance [ ]
S	The lighting area of the PV module [m^2]
T	The PV cell temperature (in [Kelvins] or [Degrees celsius])
$V_{OCN,25}$	The normalized open-circuit voltage at temperature of 25 °C [ ]
V_{MPP}	Voltage at Pmax [V]
V_{oc}	The open circuit voltage [V]
V_{pv}	The photovoltaic generator output voltage [V]
$V_{t,25}$	The junction thermal voltage of the solar cell at 25° C; [V]
η	The efficiency [%]

PUBLICATIONS AND CONFERENCES

1. **R. Boukenoui, R. Bradai, A. Mellit, M. Ghanes, and H. Salhi, "Comparative analysis of P&O, modified hill climbing-FLC, and adaptive P&O-FLC MPPTs for microgrid standalone PV system," in International Conference on Renewable Energy Research and Applications (ICRERA), Italy, (2015), 1095-1099.**

2. **R. Boukenoui, R. Bradai, H. Salhi, and A. Mellit, "Modeling and simulation of photovoltaic strings under partial shading conditions using Matlab/Simscape," in International Conference on Clean Electrical Power (ICCEP), Italy, (2015), 73-77.**

3. **R. Boukenoui, H. Salhi, R. Bradai, and A. Mellit, "A new intelligent MPPT method for stand-alone photovoltaic systems operating under fast transient variations of shading patterns," Solar Energy, V. 124, (2016), 124-142,.**

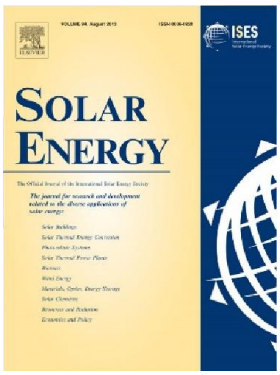

CiteScore: 4.52

Impact Factor: 4.018 (*2017 Journal Citation Reports*)

5-Year Impact Factor: 4.739 (*2017 Journal Citation Reports*)

Source Normalized Impact per Paper (SNIP): 1.957

SCImago Journal Rank (SJR): 2.063

4. **Kheldoun, R. Bradai, R. Boukenoui, and A. Mellit, "A new Golden Section method-based maximum power point tracking algorithm for photovoltaic systems," Energy Conversion and Management, V. 111, (2016), 125–136.**

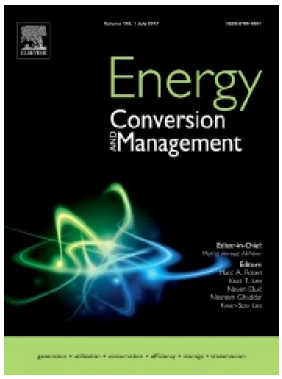

CiteScore: 6.04

Impact Factor: 5.589 (*2017 Journal Citation Reports*)

5-Year Impact Factor: 5.472 (*2017 Journal Citation Reports*)

Source Normalized Impact per Paper (SNIP): 1.948

SCImago Journal Rank (SJR): 2.156

5. **R. Bradai, R. Boukenoui, A. Kheldoun, H. Salhi, M. Ghanes, J. P. Barbot, A. Mellit., "Experimental assessment of new fast MPPT algorithm for PV systems under non-uniform irradiance conditions," Applied Energy, V. 199, (8/1/ 2017), 416-429.**

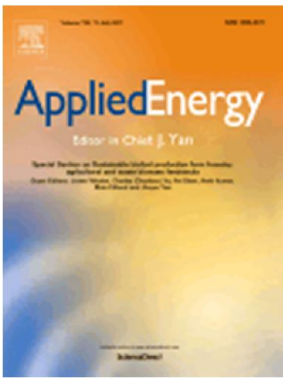

CiteScore: 7.78

Impact Factor: 7.182 (*2017 Journal Citation Reports*)

5-Year Impact Factor: 7.500 (*2017 Journal Citation Reports*)

Source Normalized Impact per Paper (SNIP): 2.439

SCImago Journal Rank (SJR): 2.998

6. **R. Boukenoui, M. Ghanes, J. P. Barbot, R. Bradai, A. Mellit, and H. Salhi, "Experimental assessment of maximum power point tracking methods for photovoltaic systems," Energy, V. 132, (8/1/ 2017), 324-340.**

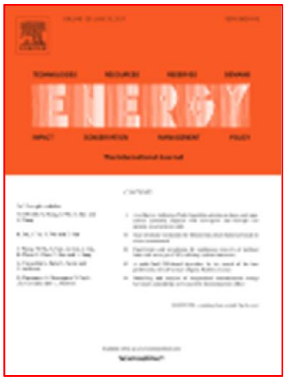

CiteScore: 5.17

Impact Factor: 4.520 (*2017 Journal Citation Reports*)

5-Year Impact Factor: 5.182 (*2017 Journal Citation Reports*)

Source Normalized Impact per Paper (SNIP): 1.898

SCImago Journal Rank (SJR): 2.350

REFERENCES

[1] Yan, J., Shamim, T., Chou, S., Desideri, U., et Li, H., “Clean, efficient and affordable energy for a sustainable future,” Applied Energy,(2016).

[2] Numbi, B. P., et Malinga, S. J., “Optimal energy cost and economic analysis of a residential grid-interactive solar PV system- case of eThekwini municipality in South Africa,” Applied Energy, V. 186, Part 1,(1/15//2017), 28-45.

[3] Zubi, G., Dufo-López, R., Pasaoglu, G., et Pardo, N., “Techno-economic assessment of an off-grid PV system for developing regions to provide electricity for basic domestic needs: A 2020–2040 scenario,” Applied Energy, V. 176,(2016), 309-319.

[4] Ammar, M. H., Benhaoua, B., et Balghouthi, M., “Simulation of tubular adsorber for adsorption refrigeration system powered by solar energy in sub-Sahara region of Algeria,” Energy Conversion and Management, V. 106,(2015), 31-40.

[5] Mekhilef, S., Saidur, R., et Safari, A., “A review on solar energy use in industries,” Renewable and Sustainable Energy Reviews, V. 15, nº 4,(2011), 1777-1790.

[6] Chatzipanagi, A., Frontini, F., et Virtuani, A., “BIPV-temp: A demonstrative Building Integrated Photovoltaic installation,” Applied Energy, V. 173,(2016), 1-12.

[7] Jiang, J.-A., Su, Y.-L., Shieh, J.-C., Kuo, K.-C., Lin, T.-S., Lin, T.-T., Fang, W., Chou, J.-J., et Wang, J.-C., “On application of a new hybrid maximum power point tracking (MPPT) based photovoltaic system to the closed plant factory,” Applied Energy, V. 124,(2014), 309-324.

[8] Assouline, D., Mohajeri, N., et Scartezzini, J.-L., “Quantifying rooftop photovoltaic solar energy potential: A machine learning approach,” Solar Energy, V. 141,(1/1/2017), 278-296.

[9] Mekhilef, S., Saidur, R., et Kamalisarvestani, M., “Effect of dust, humidity and air velocity on efficiency of photovoltaic cells,” Renewable and Sustainable Energy Reviews, V. 16, nº 5,(2012), 2920-2925.

[10] Ma, T., Yang, H., et Lu, L., “Solar photovoltaic system modeling and performance prediction,” Renewable and Sustainable Energy Reviews, V. 36, nº 0,(2014), 304-315.

[11] Ma, T., Yang, H., et Lu, L., “Development of a model to simulate the performance characteristics of crystalline silicon photovoltaic modules/strings/arrays,” Solar Energy, V. 100,(28/02/2014), 31-41.

[12] Boutana, N., Mellit, A., Lughi, V., et Massi Pavan, A., “Assessment of implicit and explicit models for different photovoltaic modules technologies,” Energy, V. 122,(3/1/2017), 128-143.

[13] Moballegh, S., et Jin, J., “Modeling, Prediction, and Experimental Validations of Power Peaks of PV Arrays Under Partial Shading Conditions,” IEEE Transactions on Sustainable Energy, V. 5, nº 1,(2014), 293-300.

[14] Farhat, M., Barambones, O., et Sbita, L., “A new maximum power point method based on a sliding mode approach for solar energy harvesting,” Applied Energy, V. 185,(2016), 1185–1198.

[15] Boukenoui, R., Salhi, H., Bradai, R., et Mellit, A., “A new intelligent MPPT method for stand-alone photovoltaic systems operating under fast transient variations of shading patterns,” Solar Energy, V. 124, nº 1,(2016), 124-142.

[16] Eccher, M., Salemi, A., Turrini, S., et Brusa, R., “Measurements of power transfer efficiency in CPV cell-array models using individual DC–DC converters,” Applied Energy, V. 142,(2015), 396-406.

[17] Belhaouas, N., Cheikh, M. S. A., Agathoklis, P., Oularbi, M. R., Amrouche, B., Sedraoui, K., et Djilali, N., “PV array power output maximization under partial shading using new shifted PV array arrangements,” Applied Energy, V. 187,(2/1/2017), 326-337.

[18] Ma, T., Yang, H., Lu, L., et Peng, J., “Pumped storage-based standalone photovoltaic power generation system: Modeling and techno-economic optimization,” Applied Energy, V. 137,(1/1/2015), 649-659.

[19] Liu, L., Meng, X., et Liu, C., “A review of maximum power point tracking methods of PV power system at uniform and partial shading,” Renewable and Sustainable Energy Reviews, V. 53,(31/01/2016), 1500-1507.

[20] Subudhi, B., et Pradhan, R., “A comparative study on maximum power point tracking techniques for photovoltaic power systems,” IEEE transactions on Sustainable Energy, V. 4, nº 1,(2013), 89-98.

[21] Gao, L., Dougal, R. A., Liu, S., et Iotova, A. P., “Parallel-connected solar PV system to address partial and rapidly fluctuating shadow conditions,” IEEE Transactions on industrial Electronics, V. 56, nº 5,(2009), 1548-1556.

[22] Salam, Z., Ahmed, J., et Merugu, B. S., “The application of soft computing methods for MPPT of PV system: A technological and status review,” Applied Energy, V. 107,(2013), 135-148.

[23] Patel, H., et Agarwal, V., “MATLAB-based modeling to study the effects of partial shading on PV array characteristics,” IEEE transactions on energy conversion, V. 23, nº 1,(2008), 302-310.

[24] Wang, Y.-J., et Hsu, P.-C., “An investigation on partial shading of PV modules with different connection configurations of PV cells,” Energy, V. 36, nº 5,(2011), 3069-3078.

[25] Syafaruddin, Karatepe, E., et Hiyama, T., “Performance enhancement of photovoltaic array through string and central based MPPT system under non-uniform irradiance conditions,” Energy Conversion and Management, V. 62, nº 0,(2012), 131-140.

[26] Wang, Y. J., et Hsu, P. C., “Analytical modelling of partial shading and different orientation of photovoltaic modules,” Renewable Power Generation, IET, V. 4, nº 3,(2010), 272-282.

[27] Balato, M., Costanzo, L., et Vitelli, M., “Series–Parallel PV array re-configuration: Maximization of the extraction of energy and much more,” Applied Energy, V. 159,(12/1/2015), 145-160.

[28] Gab-Su, S., Jong-Won, S., Bo-Hyung, C., et Kyu-Chan, L., “Digitally Controlled Current Sensorless Photovoltaic Micro-Converter for DC Distribution,” IEEE Transactions on Industrial Informatics, , V. 10, nº 1,(2014), 117-126.

[29] Romero Rodríguez, L., Salmerón Lissén, J. M., Sánchez Ramos, J., Rodríguez Jara, E. Á., et Álvarez Domínguez, S., “Analysis of the economic feasibility and reduction of a building’s energy consumption and emissions when integrating hybrid solar thermal/PV/micro-CHP systems,” Applied Energy, V. 165,(3/1/2016), 828-838.

[30] Saravanan, S., et Ramesh Babu, N., “Analysis and implementation of high step-up DC-DC converter for PV based grid application,” Applied Energy, V. 190,(3/15/2017), 64-72.

[31] Bidram, A., Davoudi, A., et Balog, R. S., “Control and circuit techniques to mitigate partial shading effects in photovoltaic arrays,” IEEE Journal of Photovoltaics, V. 2, nº 4,(2012), 532-546.

[32] Elserougi, A. A., Diab, M. S., Massoud, A. M., Abdel-Khalik, A. S., et Ahmed, S., “A switched PV approach for extracted maximum power enhancement of PV arrays during partial shading,” IEEE Transactions on Sustainable Energy, V. 6, nº 3,(2015), 767-772.

[33] Ahmed, J., et Salam, Z., “A critical evaluation on maximum power point tracking methods for partial shading in PV systems,” Renewable and Sustainable Energy Reviews, V. 47,(2015), 933-953.

[34] Lappalainen, K., et Valkealahti, S., “Output power variation of different PV array configurations during irradiance transitions caused by moving clouds,” Applied Energy, V. 190,(3/15/2017), 902-910.

[35] Liu, F., Duan, S., Liu, F., Liu, B., et Kang, Y., “A variable step size INC MPPT method for PV systems,” IEEE Transactions on industrial electronics, V. 55, nº 7,(2008), 2622-2628.

[36] Mohd Zainuri, M., Radzi, M., Amran, M., Soh, A. C., et Rahim, N., “Development of adaptive perturb and observe-fuzzy control maximum power point tracking for photovoltaic boost dc-dc converter,” Renewable Power Generation, IET, V. 8, nº 2,(2014), 183-194.

[37] Alajmi, B. N., Ahmed, K. H., Finney, S. J., et Williams, B. W., “A Maximum Power Point Tracking Technique for Partially Shaded Photovoltaic Systems in Microgrids,” IEEE Transactions on Industrial Electronics, , V. 60, nº 4,(2013), 1596-1606.

[38] Sundareswaran, K., Sankar, P., Nayak, P., Simon, S. P., et Palani, S., “Enhanced energy output from a PV system under partial shaded conditions through artificial bee colony,” IEEE Transactions on Sustainable Energy, V. 6, nº 1,(2015), 198-209.

[39] Lyden, S., et Haque, M. E., “A simulated annealing global maximum power point tracking approach for PV modules under partial shading conditions,” IEEE Transactions on Power Electronics, V. 31, nº 6,(2016), 4171-4181.

[40] Lian, K., Jhang, J., et Tian, I., “A maximum power point tracking method based on perturb-and-observe combined with particle swarm optimization,” IEEE journal of photovoltaics, V. 4, nº 2,(2014), 626-633.

[41] Sundareswaran, K., Vigneshkumar, V., Sankar, P., Simon, S. P., Nayak, P. S. R., et Palani, S., “Development of an Improved P&O Algorithm Assisted Through a Colony of Foraging Ants for MPPT in PV System,” IEEE Transactions on Industrial Informatics, V. 12, nº 1,(2016), 187-200.

[42] Cherdak, A. S., et Douglas, J. L., "Maximum power point tracker," Google Patents, 1971.

[43] Masoum, M. A. S., Dehbonei, H., et Fuchs, E. F., “Theoretical and experimental analyses of photovoltaic systems with voltage and current-based maximum power-point tracking,” IEEE Transactions on Energy Conversion, V. 17, nº 4,(2002), 514-522.

[44] Phang, J., Chan, D., et Phillips, J., “Accurate analytical method for the extraction of solar cell model parameters,” Electronics Letters, V. 20, nº 10,(1984), 406-408.

[45] Khatib, T. T., Mohamed, A., Amin, N., et Sopian, K., “An efficient maximum power point tracking controller for photovoltaic systems using new boost converter design and improved control algorithm,” WSEAS Transactions on power systems, V. 5, nº 2,(2010), 53-63.

[46] Ishaque, K., Salam, Z., et Lauss, G., “The performance of perturb and observe and incremental conductance maximum power point tracking method under dynamic weather conditions,” Applied Energy, V. 119,(2014), 228-236.

[47] Mule, S., Hardas, R., et Kulkarni, N. R., "P&O, IncCon and Fuzzy Logic implemented MPPT scheme for PV systems using PIC18F452," in 2016 International Conference on Wireless Communications, Signal Processing and Networking (WiSPNET),(23-25 March 2016), 1320-1325.

[48] Verma, D., Nema, S., Shandilya, A., et Dash, S. K., “Maximum power point tracking (MPPT) techniques: Recapitulation in solar photovoltaic systems,” Renewable and Sustainable Energy Reviews, V. 54,(2016), 1018-1034.

[49] Teulings, W., Marpinard, J., Capel, A., et O'Sullivan, D., "A new maximum power point tracking system," in 24th Annual IEEE on Power Electronics Specialists Conference PESC, , 833-838.

[50] Xiao, W., et Dunford, W. G., "A modified adaptive hill climbing MPPT method for photovoltaic power systems," in IEEE 35th Annual on Power Electronics Specialists Conference PESC, , 1957-1963.

[51] Koutroulis, E., Kalaitzakis, K., et Voulgaris, N. C., “Development of a microcontroller-based, photovoltaic maximum power point tracking control system,” IEEE transactions on power electronics, V. 16, nº 1,(2001), 46-54.

[52] Boukenoui, R., Bradai, R., Mellit, A., Ghanes, M., et Salhi, H., "Comparative analysis of P&O, modified hill climbing-FLC, and adaptive P&O-FLC MPPTs for microgrid standalone PV system," in 2015 International Conference on Renewable Energy Research and Applications (ICRERA),(22-25 Nov. 2015), 1095-1099.

[53] Fangrui, L., Yong, K., Yu, Z., et Shanxu, D., "Comparison of P&O and hill climbing MPPT methods for grid-connected PV converter," in 3rd IEEE Conference on Industrial Electronics and Applications, ,(3-5 June 2008), 804-807.

[54] Liu, B., Duan, S., Liu, F., et Xu, P., “Analysis and improvement of maximum power point tracking algorithm based on incremental conductance method for photovoltaic array,” in 7th International Conference on Power Electronics and Drive Systems, 637-641.

[55] Bendib, B., Belmili, H., et Krim, F., “A survey of the most used MPPT methods: Conventional and advanced algorithms applied for photovoltaic systems,” Renewable and Sustainable Energy Reviews, V. 45, nº 0,(2015), 637-648.

[56] Hohm, D., et Ropp, M. E., “Comparative study of maximum power point tracking algorithms,” Progress in photovoltaics: Research and Applications, V. 11, nº 1,(2003), 47-62.

[57] De Brito, M. A. G., Galotto, L., Sampaio, L. P., e Melo, G. d. A., et Canesin, C. A., “Evaluation of the main MPPT techniques for photovoltaic applications,” IEEE transactions on industrial electronics, V. 60, nº 3,(2013), 1156-1167.

[58] Pandey, A., Dasgupta, N., et Mukerjee, A. K., “High-performance algorithms for drift avoidance and fast tracking in solar MPPT system,” IEEE Transactions on Energy Conversion, V. 23, nº 2,(2008), 681-689.

[59] Piegari, L., et Rizzo, R., “Adaptive perturb and observe algorithm for photovoltaic maximum power point tracking,” IET Renewable Power Generation, V. 4, nº 4,(2010), 317-328.

[60] Zhang, L., Al-Amoudi, A., et Bai, Y., "Real-time maximum power point tracking for grid-connected photovoltaic systems," in Eighth International Conference on Power Electronics and Variable Speed Drives, , 124-129.

[61] Al-Diab, A., et Sourkounis, C., "Variable step size P&O MPPT algorithm for PV systems," in 12th International Conference on Optimization of Electrical and Electronic Equipment (OPTIM),, 1097-1102.

[62] Yang, Y., et Zhao, F. P., “Adaptive perturb and observe MPPT technique for grid-connected photovoltaic inverters,” Procedia Engineering, V. 23,(2011), 468-473.

[63] Mamarelis, E., Petrone, G., et Spagnuolo, G., “A two-steps algorithm improving the P&O steady state MPPT efficiency,” Applied Energy, V. 113,(31/01/2014), 414-421.

[64] Ahmed, J., et Salam, Z., “An improved perturb and observe (P&O) maximum power point tracking (MPPT) algorithm for higher efficiency,” Applied Energy, V. 150,(7/15/2015), 97-108.

[65] Sheik Mohammed, S., Devaraj, D., et Imthias Ahamed, T. P., “A novel hybrid Maximum Power Point Tracking Technique using Perturb & Observe algorithm and Learning Automata for solar PV system,” Energy, V. 112,(10/1/2016), 1096-1106.

[66] Mellit, A., et Kalogirou, S. A., “MPPT-based artificial intelligence techniques for photovoltaic systems and its implementation into field programmable gate array chips: Review of current status and future perspectives,” Energy, V. 70, nº 0,(2014), 1-21.

[67] Alabedin, A. Z., El-Saadany, E., et Salama, M., "Maximum power point tracking for Photovoltaic systems using fuzzy logic and artificial neural networks," in 2011 IEEE Power and Energy Society General Meeting, ,(24/06), 1-9.

[68] Xu, J., Shen, A., Yang, C., Rao, W., et Yang, X., "ANN based on IncCond algorithm for MPP tracker," in 2011 sixth international conference on bio-inspired computing: theories and applications (BIC-TA), ,(27/09), 129-134.

[69] Jie, L., et Ziran, C., "Research on the MPPT algorithms of photovoltaic system based on PV neural network," in 2011 Chinese Control and Decision Conference (CCDC), ,(23/05), 1851-1854.

[70] Veerachary, M., Senjyu, T., et Uezato, K., “Neural-network-based maximum-power-point tracking of coupled-inductor interleaved-boost-converter-supplied PV system using fuzzy controller,” IEEE Transactions on Industrial Electronics, V. 50, nº 4,(2003), 749-758.

[71] Ramaprabha, R., Gothandaraman, V., Kanimozhi, K., Divya, R., et Mathur, B., "Maximum power point tracking using GA-optimized artificial neural network for Solar PV system," in 1st international conference on electrical energy systems (ICEES), , 264-268.

[72] Simoes, M. G., et Franceschetti, N., “Fuzzy optimisation based control of a solar array system,” IEE Proceedings-Electric Power Applications, V. 146, nº 5,(1999), 552-558.

[73] Won, C.-Y., Kim, D.-H., Kim, S.-C., Kim, W.-S., et Kim, H.-S., "A new maximum power point tracker of photovoltaic arrays using fuzzy controller," in 25th Annual IEEE Power Electronics Specialists Conference PESC'94., ,(20/06), 396-403.

[74] Masoum, M., et Sarvi, M., "Design, simulation and construction of a new fuzzy-based maximum power point tracker for photovoltaic applications," in Proceedings of the Australasian University Power System Engineering Conference (AUPEC’02),.

[75] Kottas, T. L., Boutalis, Y. S., et Karlis, A. D., “New maximum power point tracker for PV arrays using fuzzy controller in close cooperation with fuzzy cognitive networks,” IEEE Transactions on Energy Conversion, V. 21, nº 3,(2006), 793-803.

[76] Wu, T.-F., Yang, C.-H., Chen, Y.-K., et Liu, Z.-R., "Photovoltaic inverter systems with self-tuning fuzzy control based on an experimental planning method," in Thirty-Fourth IAS Annual Meeting on IEEE Industry Applications Conference, , 1887-1894.

[77] Larbes, C., Aït Cheikh, S. M., Obeidi, T., et Zerguerras, A., “Genetic algorithms optimized fuzzy logic control for the maximum power point tracking in photovoltaic system,” Renewable Energy, V. 34, nº 10,(31/10/2009), 2093-2100.

[78] Alajmi, B. N., Ahmed, K. H., Finney, S. J., et Williams, B. W., “Fuzzy-logic-control approach of a modified hill-climbing method for maximum power point in microgrid standalone photovoltaic system,” IEEE Transactions on Power Electronics, , V. 26, nº 4,(2011), 1022-1030.

[79] Messai, A., Mellit, A., Pavan, A. M., Guessoum, A., et Mekki, H., “FPGA-based implementation of a fuzzy controller (MPPT) for photovoltaic module,” Energy conversion and management, V. 52, nº 7,(2011), 2695-2704.

[80] Messai, A., Mellit, A., Guessoum, A., et Kalogirou, S., “Maximum power point tracking using a GA optimized fuzzy logic controller and its FPGA implementation,” Solar Energy, V. 85, nº 2,(2011), 265-277.

[81] Al Nabulsi, A., et Dhaouadi, R., “Efficiency optimization of a DSP-based standalone PV system using fuzzy logic and dual-MPPT control,” IEEE Transactions on Industrial Informatics, V. 8, nº 3,(2012), 573-584.

[82] Rajesh, R., et Mabel, M. C., “Design and real time implementation of a novel rule compressed fuzzy logic method for the determination operating point in a photovoltaic system,” Energy, V. 116, Part 1,(12/1/2016), 140-153.

[83] Chao, P. C.-P., Chen, W.-D., et Chang, C.-K., “Maximum power tracking of a generic photovoltaic system via a fuzzy controller and a two-stage DC–DC converter,” Microsystem technologies, V. 18, nº 9-10,(2012), 1267-1281.

[84] El Khateb, A., Rahim, N. A., Selvaraj, J., et Uddin, M. N., “Fuzzy-logic-controller-based SEPIC converter for maximum power point tracking,” IEEE Transactions on Industry Applications, V. 50, nº 4,(2014), 2349-2358.

[85] Guenounou, O., Dahhou, B., et Chabour, F., “Adaptive fuzzy controller based MPPT for photovoltaic systems,” Energy Conversion and Management, V. 78,(2014), 843-850.

[86] Chen, Y.-T., Jhang, Y.-C., et Liang, R.-H., “A fuzzy-logic based auto-scaling variable step-size MPPT method for PV systems,” Solar Energy, V. 126,(31/03/2016), 53-63.

[87] Ishaque, K., Salam, Z., Shamsudin, A., et Amjad, M., “A direct control based maximum power point tracking method for photovoltaic system under partial shading conditions using particle swarm optimization algorithm,” Applied Energy, V. 99, nº 0,(2012), 414-422.

[88] Ishaque, K., Salam, Z., Amjad, M., et Mekhilef, S., “An improved particle swarm optimization (PSO)–based MPPT for PV with reduced steady-state oscillation,” IEEE transactions on Power Electronics, V. 27, nº 8,(2012), 3627-3638.

[89] Chao, K.-H., Lin, Y.-S., et Lai, U.-D., “Improved particle swarm optimization for maximum power point tracking in photovoltaic module arrays,” Applied Energy, V. 158,(2015), 609-618.

[90] Babu, T. S., Rajasekar, N., et Sangeetha, K., “Modified particle swarm optimization technique based maximum power point tracking for uniform and under partial shading condition,” Applied Soft Computing, V. 34,(2015), 613-624.

[91] Ahmed, J., et Salam, Z., “A Maximum Power Point Tracking (MPPT) for PV system using Cuckoo Search with partial shading capability,” Applied Energy, V. 119,(2014), 118-130.

[92] Jiang, L. L., Maskell, D. L., et Patra, J. C., “A novel ant colony optimization-based maximum power point tracking for photovoltaic systems under partially shaded conditions,” Energy and Buildings, V. 58, nº 0,(2013), 227-236.

[93] soufyane Benyoucef, A., Chouder, A., Kara, K., et Silvestre, S., “Artificial bee colony based algorithm for maximum power point tracking (MPPT) for PV systems operating under partial shaded conditions,” Applied Soft Computing, V. 32,(2015), 38-48.

[94] Shaiek, Y., Ben Smida, M., Sakly, A., et Mimouni, M. F., “Comparison between conventional methods and GA approach for maximum power point tracking of shaded solar PV generators,” Solar Energy, V. 90, nº 0,(2013), 107-122.

[95] Daraban, S., Petreus, D., et Morel, C., “A novel MPPT (maximum power point tracking) algorithm based on a modified genetic algorithm specialized on tracking the global maximum power point in photovoltaic systems affected by partial shading,” Energy, V. 74,(9/1//2014), 374-388.

[96] Rizzo, S. A., et Scelba, G., “ANN based MPPT method for rapidly variable shading conditions,” Applied Energy, V. 145, nº 0,(2015), 124-132.

[97] Sundareswaran, K., Vigneshkumar, V., et Palani, S., “Development of a hybrid genetic algorithm/perturb and observe algorithm for maximum power point tracking in photovoltaic systems under non-uniform insolation,” IET Renewable Power Generation, V. 9, nº 7,(2015), 757-765.

[98] Shi, J., Zhang, W., Zhang, Y., Xue, F., et Yang, T., “MPPT for PV systems based on a dormant PSO algorithm,” Electric Power Systems Research, V. 123, nº 0,(2015), 100-107.

[99] Manickam, C., Raman, G. R., Raman, G. P., Ganesan, S. I., et Nagamani, C., “A Hybrid Algorithm for Tracking of GMPP Based on P&O and PSO With Reduced Power Oscillation in String Inverters,” IEEE Transactions on Industrial Electronics, V. 63, nº 10,(2016), 6097-6106.

[100] Punitha, K., Devaraj, D., et Sakthivel, S., “Development and analysis of adaptive fuzzy controllers for photovoltaic system under varying atmospheric and partial shading condition,” Applied Soft Computing, V. 13, nº 11,(2013), 4320-4332.

[101] Ji, Y.-H., Jung, D.-Y., Kim, J.-G., Kim, J.-H., Lee, T.-W., et Won, C.-Y., “A real maximum power point tracking method for mismatching compensation in PV array under partially shaded conditions,” IEEE Transactions on power electronics, V. 26, nº 4,(2011), 1001-1009.

[102] Farivar, “Design of smart power grid renewable energy systems“: John Wiley & Sons, (2011).

[103] Pilawa-Podgurski, R. C. N., et Perreault, D. J., “Submodule Integrated Distributed Maximum Power Point Tracking for Solar Photovoltaic Applications,” IEEE Transactions on Power Electronics, , V. 28, nº 6,(2013), 2957-2967.

[104] Olalla, C., Clement, D., Rodriguez, M., et Maksimovic, D., “Architectures and Control of Submodule Integrated DC-DC Converters for Photovoltaic Applications,” IEEE Transactions on Power Electronics, , V. 28, nº 6,(2013), 2980-2997.

[105] Farivar, G., et Asaei, B., “A New Approach for Solar Module Temperature Estimation Using the Simple Diode Model,” IEEE Transactions on Energy Conversion, , V. 26, nº 4,(2011), 1118-1126.

[106] Luque, A., et Hegedus, S., “Handbook of photovoltaic science and engineering“: John Wiley & Sons, (2011).
[107] Boukenoui, R., Bradai, R., Salhi, H., et Mellit, A., "Modeling and simulation of photovoltaic strings under partial shading conditions using Matlab/Simscape," in International Conference on Clean Electrical Power (ICCEP), ,(16-18 June 2015), 73-77.
[108] MathWorks. https://www.mathworks.com/products/matlab.html.
[109] MathWorks-Simulink. https://www.mathworks.com/products/simulink.html.
[110] MathWorks_Simscape_features. https://www.mathworks.com/products/simscape/features.html.
[111] Tian, H., Mancilla-David, F., Ellis, K., Muljadi, E., et Jenkins, P., “A cell-to-module-to-array detailed model for photovoltaic panels,” Solar Energy, V. 86, nº 9,(9///2012), 2695-2706.
[112] Moballegh, S., et Jiang, J., "Partial shading modeling of photovoltaic system with experimental validations," in IEEE Power and Energy Society General Meeting,, 1-9.
[113] Abdulazeez, M., et Iskender, I., "Simulation and experimental study of shading effect on series and parallel connected photovoltaic PV modules," in 7th International Conference on Electrical and Electronics Engineering (ELECO), ,(1-4 Dec. 2011), I-28-I-32.
[114] Kumar, S. G., et Rao, K. K., “Physics and chemistry of CdTe/CdS thin film heterojunction photovoltaic devices: fundamental and critical aspects,” Energy & Environmental Science, V. 7, nº 1,(2014), 45-102.
[115] Wolden, C. A., Kurtin, J., Baxter, J. B., Repins, I., Shaheen, S. E., Torvik, J. T., Rockett, A. A., Fthenakis, V. M., et Aydil, E. S., “Photovoltaic manufacturing: Present status, future prospects, and research needs,” Journal of Vacuum Science & Technology A, V. 29, nº 3,(2011), 030801.
[116] Shockley, W., et Queisser, H. J., “Detailed balance limit of efficiency of p-n junction solar cells,” Journal of applied physics, V. 32, nº 3,(1961), 510-519.
[117] NREL, ""Best research-cell efficiencies",The National Renewable Energy Laboratory (NREL), ," 2016.
[118] Jiang, Y., Shen, H., Pu, T., Zheng, C., Tang, Q., Gao, K., Wu, J., Rui, C., Li, Y., et Liu, Y., “High efficiency multi-crystalline silicon solar cell with inverted pyramid nanostructure,” Solar Energy, V. 142,(1/15//2017), 91-96.
[119] REN21. "Renewables 2015 Global Status Report (Paris: REN21 Secretariat). ."
[120] Renewables 2016 Global Status Report (Paris: REN21 Secretariat). , 2016.
[121] Phinikarides, A., Makrides, G., Zinsser, B., Schubert, M., et Georghiou, G. E., “Analysis of photovoltaic system performance time series: Seasonality and performance loss,” Renewable Energy, V. 77,(2015), 51-63.
[122] Reinhard, P., Chirila, A., Blosch, P., Pianezzi, F., Nishiwaki, S., Buechelers, S., et Tiwari, A. N., “Review of progress toward 20% efficiency flexible CIGS solar cells and manufacturing issues of solar modules,” IEEE Journal of Photovoltaics, , V. 3, nº 1,(2013), 572-580.
[123] Burst, J. M., Duenow, J. N., Albin, D. S., Colegrove, E., Reese, M. O., Aguiar, J. A., Jiang, C.-S., Patel, M., Al-Jassim, M. M., et Kuciauskas, D., “CdTe solar cells with open-circuit voltage breaking the 1 V barrier,” Nature Energy, V. 1,(2016), 16015.
[124] Major, J., Treharne, R., Phillips, L., et Durose, K., “A low-cost non-toxic post-growth activation step for CdTe solar cells,” Nature, V. 511, nº 7509,(2014), 334-337.

[125] Caballero, R., Kaufmann, C. A., Eisenbarth, T., Unold, T., Klenk, R., et Schock, H. W., “High efficiency low temperature grown Cu (In, Ga) Se2 thin film solar cells on flexible substrates using NaF precursor layers,” Progress in Photovoltaics: Research and Applications, V. 19, nº 5,(2011), 547-551.

[126] www.lsi-lastem.it, "ata logger for environmental applications MW8024-02/10, Global radiation 43 sensors pyranometers MW8008.1-05/11, Pt100 1/3 DIN – IEC 751."

[127] www.hobut.co.uk, "Standard brass ended shunts."

[128] Yıldıran, N., et Tacer, E., “Identification of photovoltaic cell single diode discrete model parameters based on datasheet values,” Solar Energy, V. 127,(2016), 175-183.

[129] Orioli, A., et Di Gangi, A., “A procedure to calculate the five-parameter model of crystalline silicon photovoltaic modules on the basis of the tabular performance data,” Applied Energy, V. 102,(2013), 1160-1177.

[130] Zhou, J., Li, H., Qiao, Y., Gao, Q., Liu, Y., et Liu, Z., "A comprehensive method to modeling and simulation of photovoltaic module under natural environment," in IEEE 40th Photovoltaic Specialist Conference (PVSC), , 1353-1357.

[131] Walker, G., “Evaluating MPPT converter topologies using a MATLAB PV model,” Journal of Electrical & Electronics Engineering, Australia, V. 21, nº 1,(2001), 49.

[132] Xiao, W., Dunford, W. G., et Capel, A., "A novel modeling method for photovoltaic cells," in IEEE 35th Annual Power Electronics Specialists Conference PESC, , 1950-1956.

[133] Ulapane, N. N., Dhanapala, C. H., Wickramasinghe, S. M., Abeyratne, S. G., Rathnayake, N., et Binduhewa, P. J., "Extraction of parameters for simulating photovoltaic panels," in 6th IEEE International Conference on Industrial and Information Systems (ICIIS),, 539-544.

[134] Chenni, R., Makhlouf, M., Kerbache, T., et Bouzid, A., “A detailed modeling method for photovoltaic cells,” Energy, V. 32, nº 9,(2007), 1724-1730.

[135] Maki, A., et Valkealahti, S., “Power losses in long string and parallel-connected short strings of series-connected silicon-based photovoltaic modules due to partial shading conditions,” IEEE Transactions on Energy Conversion, , V. 27, nº 1,(2012), 173-183.

[136] Massi Pavan, A., Mellit, A., De Pieri, D., et Lughi, V., “A study on the mismatch effect due to the use of different photovoltaic modules classes in large-scale solar parks,” Progress in photovoltaics: research and applications, V. 22, nº 3,(2014), 332-345.

[137] McEvoy, A., Markvart, T., Castañer, L., Markvart, T., et Castaner, L., “Practical handbook of photovoltaics: fundamentals and applications“: Elsevier, (2003).

[138] Yang, W. Y., Cao, W., Chung, T.-S., et Morris, J., “Applied numerical methods using MATLAB“: John Wiley & Sons, (2005).

[139] Lu, Y., “A golden section approach to optimization of automotive friction materials,” Journal of materials science, V. 38, nº 5,(2003), 1081-1085.

[140] Ta, C.-M., et Hori, Y., “Convergence improvement of efficiency-optimization control of induction motor drives,” IEEE Transactions on Industry Applications, V. 37, nº 6,(2001), 1746-1753.

[141] Valentini, M., Raducu, A., Sera, D., et Teodorescu, R., "PV inverter test setup for European efficiency, static and dynamic MPPT efficiency evaluation," in 11th International Conference on Optimization of Electrical and Electronic Equipment, ,(22-24 May 2008), 433-438.

[142] Andrejasic, T., Jankovec, M., et Topic, M., “Comparison of direct maximum power point tracking algorithms using EN 50530 dynamic test procedure,” IET renewable power generation, V. 5, nº 4,(2011), 281-286.

[143] Kharb, R. K., Shimi, S., Chatterji, S., et Ansari, M. F., “Modeling of solar PV module and maximum power point tracking using ANFIS,” Renewable and Sustainable Energy Reviews, V. 33,(2014), 602-612.

[144] Liu, Y.-H., Liu, C.-L., Huang, J.-W., et Chen, J.-H., “Neural-network-based maximum power point tracking methods for photovoltaic systems operating under fast changing environments,” Solar Energy, V. 89,(31/03/2013), 42-53.

[145] Okoye, C. O., et Solyalı, O., “Optimal sizing of stand-alone photovoltaic systems in residential buildings,” Energy, V. 126,(2017), 573-584.

[146] Qazi, S., "Chapter 2 - Fundamentals of Standalone Photovoltaic Systems," Standalone Photovoltaic (PV) Systems for Disaster Relief and Remote Areas: Elsevier, (2017), 31-82.

[147] Bouilouta, A., Mellit, A., et Kalogirou, S. A., “New MPPT method for stand-alone photovoltaic systems operating under partially shaded conditions,” Energy, V. 55, nº 0,(2013), 1172-1185.

[148] Weidong, X., Ozog, N., et Dunford, W. G., “Topology Study of Photovoltaic Interface for Maximum Power Point Tracking,” IEEE Transactions on Industrial Electronics,, V. 54, nº 3,(2007), 1696-1704.

[149] Patel, H., et Agarwal, V., “Maximum power point tracking scheme for PV systems operating under partially shaded conditions,” IEEE transactions on industrial electronics, V. 55, nº 4,(2008), 1689-1698.

Boukenoui Rachid was born in Blida, Algeria, 1990. He received the Master degree (Top of his class at the electronics department of Blida 1 university) in electrical machines, 2013, and the PhD degree in Electrical Engineering from Blida 1 University, in 2017.

He is a member of the project titled « Modélisation et gestion d'énergie des procédés à énergies renouvelables », established at Quartz laboratory EA 7393 located in ''l'École Nationale Supérieure de l'Èlectronique et de ses Applications (ENSEA), France''. His current research interests include: Photovoltaic modelling and control, energy conversion and power electronics.